INFORMATION TO USERS

This manuscript has been reproduced from the microfilm master. UMI films the text directly from the original or copy submitted. Thus, some thesis and dissertation copies are in typewriter face, while others may be from any type of computer printer.

The quality of this reproduction is dependent upon the quality of the copy submitted. Broken or indistinct print, colored or poor quality illustrations and photographs, print bleedthrough, substandard margins, and improper alignment can adversely affect reproduction.

In the unlikely event that the author did not send UMI a complete manuscript and there are missing pages, these will be noted. Also, if unauthorized copyright material had to be removed, a note will indicate the deletion.

Oversize materials (e.g., maps, drawings, charts) are reproduced by sectioning the original, beginning at the upper left-hand corner and continuing from left to right in equal sections with small overlaps.

ProQuest Information and Learning
300 North Zeeb Road, Ann Arbor, MI 48106-1346 USA
800-521-0600

A COMBINED APPROACH FOR ANALYSIS OF SINGLE CRYSTAL NICKEL BASE SUPERALLOYS

by

Gilbert BANDE

Department of Mechanical Engineering
McGill University, Montréal

July 2001

A thesis submitted to the Faculty of Graduate Studies and Research
in partial fulfillment of the requirements of the degree of
Doctor of Philosophy

DEDICATION

To my uncle,

Ebe Evina Moise

To you, who guided and supported me throughout my life and studies,
may this document be a testimony of my eternal gratitude to you.

ABSTRACT

The purpose of this research is to develop a new tool for mechanical design and analysis of single crystal (SC) nickel base superalloys used in gas turbine engine components. The principle of this tool is based on the extension of the predictive models for isotropic material behavior to anisotropic materials such as SC nickel base superalloys. This objective is achieved by combining the two main approaches used in the literature for SC materials development: the macroscopic approach and the microscopic approach. For that reason, this theory is designated as the "**combined approach**" (CA).

The structure of the CA theory requires two main elements: a viscoplastic model (that admits a yield function) and a slip factor. The viscoplastic model describes the behavior of the material in the macroscopic level. Conversely, the slip factor based on the crystallographic theory, accounts for the micro-slip state that dominates SC materials during deformation.

In order to determine the slip factor, a preliminary slip trace study of the crystal is established. Also to determine material constants from experimental data, a procedure has been developed to reduce the 3D basic equations into a one-dimensional form. The model has been evaluated for its predictive capability on SC material behavior including orientation dependence of the initial yielding, tension/compression asymmetry, stress-strain response, fully reversed cyclic response, creep response and relaxation response. In almost all the cases, good correlation has been observed between the predicted responses and experimental data, when available. Furthermore, it is believable that the CA can be successfully used for many other SC materials such as the body-centered-cubic (b.c.c) or the hexagonal-closed-packet (h.c.p). In view of all these results, the CA theory seems to offer the greatest promise in this regard. Limitations and future development needs are discussed.

RÉSUMÉ

Le but de cette recherche est de développer un nouvel outil pour la conception et l'analyse des superalliages monocrystallins (MC) à base du nickel, souvent utilisé dans la fabrication des composants des réacteurs. Le principe de cet outil est basé sur l'extension de la prédiction du comportement des matériaux isotropes, à l'étude des matériaux anisotropes tel que les superalliages MC à base du nickel. Cet objectif est conduit en combinant les deux grandes approches utilisées dans la littérature pour l'analyse des MC: l'approche macroscopique et l'approche microscopique. Pour cette raison, la théorie est désignée par l' "**approche combinée**" (AC).

La structure de la théorie de l'AC requiert deux éléments majeurs: un model visco-plastique (qui admet une fonction d'écrouissage), et un facteur de glissement. Le modèle viscoplastique décrit le comportement du matériaux à l'échelle macroscopique, tandis que le facteur de glissement, basé sur la théorie crystallographique, décrit l'état global des micro-glissements souvent prédominent dans la déformation des matériaux MC.

Afin de déterminer le facteur de glissement, une étude préliminaire de la structure du crystal est établit. Aussi, pour déterminer les constantes du matériaux à partir des données expérimentales, une procédure a été développée afin de réduire les équations de base définies en 3D à une dimension. Le model a été évalué pour sa capacité à prédire le comportement des matériaux monocrystallins incluant l'influence de l'orientation sur la limite élastique, la symétrie entre la tension et la compression, la réponse entre la contrainte et la déformation, la réponse cyclique, la réponse en fluage et relaxation. Dans presque tous les cas ci-dessus mentionnés, une bonne corrélation a été observée entre les réponses prédites et les données expérimentales quand disponibles. De plus, il est possible que la théorie de l'AC soit utilisée avec succès pour d'autres MC tel que "the body-centered-cubic" (b.c.c) ou "the hexagonal-closed-packet" (h.c.p). Au vu de tous ces résultats, la théorie de l'AC semble offrir une grande promesse à cet égard. Les limitations ainsi que les développements futurs requis ont aussi été discutés.

ACKNOWLEDGMENTS

I would like to express my sincere gratitude and thanks to Professor Jim Nemes for his guidance, assistance, suggestions, and patience in the completion of this research topic. I am also thankful to all professors in the department of Mechanical Engineering and particularly to Professors Larry Lessard, Rabi B. Baliga, David Frost, Misra Arun, Price Stuart, Ahmed Abdul and Michael Paidoussis, and staff members Jean Milliken and Anna Cianci, for all their help and encouragement. I would like to express my sincere gratitude to Mrs Judith Stymest, Maryse Bergevin and all the staff of the Student Aid Office for all their support, during my time in this program.

Special thanks to the University of Douala in Cameroon for making this program possible, and particularly to Professor Bekolo Ebe Brunot, Rector of the University of Yaounde II, for his help and encouragement for the accomplishment of this work.

I would like to thank Pratt & Whitney Canada for their financial support of part of this work. Special thanks to Dr. Mass Hongoh and Dr. Dave Nissley from Pratt & Whitney USA and to Mrs. Beverly and David Purdy from the NASA Center for Aerospace Information, for their help in kindly providing to me suggestions and or necessary information for getting experimental data used in the present work.

I thank my wife Chantal and my children George William and Mylène Sonia for their love and support. I also want to express my deep sense of gratitude and indebtedness to my families, relatives and friends in Cameroon whose encouragement and support have provided me with the motivation to complete this work.

I also thank all the members of Côte des Neiges Presbyterian Church for their support during the time I have spent in Canada. Their prayers have always comforted my family and me. Special thanks to the Minister Reverend William Manson and M. Richard Lancing for their financial support, and Roland and Becky DeVries for correcting this thesis.

Lancing for their financial support, and Roland and Becky DeVries for correcting this thesis.

Finally, I thank all of those who have contributed in someway, large or small, to the completion of this project, and particularly to Dr. Jean Pierre Kenne, Dr. Ngandhui Eloi, M. Maurice Tchio, M Mboup Cheikh, M Zoumana Koné, Mrs Aminata Dabo Diakité, my room mate Dr. Stephen Hugh Garrioch, M. Nima Atabaki, M. David Scott and all their family for their help and support during the time of my research.

STATEMENT OF ORIGINALITY

In the present dissertation, a new approach for SC materials analysis such as nickel base superalloys is proposed. That approach named the "**combined approach**" (CA), is based on the combination of both macroscopic and microscopic approaches. Its principle consists of extending the predicted models of isotropic material behavior to anisotropic materials such as SC nickel base superalloys used in the gas turbine engine. Its originality is based on:

- The incorporation of a slip factor into the Chaboche's viscoplastic model. That slip factor, based on the crystallographic theory, accounts for the micro slip-state that dominates SC materials during their deformation. In addition, the same slip factor confers a significant portion of the model to be based on the physics of the deformation mechanism.
- The determination of the material parameters for several SC nickel alloys at different temperatures.
- Theoretical description of initial yielding and tension compression asymmetry in a macroscopic theory.
- Comparison of predicted tensile, cyclic, creep and relaxation responses to experiments.

The elements mentioned above confer to the CA theory the suitability and the simplicity of the macroscopic viscoplastic theory on one hand, and the accuracy of the crystallographic theories on the other hand.

TABLE OF CONTENTS

LIST OF FIGURES

LIST OF TABLES

LIST OF SYMBOLS

$[B_m]$, $[C_m]$	Structural matrices on the octahedral slip system along the $[\bar{1}\,0\,1]$ and $[1\,\bar{2}\,1]$ orientations
D_{ij}	Components of the elasticity matrix
$\{e\}$, $\{v\}$	Applied stress and strain unit vectors in the global coordinate system.
$E_{[hkl]}$, $G_{[hkl]}$	Young's modulus and shear modulus along the [h k l] orientation
M_{ij}	Anisotropy matrix's components
$[H_m]$	Structural matrix on the cube slip system
H_0	Activation enthalpy of cross slip
[h k l]	Miller's indices
Q_{cij}, Q_{dij}	Components of the stress and strain rotation matrices
$Sf_{[hkl]}$	Slip factor along the [h k l] orientation
$(S_i)_{[hkl]}$	Maximum shear stress in the slip system along the [h k l] orientation
T	Absolute Temperature in (° K)
τ_{RT}	Critical Resolved Shear Stress (CRSS) on [0 0 1] orientation, at RT
(θ, ψ)	Euler's angles, (related to Miller's indices)
$\mu_i(\theta, \psi)$	Orientation functions
$\nu_{[hkl]}$	Poisson's ratio along the [h k l] orientation
τ	Resolved Shear Stress (RSS)
τ_3	RSS on the cube slip system along the $[\bar{1}\,0\,1]$ orientation

CHAPTER I

INTRODUCTION

I.1 – BACKGROUND AND MOTIVATION

The absence of grain boundaries in single crystal (SC) nickel base super-alloys confers on them thermal fatigue and creep properties that are far superior to those of conventional super-alloys. Also, the absence of grain boundary strengthening elements in SC provides considerable alloying and heat treatment flexibility (Gell et al. 1980), which also improves the strength and life of the material (Kear and Piearcey 1967), as well as corrosion and oxidation resistance (Swanson et al. 1986). This explains very well their use in the gas turbine engine manufacturing and many others applications in which higher operating temperature are sought. However, the lack of grain boundaries in SC alloys renders these materials strongly anisotropic, giving rise to complicated thermal mechanical responses and increasing the difficulty in mathematical characterization of their behavior for design of engine components. In order to improve the knowledge base and our understanding of their mechanical behavior when subjected to the external load, several analytical models have been proposed in the last four decades. All of the developed models in the form suitable for highly anisotropic single crystals found in the literature fall into two categories: the macroscopic approach and the microscopic approach.

In the first category, the theory is based on the continuum mechanics approach. The deformation study of the material is tackled on the macroscopic level. The anisotropic

property of the material is introduced in the model by generalizing a fourth order tensor and by exploiting the symmetry conditions derived from the crystal geometry. The principal argument in favor of the models based on that approach is their relative numerical simplicity. In addition, while implementing in a finite element code, these models are somewhat less complicated and generally require less calculation than those based on the microscopic approach. However, the most significant disadvantage of this approach is that the actual deformation mechanisms are not correlated to the theory. This lack of correlation limits the predictive capability of the models for single crystal materials.

In the second category, also called the crystallographic approach, the deformation study of the material is tackled on the microscopic level. The constitutive equations are introduced at each of the active slips, then, are summed up from all the slip systems to obtain the overall crystal deformation. In contrast to the first approach, models based on this approach give, in several cases, a better correlation with experimental data. However, such models have been found difficult to be implemented in finite element codes and, in addition, they require increased computational cost because of the number of slip systems to be considered at each point in the body. Furthermore, the response at the crystallographic level is not necessarily easy to determine.

Therefore, with the idea of increasing our knowledge and understanding of SC nickel base superalloys behavior, a new tool, the so-called **combined approach** (CA) is proposed in this work. It takes advantage of the combination of the simplicity of the macroscopic approach and the efficiency of the microscopic approach for the analysis of these superalloys. In this research, the constitutive theory is developed and the predicted results are compared with some of the experimental data available in the literature.

I.2 – OBJECTIVE AND SCOPE OF THE STUDY

In the light of advantages and disadvantages observed for both the macroscopic and microscopic approaches mentioned above, the main goal in the present dissertation is to propose a new phenomenological approach for mechanical design and analysis of SC

turbine blade components. The new tool so defined is based on the combination of both approaches. It thus takes advantage of combining the simplicity of the former and the accuracy of the latter. This main objective is achieved through:

- the development of the constitutive model based on the combined approach theory for a general global stress state,
- describing the orientation dependence of: the initial yielding, tension compression asymmetry, stress-strain response, fully reversed cyclic responses, primary and secondary creep responses and the relaxation response, and finally,
- The validation of the theory by comparing the predicted results with the available experimental data or those for other theories.

However, the investigation of the present approach will be limited to case of small, visco-plastic and incompressible isothermal deformation. In the case of creep, only the primary and the secondary stage will be taken into account. The tertiary creep stage, and the failure mechanisms, as well as methods for life predictions are out beyond the scope of this work. Furthermore, for this first attempt of the combined approach, the study will be restricted only to the translation and the expansion of the initial yield surface obtained from the virgin state. Subsequent yield surfaces will not be taken into account. In addition, although it is applicable to other viscoplastic models, only the Chaboche's viscoplastic model is applied to the approach. Several studies of SC nickel base super-alloys available in the literature show that these alloys are strongly sensitive to at least four parameters. These include the temperature, the applied stress with respect to its orientation, the strain rate, and the size and volume fractions of the γ' particles in the solid solution. According to the value considered for each of these parameters, the material response may be strongly affected. Because of the lack of experimental data, this first attempt of the CA will be limited to only two parameters: the orientation and the temperature dependence of SC material's features.

I.3 – STRUCTURE OF THE SC NICKEL BASE SUPERALLOYS

In this work, the heat treatment, chemistry and structure studies of superalloys used are limited to brief summaries. However, more detailed studies are listed in the references where experimental data were found.

SC nickel base superalloys are based on the Ni-Cr-Al alloy system. Chemical compositions vary among alloys developed by different companies. In Table 1.1 the chemical compositions for some common SC super-alloys are listed. One of their particularities is the existence of two alloys phase with a large volume fraction of γ' precipitates shown in Figures 1.1 and 1.2. An ordered, face-centered-cubic f.c.c Ni_3Al inter-metallic compound, interspersed in a coherent f.c.c γ solid solution as shown in Figure 1.1. The strength of the alloy is a function of the γ' size and the volume fraction of γ'. The composition may be quite different among modern SC super-alloys, but their microstructures are similar. For example, PWA 1480 has much more Ta less W, no Mo or Nb, and a much higher ratio of Al to Ti compared to Rene N4. However, both alloys have a similar γ' volume fraction of about 60-65% and a γ' size of about 0.25 μm, as well as similar mechanical properties as reported in Miner et al. (1986.a).

I.4 – MECHANICAL PROPERTIES

It has been established in a number of studies that the lack of grain boundaries in SC alloys renders these materials strongly anisotropic. This fact can be observed in Figures 1.3 and 1.4. Although the same material has been tested in tension at the same temperature along three distinct orientations, the corresponding responses are known to be different. This graph shows the strong anisotropic nature of these alloys and confirms the orientation dependence of their initial yield strength, as well as their elastic constants (not shown in this graph) and their general responses. These findings agree with the observations of Gabb et al. (1986), Milligan and Antolovich (1987), and Li and Smith (1995a), (1995b), (1995c) and (1995d).

Table 1.1 Chemical composition (% per wt.) of PWA 1480 and some nickel base super-alloys.

Alloy	Al	Cr	W	Co	Ta	Ti	C	Mo	Nb	Ref.
PWA 1480	4.8	10.4	4.1	5.3	11.9	1.3	---	---	---	1, 4
Rene N4	3.77	9.26	5.88	7.35	3.96	4.24	---	---	---	2, 3
MAR-M200	5.1	8.82	12.85	10.2	---	2.19	0.014	---	---	7
Rene VF317	3.6	8.7	6.0	7.4	4.1	4.6	---	1.6	0.6	6
SRR99	5.5	8.5	9.5	5.0	2.8	2.2	0.015	---	---	5

Table 1.2 Heat treatment and trademark of some SC nickel base super alloys listed in Table 1.1.

Alloy	Trademark	Heat Treatments			Ref.
		Solution	Aging 1	Aging 2	
PWA 1480	Pratt & Whiteney	1288° C/4 h air cool	1079° C/4 h	871° C/32 h	4
Rene N4	General Electric Company	1260° C/2 h gas quench	1080° C/4 h air cool	900° C/16 h air cool	2, 6
Rene VF317	General Electric Company	1260° C/2 h gas quench	1080° C/4 h air cool	900° C/16 h air cool	6
MAR-M200	Martin Marietta				7
SRR99	Hopgood & Martin	1300° C/4 h water quench	1100° C/1 h	871° C/16 h	5

1 – Swanson et al. (1986); 2 – Miner et al. (1986.a); 3 – Gabb et al. (1986);

4 – Milligan and Antolovich (1987); 5 – Hopgood and Martin (1986);

6 – Wukusick (1980); 7 – Dandeker and Kelley. (1981).

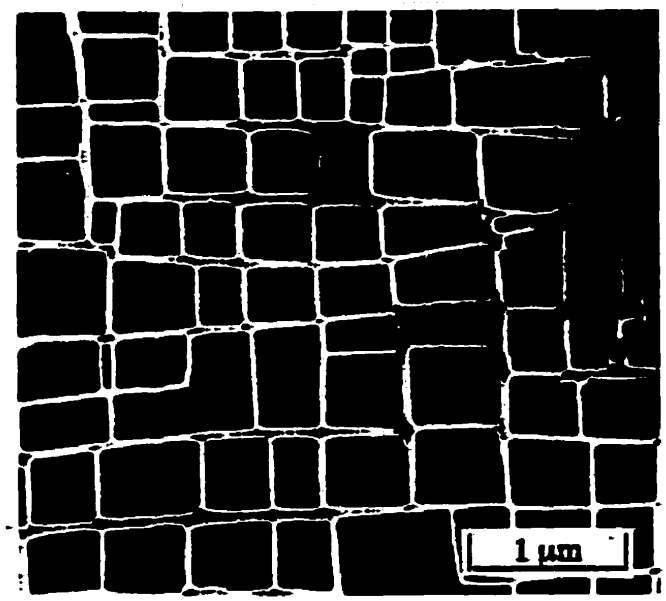

Figure 1.1 Microstructure of SC Nickel base superalloys CMSX4+Y. Aspect of aligned γ' particles (dark areas) in γ matrix (with lines). From Marchionni et al. (1993).

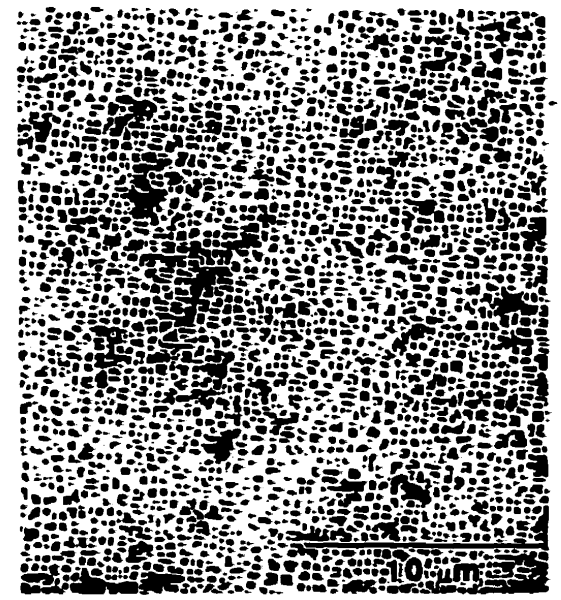

Figure 1.2 Microstructure of SC Nickel base superalloys Rene N4. From Gabb et al. (1986).

The elastic strains are associated with crystal lattice distortions and are fully recoverable whereas inelastic strains result from the movement of dislocations through the lattice and are not recoverable. In the elastic range, the stress-strain relationship obeys Hooke's law and may be written in the principal material directions or crystallographic axes (defined in Chapter III) as follows:

$$\{\sigma\}=[D]\{\varepsilon\} \tag{1.1}$$

where $\{\sigma\}$ and $\{\varepsilon\}$ are respectively stress and strain vectors, and [D] is the elasticity matrix defined in Eq.(1.2). Since SC nickel base superalloys exhibit cubic symmetry structure in the elastic range, the elasticity matrix [D], may be reduced to only three independent elastic parameters: D_{11} , D_{12} and D_{44}. Thus, the matrix [D] has the form:

$$[D]=\begin{bmatrix} D_{11} & D_{12} & D_{12} & 0 & 0 & 0 \\ D_{12} & D_{11} & D_{12} & 0 & 0 & 0 \\ D_{12} & D_{12} & D_{11} & 0 & 0 & 0 \\ 0 & 0 & 0 & D_{44} & 0 & 0 \\ 0 & 0 & 0 & 0 & D_{44} & 0 \\ 0 & 0 & 0 & 0 & 0 & D_{44} \end{bmatrix} \tag{1.2}$$

The rotation of the elastic matrix to another orientation can fully populate the matrix, which is shown in Chapter III. The inelastic response of SC materials is quite different from the inelastic behavior of polycrystalline nickel base superalloys. The yield strength of SC alloys is a function of the material orientation relative to the direction of the applied stress.

SC nickel base super alloys also exhibit significant tension/compression asymmetry in yield strength. This feature, shown in Figure 1.4, is primarily due to slip on the octahedral slip system as discuss in section 2.1.2, (i.e. between the dislocation in (111)

planes similar to $[\bar{1}\,0\,1]$ and $[\bar{1}\,2\,1]$[1]). The tension/compression asymmetry is negligible near the $[\bar{1}\,1\,1$ orientation where cube slip (i.e. dislocation in the (010) planes) is found to be the primary slip system. Furthermore, the orientation dependence and tension/compression asymmetry decreases as a function of increasing temperature above a critical temperature. These features are shown in Figures (1.5) and (1.6). Another familiar behavior observed in these alloys is the increase in flow stress with increasing temperature at the intermediate temperature (about 700°-760° C for Rene N4). This increase is followed by a sharp drop in the yield strength above the intermediate temperature as shown in Figure 1.5. This anomalous temperature dependence on the yield stress was satisfactorily explained by Takeuchi and Kuramoto (1973) to be the thermally activated transition of the moving screw dislocation from the (111) $[\bar{1}\,0\,1]$ octahedral slip system to the (010) $[\bar{1}\,0\,1]$ cube slip system. The [0 1 1] orientation is generally characterized by the lowest room temperature tensile strength and the greatest ductility and invariably produces an elliptically deformed (initially circular cross section) test sample. In contrast, the $[\bar{1}\,1\,1$ orientation has the highest ultimate strength between 700° C and 760° C. These results are generally consistent with Rene N4 data published by Miner et al. (1986). Similar to isotropic nickel base superalloys, single crystal alloys exhibit strain rate sensitivity and cyclic hardening. These features, illustrated in Figures 1.7 and 1.8 respectively, have been published and confirmed in Milligan and Antolovich, (1987), Swanson (1984.a, 1984.b), Swanson et al. (1986) and Stouffer and Bodner (1979) for SC PWA 1480 nickel base alloys data. The yield strength was constant and independent of strain rate up to 760° C, above which it dropped rapidly and strongly as a function of strain rate.

[1] The symbol [h k l] indicates the Miller indices defined in Appendix B.

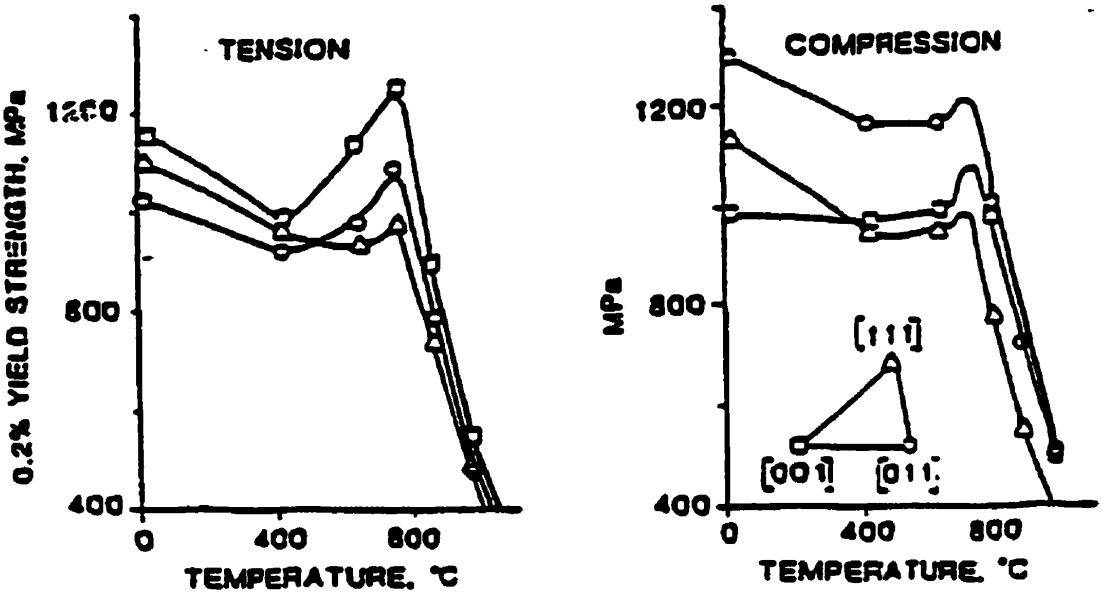

Figure 1.5 Yield strength of PWA 1480 as a function of temperature for the [0 0 1]-[0 1 1] and [1 1 1] orientations in tension and compression. From Shah and Duhl (1984).

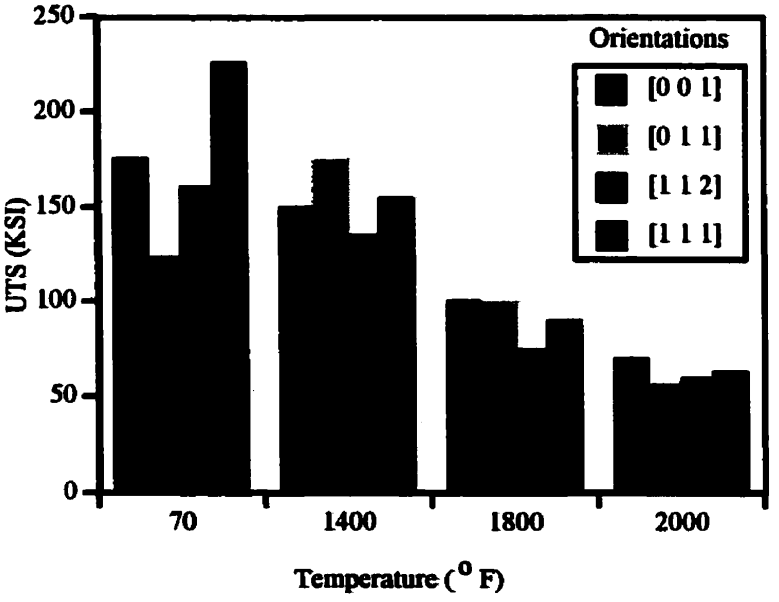

Figure 1.6 Effect of temperature on the ultimate tensile strength of SC nickel base super alloys along the [0 0 1], [0 1 1], [1 1 2] and [1 1 1] orientations. From Sheh (1988).

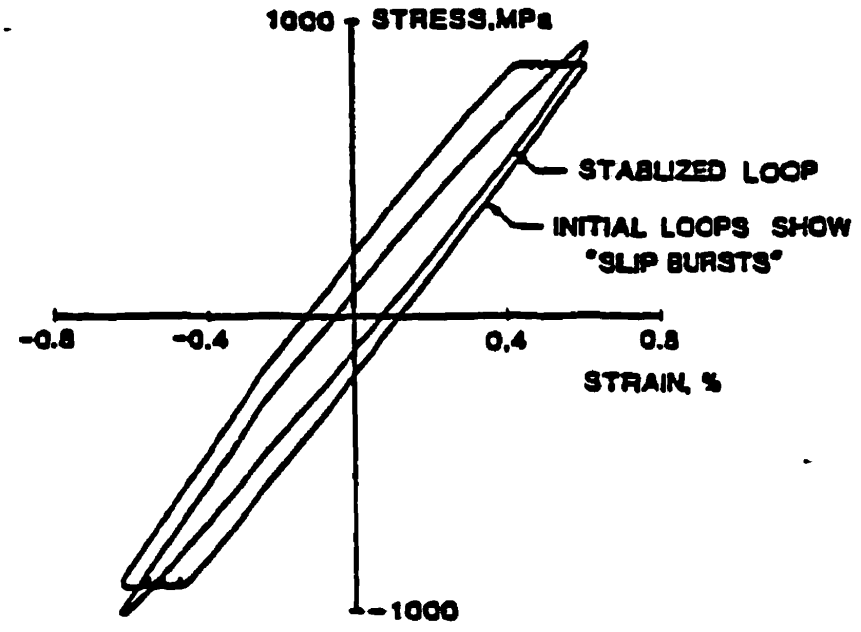

Figure 1.7 Cyclic hardening of PWA 1480 in the [3 2 1] orientation at 760° C. From Swanson (1984.b).

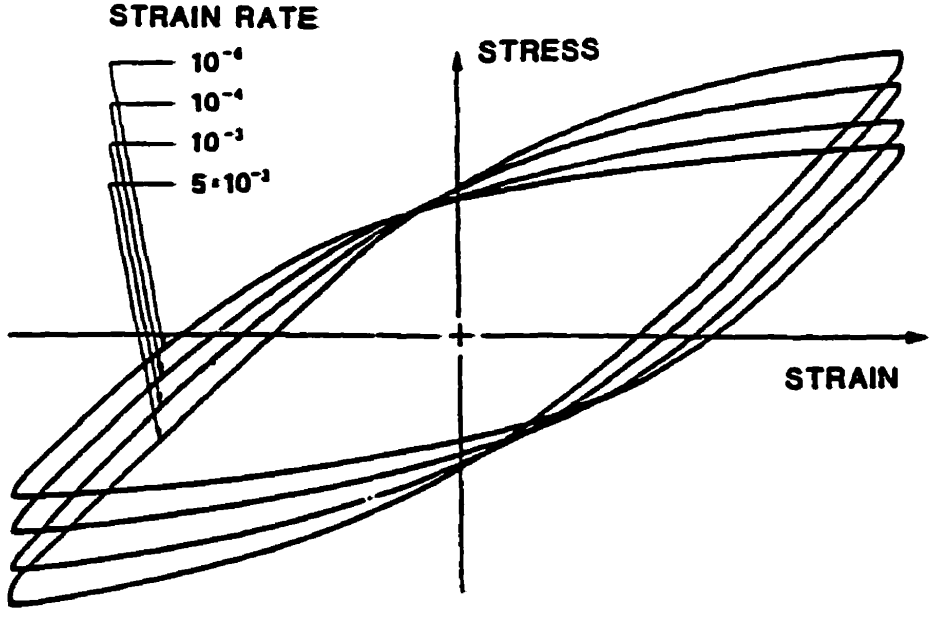

Figure 1.8 Strain rate sensitivity of PWA 1480 at 971° C in the [1 1 1] orientation. From Swanson (1984.a).

1.5 – OUTLINE

This dissertation is divided into seven chapters. Chapter II constitutes a literature review of the two main approaches (macroscopic and microscopic) used for analysis of material structure in general and SC nickel base super alloys in particular. Two models based on the above approaches were selected and presented in more detail with the goal of reaching a better understanding of their principles.

In Chapter III, the structure of the combined approach (CA) theory is defined, developed, and finally applied to the determination of the initial yielding. In the same Chapter, the orientation and temperature dependence of elastic constants developed respectively in Leknetskii (1962) and Li and Smith (1995.a) are summarized.

Chapter IV shows how the CA theory can be applied to the Chaboche model to account for the micro slip effects that dominate SC materials during their deformation process. Recall that the above phenomenon is neither treated in the original theory nor in its modified theories presented in the literature so far. The theory may therefore be extended beyond the elastic domain. The basic equations of the model are presented in the three-dimensional form and are finally reduced in the one-dimensional form.

In Chapter V, three SC nickel base super alloys (widely used in manufacturing jet engine turbine blades) were selected for the present work. The available experimental database cited in different references was collected, categorized and presented. In the same chapter, all the constants used in the theory and the material parameters used in the basic equations of the model were determined. A sensitivity study of the model was performed to illustrate the effect of small changes in the nominal values of the parameters. Values were modified and better agreement was achieved between theory and experimental results.

In the sixth Chapter, the predictive capabilities of the theories were explored and compared with other theories or experimental data available. The comparisons included

i) the orientation and temperature dependence of the initial yielding, ii) the tension compression asymmetry, iii) the stress-strain tensile response, iv) the creep response, vi) the fully reversed cyclic response and vii) the relaxation response. Whenever experimental data were not available, qualitative comparisons only were made between theories.

The seventh and final Chapter of the dissertation was devoted to drawing general conclusions based on the results and findings achieved. Moreover, recommendations for future work in areas related to the present approach were singled out.

CHAPTER II

THE CONSTITUTIVE MODELING THEORIES REVIEW

In the published literature, constitutive modeling of anisotropic materials such as single crystal (SC) superalloys falls into two categories: the micro-mechanical approach and the macroscopic approach.

In the first category, the constitutive equations are introduced at the microscopic level, on each of the known potentially active slip systems. The overall crystal deformation is then obtained by summing the slip from all the slip systems.

In the second category, the constitutive equations are introduced at the macroscopic level. For most of the models in this category, assuming the yield function (see Table 2.1), the anisotropy in the material is modeled by utilizing a fourth order tensor in the yield function and by exploiting the symmetric conditions known from the crystal geometry.

In the rest of this chapter, the two approaches in question will be described. Emphasis will be given to the Chaboche's viscoplastic model[1] retained in this work for the purpose of the **combined approach** (CA) theory development.

2.1- THE CRYSTALLOGRAPHIC APPROACH

The crystallographic or the micro-mechanical approach is based on identifying the active slip planes and slip directions as shown in Appendix A. Shear stresses are computed on each of the slip planes from the applied stress. The slip deformation is computed on each

[1] A unified viscoplastic model based on the continuum mechanics approach.

slip system. The macroscopic inelastic strain rates or strain increments are then obtained from the sum of the contributions from each individual slip system.

As an application of the crystallographic approach to single crystal nickel base super-alloys, several models exist in the published literature using the same concept. The principal advantages of the crystallographic approach are that:

- The theory is based on the physics of the deformation mechanisms. Presumably, this will enhance the predictive capability of the model.
- The developed theories based on this approach give better results than those based on the classical phenomenological approach.

However, major disadvantages of this approach are as follows:

- There is difficulty in numerically implementing crystallographic models in finite element codes, and there are increasing computational requirements due to the large number of slip systems to be considered at each point in the body with a large number of state variables at each iteration. Furthermore, the response at the crystallographic level is not necessarily easy to determine.
- The need for good understanding of the metallurgy and interaction between mechanisms.

2.1.1- Constitutive modeling history

Early study of crystalline plasticity is attributed to Ewing and Rosenhair (1899,1900). They published a series of papers that summarized their metallographic studies of plastic deformation of polycrystalline metals. One of the important conclusions obtained by Ewing and Rosenhaim in the 1890s is that the plastic deformation occurs by slip on certain crystallographic planes in certain crystallographic directions. Their findings form the basis of any recent physical plasticity theory.

Frenkel (1926) first gave the elementary theory of the shear strength's estimation for a perfect crystal. Based on the concept of a slip plane, the estimated strength of crystals has been found to be several orders higher than the observed one. Such a large disparity

inevitably suggests that the simple model proposed by Frenkel does not represent the actual behavior of crystals during plastic deformation. Indeed that disparity has been satisfactorily explained by Taylor (1934), Polanyi (1934), and Orowan (1934), using the concept of dislocations.

The mathematical representation of the physical phenomena of plastic deformation in terms of SC deformation was pioneered by Taylor (1938). Long before that, however, Schmid (1924) had proposed the concept of the critical resolved shear stress (CRSS). Schmid asserted that the resolved shear stress reaches a critical value, τ_c, for slip to occur. More rigorous and rational formulations of SC plasticity have been provided by Hill (1966), Hill and Rice (1972), Azaro and Rice (1977), Hill and Havner (1982), and more recently in Wagoner and Chenot (1996). A comprehensive review of this subject can be found in Asaro (1983), Lemaitre and Chaboche (1990), and Khan (1995). The same formulation has been used widely in polycrystal plasticity by Hill (1966), Asaro (1983) and localized plastic deformation by Asaro and Rice (1977); Pierce et al. (1982, 1983); Asaro and Needleman (1984). The same approach was successfully used in the modeling of texture evolution for both faced centered cubic (f.c.c) and body centered cubic (b.c.c) materials by Meric et al.(1991); Jordan and Walker (1992), Ohno and Takeuchi (1994). Takeuchi and Kuramoto (1973) first made a major step in better understanding of metallurgical behavior of (SC) materials. In their study of a SC Ni_3G_a, they proposed that the increase in CRSS up to the critical temperature, and the non Schmid's law behavior observed in these alloys, are results of cross slip of screw dislocation segments from the octahedral to the cube plane. The cross slip segments pin the dislocations and therefore increase the flow stress. They further proposed that the cross slip mechanism is thermally activated and is driven by the resolved shear stress in the (010)[1 0 1] system. However, their model did not fully explain the tension / compression asymmetry or the orientation dependence observed in other single crystal alloys. Lall, Chin and Pope (1979) made an improvement in Takeuchi and Kuramuto's model. In their theory, the octahedral $\frac{a}{2}[\bar{1}\,0\,1]$ dislocation is an extended dislocation

consisting of two Shockley partial dislocation pairs, $\frac{a}{6}[\bar{2}11]+\frac{a}{6}[\bar{1}\,\bar{1}\,2]$. In order to cross slip, the pair must constrict into a single $\frac{a}{2}[\bar{1}\,0\,1]$ dislocation. The constriction is aided by a shear stress on the (111) plane in the $[1\,\bar{2}\,1]$ direction. It is important to note that a shear stress in the opposite direction extends the dislocation pair and thus inhibits cross slip. This effect is generally referred to as the "core width effect" and gives rise to the tension/compression asymmetry observed in these alloys. Lall, Chin and Pope also proposed that the change in flow stress $\Delta\tau_{(111)}$ on the octahedral plane in the $[\bar{1}\,0\,1]$, for example from a reference state at 0°K, is given by

$$\Delta\tau_{(111)} = \tau_{(111)}(T) - \tau_{(111)}(0^0) = A_0 \exp\left(-\frac{H}{kT}\right) \tag{2.1}$$

$H=H(\tau_2,\tau_3)$ is a function of the resolved shear stress, τ_2, on the (1 1 1) plane in the $[\bar{1}\,2\,\bar{1}]$ direction, and the resolved shear stress, τ_3, on the (0 1 0) plane in the $[\bar{1}\,0\,1]$direction. The stress components, τ_2, and, τ_3, are shown in Figures A1 and A2 in appendix A. Extending H in a Taylor series about the reference condition H_0, Equation (2.1) becomes

$$\Delta\tau_{(111)} = A_0 \exp\left(\frac{-H_0+\delta V_1\tau_2+V_2\tau_3+\cdots}{kT}\right) \tag{2.2}$$

Where, A_0, V_1, and, V_2, are material constants, T is an absolute temperature, k is the Boltzmann's constant and H_0 is the natural activation energy, δ equal +1 for a tension stress and −1 for a compressive stress. Eq.(2.2) is similar to the one proposed by Takeuchi and Kuramuto (1973), differing only by the term $\delta V_1\tau_2$ that accounts for the stress-aided shockley partial pair constriction. In the orientations and at temperatures

where cube slip is dominant, the orientation dependence and tension/compression asymmetry are reduced considerably. Therefore, it is believed that Schmid's law can be used to relate the slip rate to the resolved shear stress on the cube planes.

2.1.2 – Slip trace study

The slip trace studies of SC alloys indicate that plastic deformation occurs by slip on certain crystallographic planes in certain crystallographic directions. In general, one or more types of slip may occur under different temperatures, orientations and strain rate conditions. These include:

- octahedral slip on the four octahedral planes in the three directions similar to the $[\bar{1}\,0\,1]$ direction (see Figure A1 in Appendix A),
- octahedral slip on the octahedral planes in the three directions similar to the $[\bar{1}\,2\,\bar{1}]$ direction, and
- Cube slip on the three cube planes in the two directions similar to the $[\bar{1}01]$ direction, (see Figure A2 in Appendix A).

The slip conditions occurring during tension/compression and creep tests are examined for use in the development of the constitutive **combined approach** theory.

2.1.2.1 – Tension and compression responses

When studying the cast SC alloy SC 7-146, Dalal et al. (1984) showed that the tensile strength is substantially less anisotropic at temperatures above 760°C (see Figures 1.5 and 1.6). The [0 1 1] orientation generally displays the lowest strength and greatest ductility and invariably produces an elliptically deformed (initially circular cross section) test sample. On the other hand, the $[\bar{1}\,1\,1]$ orientation has the highest ultimate strength around 760°C. These results are generally consistent with Rene N4 data published by Miner et al. (1986.b).

2.1.2.2 – Creep response

In Nathal and Ebert (1985), creep behavior of SC NASAIR 100 at temperatures of 925°C and 1000°C was investigated. The authors came to the conclusion that for loading in directions other than the [1 0 0] orientation, creep behavior is significantly anisotropic. In general, creep loading near the [0 1 1] orientation has a much shorter rupture life than near the [1 0 0] orientation. Kear and Piercey (1967), Mackay and Maier (1982), and Sheh (1988) confirmed these results. This finding was initially explained by Leverant and Kear (1970), using Schmid's law as multiplicity of slip for the (111) [1 1 2] slip systems. Mackay and Maier (1982) later found that the stress rupture lives at intermediates were greatly affected by the amount of lattice rotation required to produce intersecting slip. For example, crystals that required rotations to become oriented for intersecting slip exhibited large primary creep strain and shorter rupture lives. In the Mackay/Maier study, the stress rupture lives was also found, to be influenced by the relative orientations of the [001]-[011] boundary to the loading axis (which represents the slope of the straight line in the elastic part of the deformation).

2.2 – DAME AND STOUFFER'S CONSTITUTIVE MODEL

The Dame and Stouffer model (1986) is based on the crystallographic approach, and it uses the concept of the unified theory, in which the total strain rate is decomposed into elastic and inelastic components. This model has been developed for structural analysis of nickel base superalloys Rene N4, as well as other SC materials. Because of the cubic symmetry these materials exhibit, elastic strains were calculated in the elastic regime using Hooke's law defined in Eq. (1.1) in Chapter I. The inelastic strains, however, were calculated by adding up the contributions of slip in each slip system. The inelastic slip rate on each slip system was computed from a local inelastic constitutive equation that depends on local resolved shear stress components in each slip direction, as well as local state variables. In both octahedral and cube slip systems, a functional form of the flow equation is similar to the exponential form developed by Bodner-Partom (1975) for isotropic materials. Dame and Stouffer's model was also based on a system of state

variables similar to the drag stress. Their model was considered successful for predicting both orientation dependence and tension/compression asymmetry for tensile and creep histories of single crystal alloy Rene N4 at 760°C. However, certain properties including cyclic response and inelastic recovery were not satisfactorily modeled. Also in the slip trace study, it is observed that the octahedral slip system is active for both tension and creep deformations, but the deformation mechanisms are different. For this reason, the model proposed by Dame (1985) has been coupled to two terms in order to characterize the effect of the dislocation network on both mechanisms.

$$\dot{\gamma}_{oct}^{\alpha\beta} = \left(\dot{\gamma}_{oct}^{\alpha\beta}\right)_1 + \left(\dot{\gamma}_{oct}^{\alpha\beta}\right)_2 \tag{2.3}$$

Where, $\dot{\gamma}^{\alpha\beta}$ is the uniform shear strain rate on the plane α, along the orientation β.

The first term is used to characterize the dislocation cutting of the γ' particles observed in the tensile test and the second is motivated by the interstitial emission and diffusion mechanism common in the creep test. The origin of this approach is clearly based on the physical motivation of two or more deformation mechanisms. The thrust of the unified strain measure is to eliminate the need to identify the coupling between the two mechanisms.

2.2.1 – Octahedral flow law

Because of a wide range of mechanical responses exhibited by SC nickel base super-alloys, Miner et al. (1986.a,b) and Dame (1985) have adopted two separate flow equations to compute the inelastic strain rate of the octahedral slip systems. In Eq.(2.3), the first term, which characterizes dislocation cutting of the γ' particles, is negligible during creep while the second term, which is motivated by interstitial emission and diffusion mechanisms, is negligible during high rate tensile tests. Both terms are active at intermediate values of stress or strain rate. One gets

$$\dot{z}^{\alpha\beta} = M_1\left(w_1 - z^{\alpha\beta}\right)\tau^{\alpha\beta}\dot{\gamma}^{\alpha\beta} \tag{2.7}$$

where M_1 and w_1 are material constants.

2.2.2 – Cube flow law

Cube slip occurs in specimens where the loading is near the $[\bar{1}\ 1\ 1]$ material direction and becomes increasingly important at high temperatures. Furthermore, Schmid's law is a good approximation for cube slip. Similar to the octahedral flow law, the cube flow law is also formulated with two terms such as,

$$\dot{\gamma}_{cub}^{\alpha\beta} = \left\{ D_1 \exp\left(-\left(\frac{z_3^{\alpha\beta}}{|\tau^{\alpha\beta}|} \right)^{n_3} \right) + D_2 \exp\left(-\left(\frac{z_2^{\alpha\beta}}{|\tau^{\alpha\beta}|} \right)^{n_4} \right) \right\} \frac{\tau^{\alpha\beta}}{|\tau^{\alpha\beta}|} \tag{2.8}$$

Once again the constants n_3 and n_4 reflect the strain rate sensitivity of the material in cube slip, and $z_3^{\alpha\beta}$ and $z_4^{\alpha\beta}$ are the state variables that include work hardening. The evolution equations that account for the work hardening are similar to that for octahedral slip defined in Eq.(2.5) and (2.6), except that the material parameters associated with the shear stress components $\tau_2^{\alpha\beta}$ and $\tau_3^{\alpha\beta}$, are excluded. These can be summarized as:

$$z_3^{\alpha\beta} = \phi_3 + z^{\alpha\beta} \tag{2.9}$$

and

$$z_4^{\alpha\beta} = \phi_4 + b z^{\alpha\beta} \tag{2.10}$$

In this case, the increase in flow resistance due to work hardening is given by

$$\dot{z}^{\alpha\beta} = M_3\left(w_3 - z^{\alpha\beta}\right)\tau^{\alpha\beta}\dot{\gamma}^{\alpha\beta} \tag{2.11}$$

Where $z^{\alpha\beta}(0)=\phi$ and w_3 and M_3 are determined from the high rate data. The parameters ϕ_3, ϕ_4 and b relate the hardening in the high rate and low rate responses for cube slip.

Some simple uniaxial tests such as the tensile, creep and cyclic tests have been simulated for Rene N4 VF317 at 760 °C by Dame (1985). Some of the predicted curves have been plotted and compared with experimental data at different orientations. See Figures (2.1), (2.2.a) and (2.2.b). From these results, the model was considered successful for predicting both orientation dependence and tension/compression asymmetry for tensile and creep histories for the single crystal alloy Rene N4 at 760°C. However certain properties, including cyclic response and inelastic recovery, were not satisfactorily modeled.

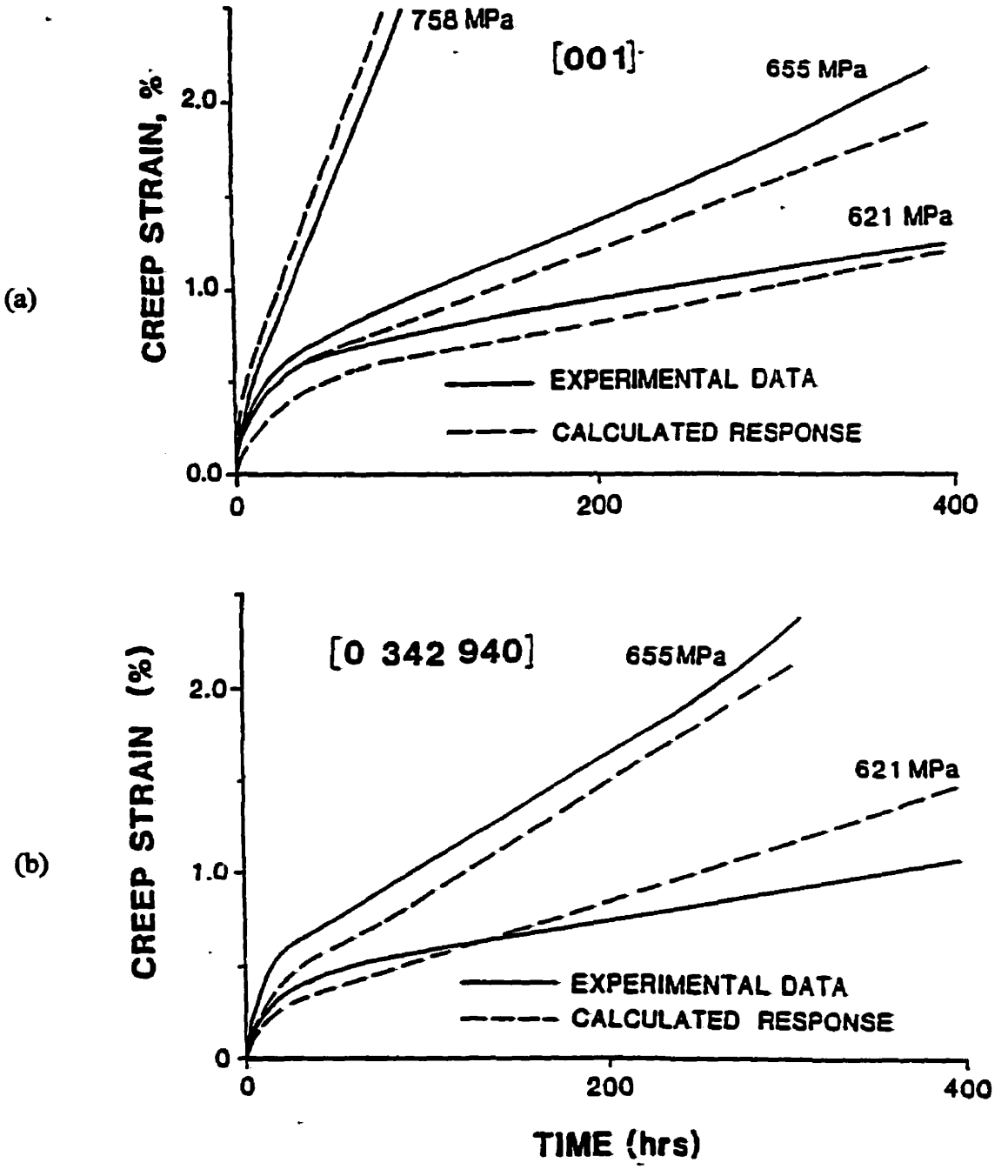

Figure 2.2 Creep responses for Rene N4 VF317 at 760° C loaded (a) in the [0 0 1] orientation, and (b) in the [0 342 940] orientation. From Dame (1985).

2.3 – THE CONTINUUM MECHANICS APPROACH

Since 1919, when Bingham and Green (1919) proposed the first one-dimensional theory for viscoplastic material behavior under simple shear, more than twenty viscoplastic constitutive theories have been proposed. These theories can be categorized into two groups, depending on whether or not a yield condition is employed:

- Theories that assume yield criteria, which separate purely elastic from combined elastic-viscoplastic deformations.
- Theories that assume no yield conditions and allow for the possible existence of elastic and viscoplastic deformations at all stages of loading.

Some of these theories are listed in two groups in Table 2.1, according to whether they assume the yield function or not. Whichever category is considered, however, their most common feature is that they solve viscoplastic problems at the macroscopic level.

2.3.1- Macroscopic viscoplastic formulation

Almost all of the viscoplastic theories presented in this section are isothermal and assume the material in its original form to be homogeneous and initially isotropic. In addition, the incompressibility and the normality of the inelastic response are assumed. A basic assumption of these theories is the decomposition of the rate of deformation tensor into elastic and inelastic components. This unified approach is more realistic when compared to the more traditional theories that decompose the inelastic strain into time-dependent creep and time-independent plastic components. Furthermore, it is supported by experimental data.

The structure of a viscoplastic theory is based on the establishment of:

- The yield condition (not used in every constitutive law), describing which stress state leads to further plastic strains.
- A flow law, giving the change of plastic strain from the stress and the internal state,
- Evolutionary equations, for describing the growth of the state variables, the values of which depend on the phenomena that the theory attempts to model.

In this section, the above three constituents of the theories will be presented, discussed and assessed for some models based on the two categories mentioned above. But, since Chaboche's viscoplastic theory is used in the **combined approach** proposed in this research, it will also be presented in more detail. The most significant particularity of the theories based on the continuum mechanics approach states that the actual deformation mechanisms for anisotropic materials (which include single crystal alloys) are not correlated to the theory. This lack of correlation limits the predictive capability of the model outside the range for which it was calibrated.

Table 2.1 – Evaluation of viscoplastic theories according to the yielding assumption.

Theories assuming the yield function	Theories without the yield function
• Perzyna (1963.a, 1966)	• Valanis (1971)
• Phillips and Wu (1973)	• Bodner and Partom (1975)
• Chaboche (1977)	• Hart (1976)
• Robinson (1978)	• Miller (1976)
• Lee and Zaverl (1978)	• Krieg (1975)
• Eisenberg and Yen (1981)	• Liu and Krempl (1979)
• Abdel-Kader (1986)	• Stouffer and Bodner(1979)
• Freed, Walker and Verrilli (1994)	• Walker (1981)
• Kurtyka and Zyezkowski (1996)	
• Wegener and Schlegel (1996)	

2.3.1.1- Yield function

The yield function is a mathematical form chosen to represent the initial and subsequent yield surface geometry in stress space. Since a yield surface is essentially an idealization that results in difficulties in multidimensional stress-strain application, there is great incentive to develop viscoplasticity theories that do not make use of this idealization. The yield surface separates the inelastic part of the deformation from the elastic part. The essential features of any viscoplasticity theory are that the inelastic deformations are rate-dependent and non-recoverable. These features must also be part of any viscoplastic theory that does not use a yield surface. Since a yield condition is absent in a viscoplasticity theory, both elastic and inelastic deformations can possibly occur during loading at every level of stress, however small. Because a yield condition does not exist, neither is a yield function required as part of the structure of the constitutive equation. In general, most continuum mechanics approaches are phenomenological. For most of the models in this category, assuming the yield function, anisotropy in the material is modeled by utilizing a fourth order tensor in the yield function and by exploiting the symmetric conditions known from the crystal geometry. For those without the benefit of a yield function, anisotropy is directly modeled by "internal or state variables", usually used to model the hardening/softening that occurs during plastic deformation. Two internal variables are widely used: These include the kinematic hardening (tensor) and the isotropic hardening (scalar). The kinematic hardening, also known as the back stress, accounts for the displacement of the yield surface, while the isotropic hardening (or the drag stress) accounts for the change in the yield surface size.

2.3.1.2- Flow law

The flow law establishes the relationship between the inelastic strain rate, $\dot{\varepsilon}^{I}$, with the stress tensor, σ , the absolute temperature, T, and the internal or state variables, α_k, such that, $\dot{\varepsilon}^{I} = f\left(\sigma, T, \alpha_k\right)$. According to the model, three main forms are commonly used to express the flow law. These include:

- the power law function,
- the exponential form, and

- The hyperbolic sine.

For the yield-based theories such as Chaboche's viscoplastic theory, the flow law is usually associated with the chosen yield function and has the general form

$$\dot{\varepsilon}^{i} = \Lambda \frac{\partial f}{\partial \sigma} \tag{2.12.a}$$

Where, σ , is the stress tensor, f, is the yield function defined in Eq.(2.12.b), and, Λ , is a non negative scalar function of f.

$$f = f\left(\sigma, T, \alpha_{k}\right) \tag{2.12.b}$$

In the stress space, Eq. (2.12.a) requires the inelastic strain rate "vector" to be normal to the loading surface; hence it is also called the normality condition. In Chaboche's theory, the yield function is specified explicitly by the Von Mises form. Conversely, the generalized Prandtl-Reuss flow law is adopted in the Bodner theory.

$$\dot{\varepsilon}^{i} = \mathfrak{I} : S \tag{2.12.c}$$

Where, $\mathfrak{I}$, is a fourth-order tensor that generally depends to the stress, temperature and state variables, and S is the deviatoric stress tensor.

In this theory, as well as in the Walker theory, the flow law is not associated with a yield condition; rather it is considered to represent a basic material equation in its own right. For isotropic hardening, Eq. (2.12.c) reduces to

$$\dot{\varepsilon}^{i} = \lambda S \tag{2.12.d}$$

Where $\lambda = \frac{\Lambda}{\Pi^{1/2}_{\sigma'-Y}}$ is a scalar function in this case, σ' is the deviatoric stress tensor, **Y** is the back stress tensor, and $\Pi_{\sigma'-Y}$ is a second invariant of σ'-**Y**.

In the Walker theory, the flow law is assumed to have the same form as that given in Eq.(2.12.a) which takes the following form in the deviatoric effective stress space.

$$\dot{e}^i = \Lambda \frac{(\sigma' - Y)}{\Pi^{1/2}_{(\sigma'-Y)}} \qquad (2.12.e)$$

2.3.1.3 – Evolutionary equations

The state variables account for different phenomena that take place in the sample during inelastic deformation. In most of the viscoplastic theories, two such variables are employed to model hardening: the scalar variable, R, models isotropic hardening while the second-order tensor, **Y**, describes anisotropic hardening and the associated Bauschinger effect.

Viscoplasticity theories do differ, however, in the functional forms assumed to represent the evolution of these variables. In spite of this, they all assume these variables to grow according to a hardening/recovery format. At large strain values, these state variables saturate to a limiting functional form which, in the Chaboche and Walker theories, are independent of strain rate at high rates of strain. In Bodner's theory, the limiting functional forms of R and **Y** depend on the strain rate even at high rates of strain.

a) – Isotropic hardening

In the Chaboche and Walker theories, the cumulative inelastic strain, p, defined in Eq.(2.13.a) is taken to measure isotropic hardening:

$$p = \int_0^t \left| \dot{e}^i \right| d\tau \qquad (2.13.a)$$

where $\left|\dot{\varepsilon}^{i}\right| = \sqrt{\sum_{k=1}^{6}\left(\dot{\varepsilon}_{k}^{i}\right)^{2}}$, is the magnitude of the inelastic strain rate $\dot{\varepsilon}^{i}$ and $\dot{\varepsilon}_{k}^{i}$ its components, defined in section 3.1.1.

Alternatively, the inelastic work w^{i}, defined in Eq. (2.13.b) is used in Bodner's theory.

$$w^{i} = \int_{0}^{t} \mathrm{tr}\left(\sigma . \dot{\varepsilon}^{i}\right) d\tau \qquad (2.13.b)$$

According to Bodner and Partom (1975), the cumulative inelastic strain rate, $\dot{p}$, is not a suitable parameter for measuring isotropic hardening since it does not reflect the influence of strain rate on the stress for sudden change in loading rate. They have shown that the use of w^{i} is better. On the contrary, Krempl and Kallianpur (1984) have concluded that the inelastic work accumulation is not a suitable parameter for modeling strain-hardening behavior of two steels and a Titanium alloy. Their results, cannot be generalized, however, since none of these materials exhibits a strong strain-rate history effect. Therefore, the use of p or w^{i} depends mainly on the material to be modeled as well as on the particular material behavioral facet of interest, such as shown by Abdel-Kader (1986). The general framework of the evolutionary equation for this variable assumes that, during inelastic deformation, isotropic hardening occurs under the action of two simultaneously competing mechanisms, a hardening process of deformation, and a softening (or recovery) process over time. The growth law of the isotropic stress is then the difference between the hardening rate and the softening rate. Now individual isotropic stress growth laws will be closely examined.

- <u>In Chaboche's theory</u>, the isotropic hardening growth law has the form

$$\dot{R} = B\left(Q - R\right)\dot{p} \qquad (2.14.a)$$

b) – Kinematic hardening

It is well known that plastic deformation induces additional anisotropy in the material. That feature, which takes place on a microscopic level during plastic deformation, is usually modeled by an internal variable, the so-called the kinematic or the back-stress hardening. The major effort in modeling the viscoplastic behavior of materials is therefore to determine the way state variables evolve with plastic deformation. Whereas minor differences are observed among the isotropic hardening evolutionary equations, considerable differences do exist in the kinematic hardening growth laws. Because of the directional nature of kinematic hardening and associated Bauschinger effect, a second-order tensor is usually used to model this phenomenon. In the case of isothermal conditions, the evolutionary equation of the kinematic hardening has the following forms:

- In Chaboche's theory,

$$\dot{\mathbf{Y}} = C\left(A\dot{\boldsymbol{\varepsilon}}^{i} - \mathbf{Y}\left|\,\dot{\varepsilon}^{i}\,\right|\right) - \chi\,\Pi_{Y}^{(m-1)/2}\,\mathbf{Y} \qquad (2.15.a)$$

The first term in Eq.(2.15.a) combines the hardening and dynamic recovery terms. The second term provides for modeling thermal (or static) recovery effects. At high strain rates, the latter term becomes insignificant in comparison with the dynamic recovery term, and the kinematic hardening stress becomes independent of strain rate and saturates to its limiting value.

- In Bodner, a new algorithm was proposed for modeling the kinematic hardening variable. Its evolutionary equation has the form,

$$\dot{\mathbf{Y}} = m_2\left(z_3\mathbf{u} - \mathbf{Y}\right)\dot{w}^{i} - A_2 z_1\left(\frac{\Pi_Y^{1/2}}{z_1}\right)^{r_2}\frac{\mathbf{Y}}{\Pi_Y^{1/2}} \qquad (2.15.b)$$

Where m_2, z_3, A_2, r_2, z_1 are material parameters, and $\mathbf{u}$ is the directional index for hardening assumed to be the current stress direction. Also, $\mathbf{u}$ is assumed to represent direction cosines of the inelastic strain rate.

$$\mathbf{u} = \frac{\sigma}{\mathrm{tr}(\sigma \bullet \sigma)} \qquad (2.15.c)$$

- In Walker's theory, the kinematic hardening stress expression has the form

$$\dot{\mathbf{Y}} = n_1 \dot{\boldsymbol{\varepsilon}}^i + \mathbf{Y}\left|\dot{\varepsilon}^i\right| - n_5 \Pi_{\mathbf{Y}}^{(m-1)/2} \mathbf{Y} - n_3 \exp\left[-n_4 \left|\log\left(\frac{\dot{p}}{\dot{p}_0}\right)\right|\right] \mathbf{I} \qquad (2.15.d)$$

where n_1, n_3, n_4, and n_5 are material parameters. It is different from Chaboche's law Eq.(2.15.a) in the last term which is added to model negative strain rate sensitivity effects associated with strain rate aging. Chaboche's form, however, represents the rate of translatory motion of the yield surface in stress space, whereas Walker's form lacks such visualization, since the theory dispenses with the notion of yield. With the emergence of so many theories, interest in comparative evaluations of them appears to be appropriate. Several comparisons have been made Cernocky (1982a, 1982b), Milly and Allen (1982), and James et al. (1987) that discuss some of the viscoplastic theories from the two categories mentioned previously. Specifically, Eftis et al. (1989) and Abdel-Kader et al. (1989), have presented theoretical and experimental comparative studies of the leading theories of Chaboche, Walker and Bodner. In these papers, the basic structures of these theories have been examined, their major advantages and limitations highlighted, and the principal similarities and differences among them explained. Also, the theories have been compared with experiments for elevated temperature application. In the two comparative studies mentioned above, the authors came to the same conclusions: the three theories are capable of modeling the main features of the inelastic behavior of Inconel 718 at 1200°F and 1100°F, respectively. Chaboche's theory however, seems to offer the greatest promise. In this regard, it has been retained for modeling the CA proposed in this work, and developed in Chapter III.

2.4 – CHABOCHE'S VISCOPLASTIC MODEL

The elastic/viscoplastic model proposed by Chaboche is an extension of Perzyna's theory, in that it adopts the same structure of that theory. However, Chaboche's theory has specific forms for the yield function, f, and the flow rule. In addition, specific rate equations governing isotropic and kinematic hardening during rate-dependent plastic deformation are introduced.

2.4.1- The multiaxial form of the model

Chaboche's theory models initially homogeneous, isotropic materials subjected to small, isothermal deformation with the plastic deformation taken to be incompressible.

2.4.1.1 – Yield function

The yield function is specified by von Mises's form, appropriately used to include isotropic and kinematic hardening.

$$F\left(\sigma', \mathbf{Y}', \hat{R}\right) = \Pi^{1/2}_{\sigma'-\mathbf{Y}'} - \hat{R}(p) \tag{2.16.a}$$

where,

- σ' and, $\mathbf{Y}'$ are respectively the total and kinematic deviatoric stress tensor,
- $\Pi_{\sigma'-\mathbf{Y}'}$ is the second invariant of the stress tensor, $(\sigma' - \mathbf{Y}')$, defined in Eq.(2.16.a). It denotes the difference between any point on the convex yield surface and the center of the yield surface.
- $\hat{R}(p)$, is the isotropic hardening variable assumed to be a scalar function of the accumulated inelastic strain, p, defined in Eqs.(2.16.b).

$$\Pi_{\sigma'-\mathbf{Y}'} = tr\left((\sigma' - \mathbf{Y}') \bullet (\sigma' - \mathbf{Y}')\right) \tag{2.16.b}$$

$$p = \int_0^{t_f} \left|\dot{\varepsilon}^i\right| d\tau = \int_0^{\varepsilon^i_f} d\left|\varepsilon^i\right| \tag{2.16.c}$$

2.4.1.2 – Flow law

Assuming that the normality condition is also applied for rate-dependent plasticity, the inelastic strain rate tensor, $\dot{\varepsilon}^{I}$, is normal to the convex yield surface, $f = 0$, and has the form

$$\dot{\varepsilon}^{I} = \Lambda \frac{\partial f}{\partial \sigma} = \Lambda \frac{(\sigma' - Y')}{\Pi^{1/2}_{\sigma' - Y'}} \tag{2.17.a}$$

Where, $\Lambda(\sigma', Y', \hat{R}) > 0$, is an arbitrary positive valued function. It is chosen to have the following functional form

$$\Lambda = \langle \varphi(f) \rangle^{n} = \begin{cases} \left(\frac{1}{K} f\right)^{n} & \text{for } f > 0 \\ 0 & \text{for } f \le 0 \end{cases} \tag{2.17.b}$$

Where K, and, n, are material constants. Combining Eqs. (2.17.a) and (2.17.b), the constitutive equation for viscoplastic strain rate has the explicit form,

$$\dot{\varepsilon}^{I} = \left[\frac{\Pi^{1/2}_{[\sigma' - Y']} - \hat{R}(p)}{K} \right]^{n} \frac{(\sigma' - Y')}{\Pi^{1/2}_{\sigma' - Y'}} \qquad \text{for} \quad f > 0, \tag{2.17.c}$$

2.4.1.3 – Evolutionary equations

Kinematic and isotropic hardening occur during the isothermal inelastic deformation and are described by postulated rate equations. For the kinematic hardening

$$\frac{dY'}{dt} = C\left(A\dot{\varepsilon}^{I} - Y' \left| \dot{\varepsilon}^{i} \right| \right) - \chi \, \Pi^{(m-1)/2}_{Y'} Y' \tag{2.18}$$

Where, A, C, m and χ are material parameters. The term with a bracket in Eq. (2.18) is the Armstrong-Frederick non-linear generalization of Prager's linear kinematic hardening rule. The first term inside the bracket models kinematic hardening under monotonic loading. The second term is introduced to model the effect of load reversals, which occur under cyclic loads. The combination of these two terms makes the modeling of the Bauschinger effect during cyclic loading possible. The last term allows recovery of the material to its original anisotropic state at high temperature. Chaboche introduces the isotropic hardening variable, $\hat{R}(p)$, that is assumed to be governed by the following rate equation

$$\frac{d\hat{R}}{dt} = B\left(Q - \hat{R}(p)\right)\left|\dot{\varepsilon}^{i}\right| \tag{2.19}$$

where, B and Q are additional material parameters. The constant Q represents the saturated value of $\hat{R}(p)$ for either isotropic hardening or softening. The basic equations of the Chaboche model can be summarized as follow:

$$\dot{\varepsilon} = \dot{\varepsilon}^{e} + \dot{\varepsilon}^{i} \tag{2.20.a}$$

$$\dot{\varepsilon}^{e} = \frac{1}{2\mu}\frac{\partial \dot{\sigma}'}{\partial t} + \frac{(1-2\nu)}{3E}\mathrm{tr}(\dot{\sigma})1 \tag{2.20.b}$$

$$\dot{\varepsilon}^{i} = \begin{cases} \left\langle \dfrac{\Pi^{1/2}_{(\sigma'-Y')} - \hat{R}}{K} \right\rangle^{n} \dfrac{(\sigma'-Y')}{\Pi^{1/2}_{(\sigma'-Y')}} & \text{if } f > 0 \\ 0 & \text{if } f \le 0 \end{cases} \tag{2.20.c}$$

Where

$$f = \Pi^{1/2}_{(\sigma'-Y')} - \hat{R} \tag{2.20.d}$$

$$p = \int_0^t \left| \dot{e}^i \right| d\tau \tag{2.20.e}$$

$$\frac{d\,Y'}{dt} = C\left(A\,\dot{e}^i - Y'\left|\,\dot{\varepsilon}^i\,\right|\right) - \chi\,\Pi_Y^{(m-1)/2}\,Y' \tag{2.20.f}$$

$$\frac{d\hat{R}}{dt} = B\left(Q-\hat{R}(p)\right)\left|\,\dot{\varepsilon}^i\,\right| = B\left(Q-\hat{R}(p)\right)\frac{dp}{dt} \tag{2.20.g}$$

The saturation value of, $\hat{R}(p)$, for either isotropic hardening or softening, may be seen from the solution of Eq.(2.19), and is given by the relation below as

$$\hat{R} = Q + \left(\hat{R}_0 - Q\right)e^{-Bp} \tag{2.21.a}$$

Examination of Eqs.(2.20)'s reveals several interesting properties of $\hat{R}(p)$. At the start of either monotonic or cyclic loading, the accumulated plastic strain, $p = 0$, and, $\hat{R}$, equals, $\hat{R}_0$, the initial yield stress. As cyclic loading proceeds, the magnitude of the accumulated plastic strain increases and ultimately $\hat{R}$ approaches Q the saturation value of $\hat{R}$. Mathematically Y' and $\hat{R}(p)$ represent, respectively, the center and the radius of the actually a cylinder centered on an axis parallel to the hydrostatic axis in stress space described by the relation $f = 0$ in the stress space. When the state of stress is within or on this hypersphere, only elastic deformation takes place. When the stress is outside the sphere, however, viscoplastic deformation commences. The total strain rate is composed of elastic and viscoplastic components. Beside elastic constants such as the Young modulus (E), the shear modulus (G), and the Poisson's ratio (ν), the basic equations above involve six additional material constants (A, B, C, K, Q, n) that have to be determined from monotonic and cyclic tests. Once these material constants are determined, Eqs.(2.20) completely characterize the elastic/viscoplastic response of the

material for general states of stress and loading. As mentioned previously, Inconel 718 has been satisfactorily modeled at 1200° F by this theory in Eftis et al. (1989).

It is better to mention that the capability of Chaboche's model is a fruit of a long process. A comparison in Table 2.2 of yield conditions and the inelastic strain rate expressions of the viscoplastic theories of Bingham, Hohenemser-Prager, Perzyna and Chaboche, reveals two points: the progressively more general, sophisticated and evolutionary nature of these constitutive equations and the essential similarity of their structure is apparent. All of these equations have the over stress characteristic. That is, viscoplastic deformation takes place only after the yield function, f, assumes positive values. In other words, in order for inelastic deformation to occur, the state of stress must lie outside the yield surface defined by $f = 0$. For the purpose of comparison, f in the Perzyna equation is shown to have a von Mises form with isotropic hardening only.

There are several important features that differentiate Chaboche's and Perzyna's theories:

- While anisotropic (kinematic) hardening is accounted for in principle, in Perzyna's theory no specific form is proposed. In Chaboche's theory, a non-linear kinematic hardening rule is specified which is suitable for modeling hardening under cyclic loading.
- Furthermore, Chaboche formulates his isotropic hardening rule in such a manner that it models effectively the stabilized cyclic hardening or softening behavior of most structural metals.
- Perzyna leaves the functional form of the yield function, f, arbitrary, to be selected on the basis of experiments. For the uniaxial case, several particular forms for f have been suggested that are capable of modeling high strain rate results. Chaboche, on the other hand proposes a particular form for f that applies for general states of stress.

Table 2.2 A comparative study of the yield stress and inelastic strain rate expressions for four distinct theories. From Chiu (1988).

Authors And Year	Yield condition	Strain-rate expressions
Bingham and Green (1919)	$\lvert\sigma_{12}\rvert > Y_s$	$\dot{\varepsilon}^i_{12} = \frac{1}{G}\langle f\rangle \lvert\sigma_{12}\rvert = \frac{1}{G}\left(1 - \frac{Y_s}{\lvert\sigma_{12}\rvert}\right)$
Hohenemser and Prager (1932)	$\Pi^{1/2}_{\sigma'} > 2K$	$\dot{\varepsilon}^i = \frac{1}{2G}\langle f\rangle \sigma' = \frac{1}{2G}\left(1 - \frac{\sqrt{2}\,K}{\Pi^{1/2}_{\sigma'}}\right)\sigma'$
Perzyna (1963.a,b)	$\Pi^{1/2}_{\sigma'} > R(w^i)$	$\dot{\varepsilon}^i = \alpha\langle\,\phi(f)\rangle\frac{\partial f}{\partial \sigma'} = \alpha\phi\left(\frac{\Pi^{1/2}_{\sigma'}}{R(w^i)} - 1\right)\frac{\sigma'}{\Pi^{1/2}_{\sigma'}}$
Chaboche (1977)	$\Pi^{1/2}_{(\sigma'-Y')} > R(p)$	$\dot{\varepsilon}^i = \langle\,\phi(f)\rangle\frac{\partial f}{\partial \sigma'} = \left(\frac{\Pi^{1/2}_{(\sigma'-Y')} - \hat{R}(p)}{K}\right)^n \frac{(\sigma' - Y')}{\Pi^{1/2}_{(\sigma'-Y')}}$

2.4.2- The uniaxial form of the model

2.4.2.1 – Basic equations

The multidimensional form of the Chaboche's model presented earlier in this chapter involves three elastic constants (E, G, ν), and eight material constants (A, B, C, K, n, Q, m, Λ), in order to completely characterize the elastic/viscoplastic response of the material for the general states of stress and loading. Given that the determination of these material parameters requires judicious assumptions and experimental data for some simple tests, the uniaxial form of the model is therefore useful. The remaining section deals with the reduction of the 3D form of the basic equations into a one-dimensional form. The physical significance of the initial value of the drag stress R_0, is also evaluated.

Let us set a stress tensor at a given point of the sample to be

$$[\sigma]=\begin{bmatrix} \sigma_{11} & \sigma_{12} & \sigma_{13} \\ \sigma_{21} & \sigma_{22} & \sigma_{23} \\ \sigma_{31} & \sigma_{32} & \sigma_{33} \end{bmatrix}, \tag{2.22.a}$$

Under uniaxial loading along the third direction, the multidimensional stress can be reduced as follow:

$$\begin{aligned} &\sigma_{33}=\sigma; \quad \sigma_{22}=\sigma_{11}=0 \\ &\sigma_{12}=\sigma_{21}=\sigma_{23}=\sigma_{32}=\sigma_{13}=\sigma_{31}=0 \end{aligned} \tag{2.22.b}$$

That corresponds to

$$[\sigma]=\begin{bmatrix} 0 & 0 & 0 \\ 0 & 0 & 0 \\ 0 & 0 & \sigma \end{bmatrix}, \tag{2.22.c}$$

The corresponding deviatoric stress tensor may be expressed as

$$[\sigma'] = [\sigma] - \frac{1}{3} I_{[\sigma]} [1]$$
$$= \frac{\sigma}{3} \begin{bmatrix} -1 & 0 & 0 \\ 0 & -1 & 0 \\ 0 & 0 & 2 \end{bmatrix} \tag{2.22.d}$$

And similarly, the deviatoric back stress tensor may be expressed as

$$[Y'] = \frac{Y}{3} \begin{bmatrix} -1 & 0 & 0 \\ 0 & -1 & 0 \\ 0 & 0 & 2 \end{bmatrix} \tag{2.22.e}$$

Using the above quantities, the square root of the second invariant of the deviatoric stress tensor reduces to

$$\Pi^{1/2}_{[\sigma']} = \left[\mathrm{tr}\left([\sigma'] \cdot [\sigma'] \right) \right]^{1/2} = \left[\sigma'_{ik} \sigma'_{ki} \right]^{1/2}$$
$$= \sqrt{\frac{2}{3}} \, |\sigma| \tag{2.23.a}$$

Similarly

$$\Pi^{1/2}_{[Y']} = \sqrt{\frac{2}{3}} \, |Y| \tag{2.23.b}$$

And finally

$$\Pi^{1/2}_{[\sigma'-Y']} = \sqrt{\frac{2}{3}} \, |\sigma - Y| \tag{2.23.c}$$

Elastic strains are

$$\begin{aligned} \varepsilon_{11}^{e} &= \varepsilon_{22}^{e} = \nu\, \varepsilon_{33}^{e} = -\nu\, \varepsilon^{e} \\ \varepsilon_{33}^{e} &= \varepsilon^{e} \\ \varepsilon_{12}^{e} &= \varepsilon_{13}^{e} = \varepsilon_{23}^{e} = 0 \end{aligned} \tag{2.24.a}$$

That becomes, in the matrix form,

$$\left[\varepsilon^{e}\right] = \varepsilon^{e} \begin{bmatrix} -\nu & 0 & 0 \\ 0 & -\nu & 0 \\ 0 & 0 & 1 \end{bmatrix} \tag{2.24.b}$$

In the inelastic strains, imposing the condition of incompressibility of plastic deformation, i.e. $\varepsilon^{i} = \varepsilon^{i\prime}$, one gets

$$I_{[\varepsilon^{i}]} = \varepsilon_{11}^{i} + \varepsilon_{22}^{i} + \varepsilon_{33}^{i} = 0 \tag{2.25.a}$$

$$\varepsilon_{22}^{i} + \varepsilon_{11}^{i} = -\varepsilon_{33}^{i} \tag{2.25.b}$$

Also from loading symmetry

$$\varepsilon_{22}^{i} = \varepsilon_{11}^{i} \tag{2.25.c}$$

therefore,

$$\varepsilon_{22}^{i} = \varepsilon_{11}^{i} = -\frac{1}{2}\varepsilon_{33}^{i} = -\frac{1}{2}\varepsilon^{i} \tag{2.25.d}$$

In the matrix form, the inelastic strain tensor may be expressed as

$$\left[\varepsilon^{i}\right]=\frac{\varepsilon^{i}}{2}\begin{bmatrix}-1 & 0 & 0\\ 0 & -1 & 0\\ 0 & 0 & 2\end{bmatrix} \tag{2.25.e}$$

The accumulated inelastic strain rate becomes

$$p=\int_{0}^{t}\left|\dot{\varepsilon}^{i}\right| d\tau \tag{2.25.f}$$

In addition to the above reductions, the following quantities are defined:

$$a=\frac{3}{2}A \tag{2.26a}$$

$$b=B \tag{2.26.b}$$

$$c=C \tag{2.26.c}$$

$$k=\left(\frac{3}{2}\right)^{\frac{(1+n)}{2n}}K \tag{2.26.d}$$

$$q=\sqrt{\frac{3}{2}}Q \tag{2.26.e}$$

and,

$$R(p)=\sqrt{\frac{3}{2}}\hat{R}(p) \tag{2.26.f}$$

Using these relations in equations (2.20), Chaboche's multidimensional isothermal stress-strain basic equations are reduced in the one-dimensional form to:

$$\dot{\varepsilon} = \dot{\varepsilon}^e + \dot{\varepsilon}^i \tag{2.27.a}$$

$$\dot{\varepsilon}^e = \frac{\dot{\sigma}}{E} \tag{2.27.b}$$

$$\dot{\varepsilon}^i = \begin{cases} \left\langle \dfrac{|\sigma - Y| - \hat{R}}{k} \right\rangle^n \operatorname{sgn}(\sigma - Y) & \text{for } f > 0 \\ 0 & \text{for } f \le 0 \end{cases} \tag{2.27.c}$$

$$f = |\sigma - Y| - R \tag{2.27.d}$$

$$\frac{dY}{dt} = c\left(a\,\dot{\varepsilon}^i - Y\,|\dot{\varepsilon}^i|\right) - \lambda\,|Y|^m \operatorname{sgn}(Y) \tag{2.27.e}$$

$$\frac{d\hat{R}}{dt} = b\left(q - R(p)\right)|\dot{\varepsilon}^i| \tag{2.27.f}$$

$$\operatorname{sgn}(\sigma - Y) = \frac{(\sigma - Y)}{|\sigma - Y|} = \pm 1 \tag{2.27.g}$$

where n, k, c, a, b, q , λ and m are the viscoplastic material constants.

In addition to the elastic constants, Chaboche's uniaxial theory is characterized by 8 more parameters. Each of these parameters plays a unique role in modeling viscoplastic response of materials. Their functions are discussed in more detail in Chiu (1988) and in Abdel-Kader (1986). The rest of the present Chapter examines the initial value of R_0.

2.4.2.2- Initial yielding (R_0)

Under uniaxial cyclic loading at constant strain rate magnitude, the rate equations (2.27.e) and (2.27.f) for the kinematic and isotropic hardening variables, Y and R, respectively, can be integrated directly giving

$$Y = a - (a - Y_0)\exp\left[-c\left(\varepsilon^i - \varepsilon_0{}^i\right)\right] \tag{2.28.a}$$

During tensile loading, and

$$Y = -a + \left(a + \overline{Y}_0\right)\exp\left[c\left(\varepsilon^i - \overline{\varepsilon}_0{}^i\right)\right] \tag{2.28.b}$$

During compressive loading, where $(Y_0, \varepsilon_0{}^i)$ and $(\overline{Y}_0, \overline{\varepsilon}_0{}^i)$ represent the initial values of Y and ε^i at the start of a tensile or compressive and reversal respectively. Similarly, for the isotropic hardening variable R,

$$R = q + (R_0 - q)\exp[-b\,p] \tag{2.29.a}$$

where R_0 is another material constant to be determined from experiments. Solving Eq. (2.27.c) for stress gives,

$$\sigma = Y + R + k\left(\dot{\varepsilon}^i\right)^{1/n} \tag{2.29.b}$$

The physical significance of the material constant R_0 has been demonstrated in Sheh (1988) as the initial uniaxial yield stress of the material when time-dependent deformation commences. In the original form of the Chaboche's model, R_0 was constant. This fact restricts all the non-linear portions of the uniaxial stress-strain curves obtained at different loading rates to initiate at one common point. In order to account for the strain rate dependence of the initial yield stress, several formulations have been proposed. Among these formulations, the one proposed by Abdel-Kader (1986), obtained by regression, seems to offer the greatest promise in this regard. R_0 is given by the relation,

$$R_0(\dot{\varepsilon}_0) = R_{00}\left[1 + \ln\left(1 + \exp\left(\sum_{k=0}^{n} \beta_k (\ln(\dot{\varepsilon}_0))^k\right)\right)\right] \qquad (2.29.c)$$

where R_{00} represents the yield stress at zero strain rate, β_k are the non-linear regression coefficients, and $\dot{\varepsilon}_0$ is a given strain rate.

For the case of Inconel 718 at 1200° F used by the author, the predictive capabilities of the model were simulated and compared with experimental data for: the stress-strain tensile response (Figure 2.3), the fully reversed cyclic response (Figure 2.4), and the creep response (Figure 2.5). In addition, a regression formulation of the initial yield strength $R_0(\dot{\varepsilon})$, was simulated from Eq.(2.29.c) for n = 5, and compared with experimental data in Figure 2.6. In that case, R_{00} was taken to be equal to 50 KSI, and the coefficients β_k used were defined in Table 2.3.

Table 2.3 – The non-linear regression coefficients values for n = 5.

β_0	β_1	β_2	β_3	β_4	β_5
48.88	18.30	2.77	0.208	0.783e-2	0.117e-3

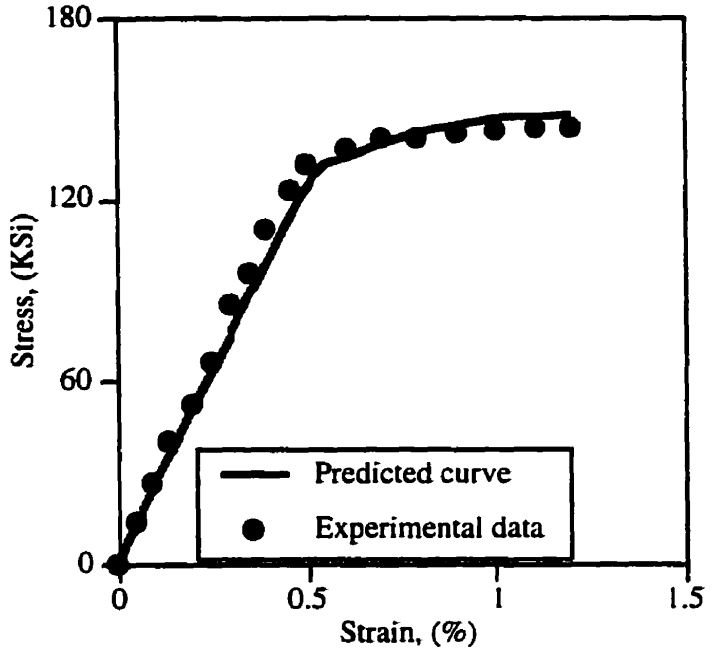

Figure 2.3 Comparison between experimental and predicted tensile stress-strain curves for Inconel 718 at 1200° F, and at $\dot{\varepsilon}$ = 1.333e-5/s. Eftis et al. (1989)

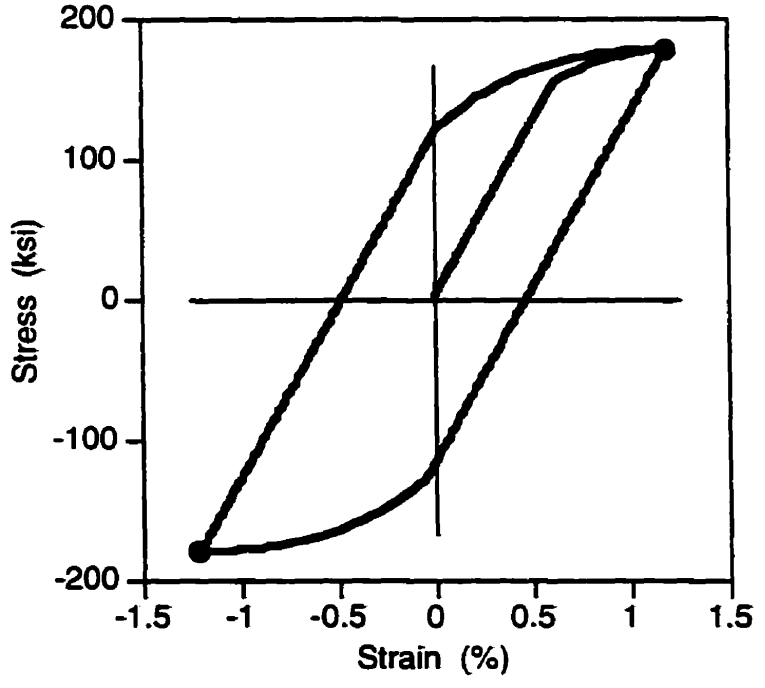

Figure 2.4 Experimental and predicted strain controlled fully reversed cyclic behavior for Inconel 718 at 1200° F at strain rate $\dot{\varepsilon}$ = 4e-5/s, and strain range $\Delta\varepsilon \cong 2\%$. Eftis et al. (1989).

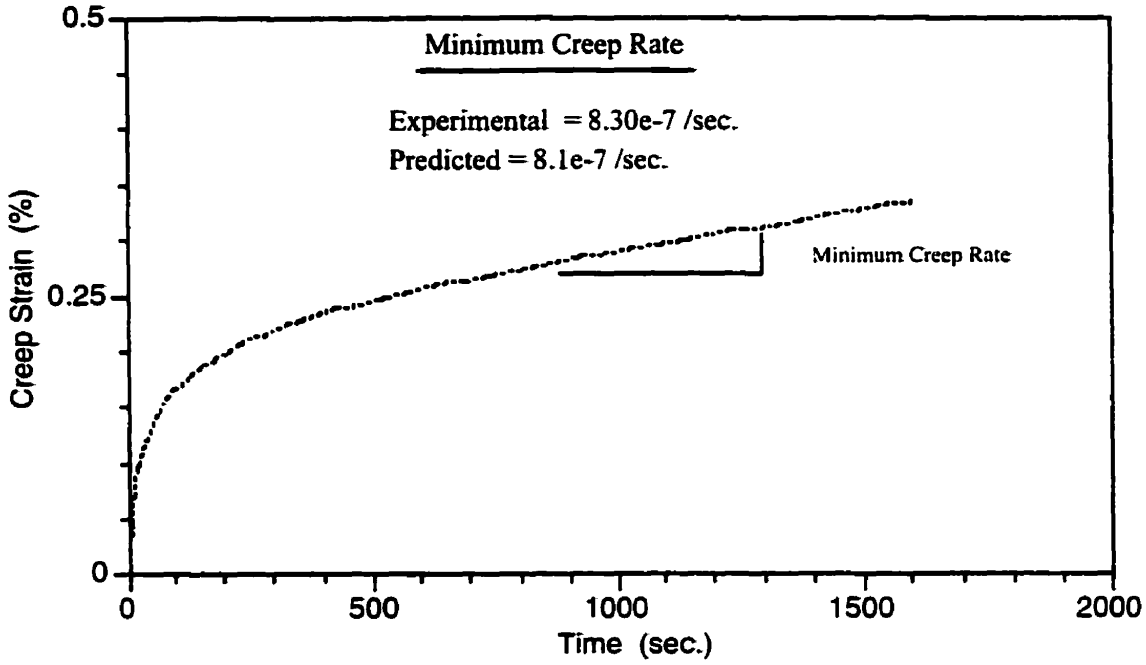

Figure 2.5 Primary and secondary creep test for Inconel 718 at 1200° F. From Eftis et al. (1989).

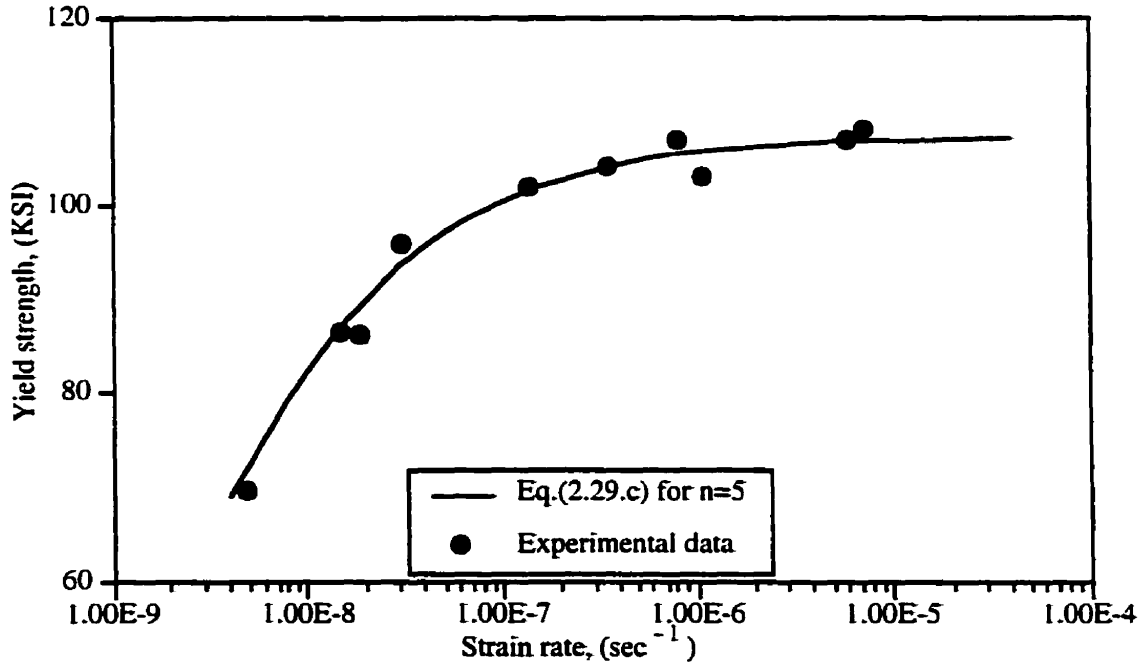

Figure 2.6 Comparison of the analytical expression of R_0 ($\dot{\varepsilon}$) with experimental data of Beaman (1984) for Inconel 718 at 1200° F. From Abdel-Kader (1986).

CHAPTER III

DEVELOPMENT OF THE CONSTITUTIVE THEORY

The purpose of this study is to develop a new tool for SC materials analysis, such as nickel base superalloys. The phenomenological model proposed in this work, combines in a certain way both macroscopic and micro-mechanical approaches presented in Chapter II. For that reason, it is called the **"combined approach"** (CA). Its principle consists of extending predictive models of isotropic material behavior to anisotropic materials such as SC nickel base superalloys. Its structure is based on the establishment of two main elements:

- a viscoplastic model, that assumes a yield function, and
- a slip factor that accounts for the micro-mechanical slip effect occurring within the crystal during the deformation process.

This chapter emphasizes the development of the combined approach theory, as well as the orientation dependence of the initial yielding (σ_y) and elastic constants such as: Young's modulus (E), shear modulus (G) and Poisson's ratio (v). The knowledge of these features is important for a good estimation and a comprehensive account of the mechanical response and mechanisms of inelastic deformation in components, such as turbine blades under service conditions. Also, emphasized are the temperature dependence of elastic constants and the initial yielding behavior of these materials. The

application of the combined approach to Chaboche's model[1] is elaborated on in the next chapter. In order to describe the common misalignment observed in the SC materials between the global coordinate system and the crystallographic coordinate system, three coordinate systems, similar to those used by Jordan and Walker (1992) have been used.

3.1 – Definitions

3.1.1 - Stress and strain vectors

Let $\{\sigma\}$ and $\{\varepsilon\}$ be respectively a 6x1 stress and strain vectors in the global co-ordinate system with components, σ_i, and, ε_i. Using the Voigt notation, the stress and strain components may be defined as:

$$\{\sigma\}^t = \{\sigma_1=\sigma_{11}, \sigma_2=\sigma_{22}, \sigma_3=\sigma_{33}, \sigma_4=\sigma_{23}, \sigma_5=\sigma_{13}, \sigma_6=\sigma_{12}\} \tag{3.1.a}$$

$$\{\varepsilon\}^t = \{\varepsilon_1=\varepsilon_{11}, \varepsilon_2=\varepsilon_{22}, \varepsilon_3=\varepsilon_{33}, \varepsilon_4=2\varepsilon_{23}, \varepsilon_5=2\varepsilon_{13}, \varepsilon_6=2\varepsilon_{12}\} \tag{3.1.b}$$

They may be expressed in the shorthand form as follows:

$$\{\sigma\} = \sigma\{\mathbf{e}\} \tag{3.1.c}$$

$$\{\varepsilon\} = \varepsilon\{\mathbf{v}\} \tag{3.1.d}$$

where

- $\sigma = \|\sigma\| = \sqrt{\sum_{i=1}^{6}(\sigma_i)^2}$, and, $\varepsilon = \|\varepsilon\| = \sqrt{\sum_{i=1}^{6}(\varepsilon_i)^2}$, are their magnitudes, and
- $\{\mathbf{e}\} = \frac{\{\sigma\}}{\|\sigma\|}$, and $\{\mathbf{v}\} = \frac{\{\varepsilon\}}{\|\varepsilon\|}$, are respectively their cosine directors.

Recall that, the symbol $\|\ \|$ is used to designate the norm of a vector.

[1] A unified viscoplastic model used for the purpose of the present work.

In the same way, the back stress may be expressed in the short hand form as

$$\{\mathbf{Y}\} = Y\{\mathbf{e}\} \tag{3.1.e}$$

where

- $Y = \|\mathbf{Y}\|$, and $\{\mathbf{e}\} = \dfrac{\{\mathbf{Y}\}}{\|\mathbf{Y}\|}$ are respectively its magnitude and its cosine director.

3.1.2 – Deviatoric Stress vector

The deviatoric stress, $\{\sigma'\}$ of the stress vector $\{\sigma\}$ has the form:

$$\{\sigma'\} = [N_0]\{\sigma\} = \sigma[N_0]\{\mathbf{e}\} \tag{3.2.a}$$

where

$$[N_0] = \begin{bmatrix} \frac{2}{3} & -\frac{1}{3} & -\frac{1}{3} & 0 & 0 & 0 \\ -\frac{1}{3} & \frac{2}{3} & -\frac{1}{3} & 0 & 0 & 0 \\ -\frac{1}{3} & -\frac{1}{3} & \frac{2}{3} & 0 & 0 & 0 \\ 0 & 0 & 0 & 1 & 0 & 0 \\ 0 & 0 & 0 & 0 & 1 & 0 \\ 0 & 0 & 0 & 0 & 0 & 1 \end{bmatrix} \tag{3.2.b}$$

3.1.3 – Maximum and minimum of the stress vector

Let $\{\mathbf{X}\}$ be a vector represented in the six dimensional space as

$$\{\mathbf{X}\}^t = \{x_1, x_2, x_3, x_4, x_5, x_6\} \tag{3.3.a}$$

where x_i are its components. In the present work, the maximum of the vector $\{\mathbf{X}\}$, denoted by $\max(\{\mathbf{X}\})$ is defined as follows

$$\max(|X|) = \max(|x_1|, |x_2|, |x_3|, |x_4|, |x_5|, |x_6|) \tag{3.3.b}$$

while, its minimum denoted as $\min(|X|)$ is defined as

$$\min(|X|) = \min(|x_1|, |x_2|, |x_3|, |x_4|, |x_5|, |x_6|) \tag{3.3.c}$$

3.1.4 – Stress-strain relationship

Because of the face-centered-cubic (f.c.c) structure of single crystal (SC) nickel base superalloys, the properties along each of the crystallographic or principal axes are assumed to be identical. Symmetry is then observed in its elastic properties along the principal axes. The generalized Hooke's law equation can be expressed in 3D in the shorthand notation below:

$$\{\sigma\} = [D]\{\varepsilon\} \tag{3.3.d}$$

Where, $\{\sigma\}$ and $\{\varepsilon\}$ are respectively the 6x1 stress and strain vectors, and [D] is the 6x6 elasticity or stiffness matrix, defined in Eq.(1.2). This form of the elasticity matrix [D], has been defined by Leknitskii (1962), and it has been used by a number of authors such as Nissley and Meyer (1992.a), Anderson et al. (1994) and, Kundel and Kollman (1996). As explained in Swanson et al. (1986), the stiffness components, D_{ij}, are usually measured by the ultrasonic wave velocity at different temperatures. In this work, the D_{ij} values used for Rene N4 as well as for Rene N4 VF317 are those for the SC nickel base superalloys PWA 1480, taken at the temperature of interest as shown in Table 3.1. Since the chemical composition of Rene N4 and PWA 1480 are very similar, their mechanical properties are also similar and therefore that assumption is realistic.

Table 3.1 Dynamic elastic constants and apparent modulus for a uniaxial bar in PWA 1480 along four orientations. From Nisley and Mayer (1992.a)

Temp. (°C)	Dynamic Elastic Constants (GPa)			Apparent Modulus (GPa)			
	D_{11}	D_{12}	D_{44}	[001]	[011]	[213]	$[\bar{1}11]$
0	251.72	162.75	131.03	124.13	229.65	229.65	320.00
37.77	250.34	162.75	128.96	122.06	226.20	226.20	316.55
93.32	248.27	161.37	127.58	121.37	224.13	224.13	313.10
148.87	246.20	160.00	126.20	120.00	222.06	222.06	308.96
204.42	244.13	159.31	124.13	118.62	219.31	219.31	305.51
259.97	242.06	157.93	122.75	117.24	216.55	216.55	301.37
315.52	240.00	157.24	120.69	115.17	213.10	213.10	299.34
371.07	237.93	156.55	118.62	113.10	209.65	209.65	293.10
426.62	235.17	155.86	116.55	111.03	206.20	206.20	288.96
482.17	233.10	154.48	114.48	109.65	203.44	203.44	284.13
537.72	230.34	153.79	113.10	107.58	200.00	200.00	280.00
593.27	227.58	152.41	111.03	105.51	195.86	195.86	275.17
648.82	225.51	151.72	108.96	103.44	192.41	192.41	271.03
704.37	222.75	151.03	106.89	100.69	188.27	188.27	266.20
759.92	219.31	150.34	104.82	97.93	184.13	184.13	261.37
815.47	216.55	149.65	102.06	94.48	179.31	179.31	256.55
871.02	213.10	148.96	100.00	91.03	174.48	174.48	251.03
926.57	209.65	147.58	97.24	87.58	169.65	169.65	245.51
982.12	206.20	146.20	94.48	84.13	163.44	163.44	238.62
1032.6	201.37	144.82	91.72	80.00	157.24	157.24	231.72
1093.2	196.55	143.44	88.27	75.17	150.34	150.34	224.13
1148.7	191.72	142.75	84.82	69.65	141.37	141.37	215.86
1204.3	186.20	142.06	81.37	63.44	132.41	132.41	207.58

Shadow rows correspond to the three temperatures used in this work.

3.1.5 – Coordinate Systems

The stress-strain relationship given by the Hooke's law in Eq.(3.3.d) requires that the stress-strain coordinate system (the geometric or global coordinate system) be aligned with the principal material directions (or the crystallographic coordinate system) shown in Figure 3.1. However, the principal directions of orthotropy often do not coincide with coordinate directions that are geometrically natural to the solution of the problem. When this occurs, material orientation relative to system axes is specified with Euler's angles, as presented in Figure 3.3. In order to describe the proposed model, three co-ordinate systems and their associated unit basis vectors are defined as follows.

3.1.5.1 – The global coordinate system

In general, the global coordinate system is located such that one axis coincides with the specimen axis in the turbine blade or test specimen axis (see Figure 3.1). Its axes are **x** , **y** , **z** with unit vectors **i** , **j** and **k**. It is also in that coordinate system that the applied loads are usually defined.

3.1.5.2 – The crystallographic coordinate system

It is convenient to locate the crystallographic coordinate system with axes aligned along the edges of a unit cell in the f.c.c structure. That coordinate system will be referred to as the **x***, **y***, **z*** system with unit vectors **i***, **j*** and **k***. This coordinate system is also convenient to define physical properties and the constitutive laws for anisotropic materials.

3.1.5.3 – The local coordinate system

Since the plastic deformation occurs by slip on certain crystallographic planes in certain crystallographic directions, the third coordinate system is defined such that the constitutive behavior of individual slip systems may be defined (see Figure 3.2). The associated unit vectors that define the basis of this system are: the unit vector { **n** }, normal to the slip plane, the unit vector { **s** }, oriented along the slip direction and finally

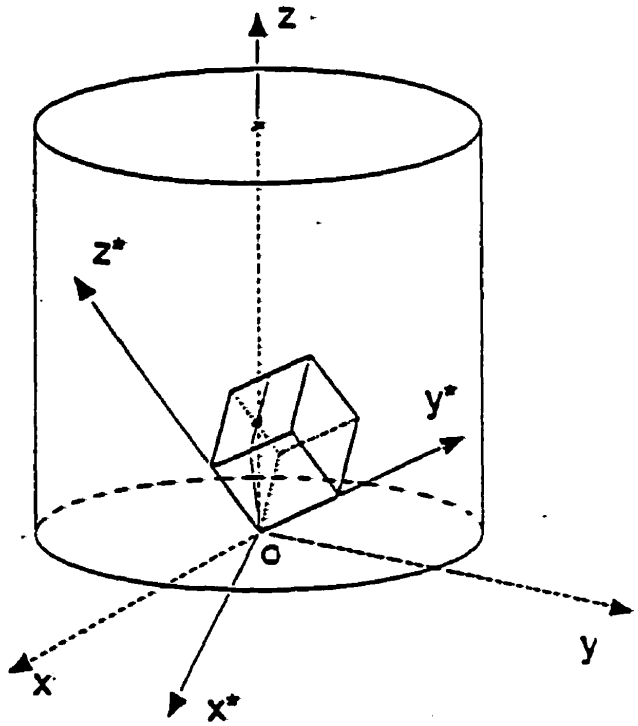

Figure 3.1 Relationship between the global and the crystallographic co-ordinate systems

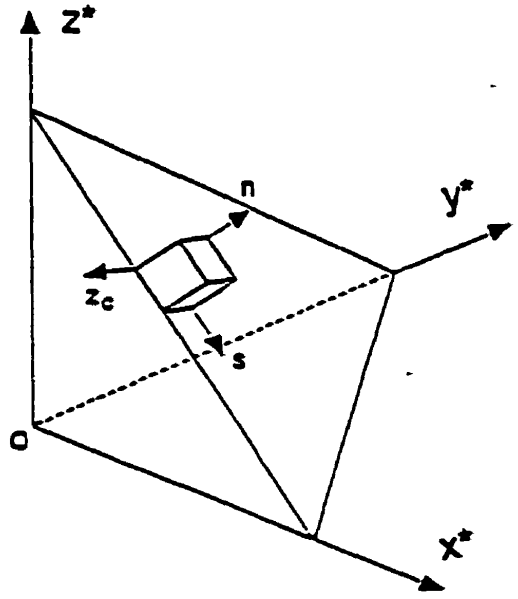

Figure 3.2 Local slip system, referred to the crystallographic system.

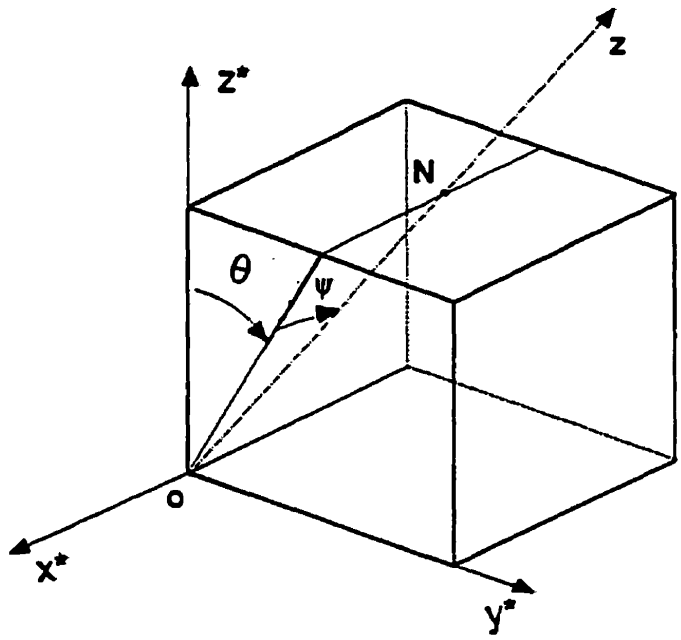

Figure 3.3 Definition of the Eulerian angles θ and ψ in the single crystal bar oriented along ON, with respect to the crystal axes x*, y*, z*.

the third unit vector, defined as $\{ z_c \} = \{ s \} \times \{ n \}$. A more detailed study of the octahedral and cube slip plane and their corresponding slip directions is done in Appendix A.

3.1.6 - Stress and strain transformations

The position of the new system, x , y , z with respect to the first system , x*, y* and z*, is given by the relation

$$\begin{Bmatrix} x^* \\ y^* \\ z^* \end{Bmatrix} = \begin{bmatrix} \alpha_1 & \beta_1 & \gamma_1 \\ \alpha_2 & \beta_2 & \gamma_2 \\ \alpha_3 & \beta_3 & \gamma_3 \end{bmatrix} \begin{Bmatrix} x \\ y \\ z \end{Bmatrix} \qquad (3.4.a)$$

Where α_i , β_i , γ_i (for i = 1, 2 or 3) are the cosines director function of the Euler's

angles shown in Figure (3.3), and defined as follows

$$\begin{aligned} \alpha_1 &= \cos(\psi) \quad ; \quad \alpha_2 = 0 \quad ; \quad \alpha_3 = -\sin(\psi) \\ \beta_1 &= \sin(\psi)\sin(\theta) \; ; \quad \beta_2 = \cos(\theta) \; ; \quad \beta_3 = \cos(\psi)\sin(\theta) \\ \gamma_1 &= \sin(\psi)\cos(\theta) \; ; \quad \gamma_2 = -\sin(\theta) \; ; \quad \gamma_3 = \cos(\psi)\cos(\theta) \end{aligned} \tag{3.4.b}$$

Knowing the stress or strain in one of the previous coordinate systems above it is therefore possible to express each of them (stress or strain) in the other coordinate systems. In Anderson et al. (1994), it is explained in more detail the way to transform stress and strain matrices from one coordinate system to another. Depending upon the form in which stresses and strains are written, different forms of the transformation matrices can be found. For example, when stresses and strains are written as 6×1 vector (form used in the present work), they are transformed by an orthogonal 6×6 rotation matrix which rotates the crystallographic axes into the global axes as shown in Figure 3.1. In the vector notation, the stress tensor, $\{\sigma\}$, and the strain tensor, $\{\varepsilon\}$, in the crystallographic system are related to stress tensor, $\{\sigma^*\}$, and the strain tensor, $\{\varepsilon^*\}$, in the global coordinate system, with the following transformation relations:

$$\{\sigma^*\} = [Q_\sigma]\{\sigma\} \tag{3.5.a}$$

$$\{\varepsilon^*\} = [Q_\varepsilon]\{\varepsilon\} \tag{3.5.b}$$

where $[Q_\sigma]$, and $[Q_\varepsilon]$ are orthogonal matrices defined in Eqs.(3.5.c) and (3.5.d) respectively.

$$[Q_c]=\begin{bmatrix} \alpha_1^2 & \alpha_2^2 & \alpha_3^2 & 2\alpha_2\alpha_3 & 2\alpha_3\alpha_1 & 2\alpha_1\alpha_2 \\ \beta_1^2 & \beta_2^2 & \beta_3^2 & 2\beta_2\beta_3 & 2\beta_3\beta_1 & 2\beta_1\beta_2 \\ \gamma_1^2 & \gamma_2^2 & \gamma_3^2 & 2\gamma_2\gamma_3 & 2\gamma_3\gamma_1 & 2\gamma_1\gamma_2 \\ \beta_1\gamma_1 & \beta_2\gamma_2 & \beta_3\gamma_3 & (\beta_2\gamma_3+\beta_3\gamma_2) & (\beta_1\gamma_3+\beta_3\gamma_1) & (\beta_1\gamma_2+\beta_2\gamma_1) \\ \gamma_1\alpha_1 & \gamma_2\alpha_2 & \gamma_3\alpha_3 & (\gamma_2\alpha_3+\gamma_3\alpha_2) & (\gamma_1\alpha_3+\gamma_3\alpha_1) & (\gamma_1\alpha_2+\gamma_2\alpha_1) \\ \alpha_1\beta_1 & \alpha_2\beta_2 & \alpha_3\beta_3 & (\alpha_2\beta_3+\alpha_3\beta_2) & (\alpha_1\beta_3+\alpha_3\beta_1) & (\alpha_1\beta_2+\alpha_2\beta_1) \end{bmatrix} \quad (3.5.c)$$

and,

$$[Q_d]=\begin{bmatrix} \alpha_1^2 & \alpha_2^2 & \alpha_3^2 & \alpha_2\alpha_3 & \alpha_3\alpha_1 & \alpha_1\alpha_2 \\ \beta_1^2 & \beta_2^2 & \beta_3^2 & \beta_2\beta_3 & \beta_3\beta_1 & \beta_1\beta_2 \\ \gamma_1^2 & \gamma_2^2 & \gamma_3^2 & \gamma_2\gamma_3 & \gamma_3\gamma_1 & \gamma_1\gamma_2 \\ 2\beta_1\gamma_1 & 2\beta_2\gamma_2 & 2\beta_3\gamma_3 & (\beta_2\gamma_3+\beta_3\gamma_2) & (\beta_1\gamma_3+\beta_3\gamma_1) & (\beta_1\gamma_2+\beta_2\gamma_1) \\ 2\gamma_1\alpha_1 & 2\gamma_2\alpha_2 & 2\gamma_3\alpha_3 & (\gamma_2\alpha_3+\gamma_3\alpha_2) & (\gamma_1\alpha_3+\gamma_3\alpha_1) & (\gamma_1\alpha_2+\gamma_2\alpha_1) \\ 2\alpha_1\beta_1 & 2\alpha_2\beta_2 & 2\alpha_3\beta_3 & (\alpha_2\beta_3+\alpha_3\beta_2) & (\alpha_1\beta_3+\alpha_3\beta_1) & (\alpha_1\beta_2+\alpha_2\beta_1) \end{bmatrix} \quad (3.5.d)$$

Using the stress strain transformation relations given in Eqs.(3.5.a) and (3.5.b), vectors $\{\sigma\}$, and $\{\varepsilon\}$ may be expressed in the crystallographic coordinate system as

$$\{\sigma^*\}=[Q_c]\{\sigma\}=\sigma\,[Q_c]\{e\} \quad (3.5.e)$$

$$\{\varepsilon^*\}=[Q_d]\{\varepsilon\}=\varepsilon\,[Q_d]\{v\} \quad (3.5.f)$$

Eqs. (3.5.e), and (3.5.f) define the relationship between the vectors, $\{\sigma^*\}$ and $\{\varepsilon^*\}$ in the crystallographic system and vectors $\{\sigma\}$ and $\{\varepsilon\}$ in the global coordinate system.

3.2 - Elastic constants

Elastic constants, which enter into equations of the generalized Hooke's law for anisotropic materials, are refered to the crystallographic coordinate system x*, y*, z*. The known elastic constants defined in the global coordinate system x, y and z should be different from those defined in the crystallographic coordinate system. Therefore, it is

convenient to express the unknown elastic constants as a function of the known constants. This study is done in detail in Leknitskii (1962).

3.2.1 – Orientation dependence of elastic constants

Consider a tensile load along the ON axes such that the unit vector of the applied load coincides with the unit vector { k }, as shown in Figure 3.3. The Euler's angles θ and ψ can then be related to Miller indices [h k l] (defined in Appendix B), by the following relations,

$$\tan(\theta) = \frac{k}{l} \tag{3.6.a}$$

$$\frac{\tan(\psi)}{\cos(\theta)} = \frac{h}{l} \tag{3.6.b}$$

According to Leknitskii (1962), elastic constants such as the Young modulus, $E_{[hkl]}$, the shear modulus $G_{[hkl]}$, and the Poisson's ratio $\nu_{[hkl]}$ along an arbitrary [h k l] orientation are defined respectively as follows.

$$E_{[hkl]} = \left[\frac{D_{11} + D_{12}}{(D_{11} + 2D_{12})(D_{11} - D_{12})} + \left(\frac{1}{D_{44}} - \frac{2}{(D_{11} - D_{12})} \right) \left(\alpha_3^2\beta_3^2 + \alpha_3^2\gamma_3^2 + \beta_3^2\gamma_3^2 \right) \right]^{-1} \tag{3.7.a}$$

$$G_{[hkl]} = \left[\frac{4(D_{11} + D_{12})\,angl - 8D_{12}\,ang2}{(D_{11} + 2D_{12})(D_{11} - D_{12})} + \frac{ang3}{D_{44}} \right]^{-1} \tag{3.7.b}$$

$$\nu_{[hkl]} = -\left[\frac{(D_{11} + D_{12})\,angl - D_{12}\,ang4}{(D_{11} + 2D_{12})(D_{11} - D_{12})} + \frac{ang2}{D_{44}} \right] E_{[hkl]} \tag{3.7.c}$$

In the above expression, D_{ij} are the components of the elasticity matrix [D] defined in section 3.1.4, and ang i are orientation functions defined in Eqs.(3.7.d).

$$\begin{aligned} ang1 &= (\alpha_1 \gamma_1)^2 + (\alpha_2 \gamma_2)^2 + (\alpha_3 \gamma_3)^2 \\ ang2 &= (\alpha_1\gamma_1 \alpha_2 \gamma_2) + (\alpha_2 \gamma_2 \alpha_3 \gamma_3) + (\alpha_3 \gamma_3 \alpha_1 \gamma_1) \\ ang3 &= (\alpha_2 \gamma_1 + \alpha_1 \gamma_2)^2 + (\alpha_3 \gamma_2 + \alpha_2 \gamma_3)^2 + (\alpha_3 \gamma_1 + \alpha_1 \gamma_3)^2 \\ ang4 &= (\alpha_2 \gamma_1)^2 + (\alpha_1 \gamma_2)^2 + (\alpha_3 \gamma_2)^2 + (\alpha_2 \gamma_3)^2 + (\alpha_1 \gamma_3)^2 + (\alpha_3 \gamma_1)^2 \end{aligned} \qquad (3.7.d)$$

Figures 3.4 and 3.5 show orientation dependence of the elastic constants above for Rene N4 at 760° C, taking $D_{11} = 227.58$ GPa, $D_{12} = 152.41$ GPa and $D_{44} = 111.03$ GPa from Table 3.1. Good correlation between theory and experimental data for Young's modulus is observed. Similar variation of elastic constants has been observed in other single crystal nickel base superalloys such as Rene N4, in Dame and Stouffer (1986), and SRR99, in Li and Smith (1995.d). In Table 3.2, the Young's modulus E, calculated on the basis of Eq. (3.7.a) at three distinct temperatures and along six orientations, is compared with the available experimental data, particularly those obtained by Dame (1985). From these results, it is seen that the best correlation is for PWA 1480 at 593° C, for which the biggest error between the theory and experimental data is 0.21%, while for Rene N4 VF 317 at 760° C and Rene N4 at 980° C, the biggest errors are respectively 9.3% and 21.2% along the same orientation [2 3 6]. This mismatch may be attributed to the fact that elastic constants D_{ij} used in the calculation of their Young's modulus are those for PWA 1480.

Table 3.2 Evaluation of the Young's modulus along six distinct orientations at three temperatures. Experimental data for Rene N4 are from Gabb et al. (1986), while those for PWA 1480 are from Nissley et al. (1992.a), (1992.b).

Orientation Eulerian angles		Young modulus E, (GPa)		
		PWA 1480 T = 593 °C	Rene N4 VF317 T = 760 °C	Rene N4 T = 980 °C
[0 0 1]	θ = 0 ψ = 0	105.517 (105.33)	104 (97.02)	90 (78.41)
[0 1 1]	θ = 45 ψ = 0	195.86 (196.28)	185 (187.73)	163 (151.66)
$[\bar{2}\,3\,6]$	θ = 33.69 ψ = 15.5	--- (196.00)	166 (183.00)	119 (151.00)
[0 2 3]	θ = 33.69 ψ = 0	--- (174.00)	170 (162.00)	153 (133.00)
$[\bar{1}\,1\,1]$	θ = 45 ψ = 35.26	275.17 (275.59)	253 (261.00)	226 (220.60)
$[\bar{1}\,4\,5]$	θ = 38.66 ψ = 8.87	--- (196.00)	181 (183.40)	166 (151.46)

values in parenthesis are calculated from the CA theory.

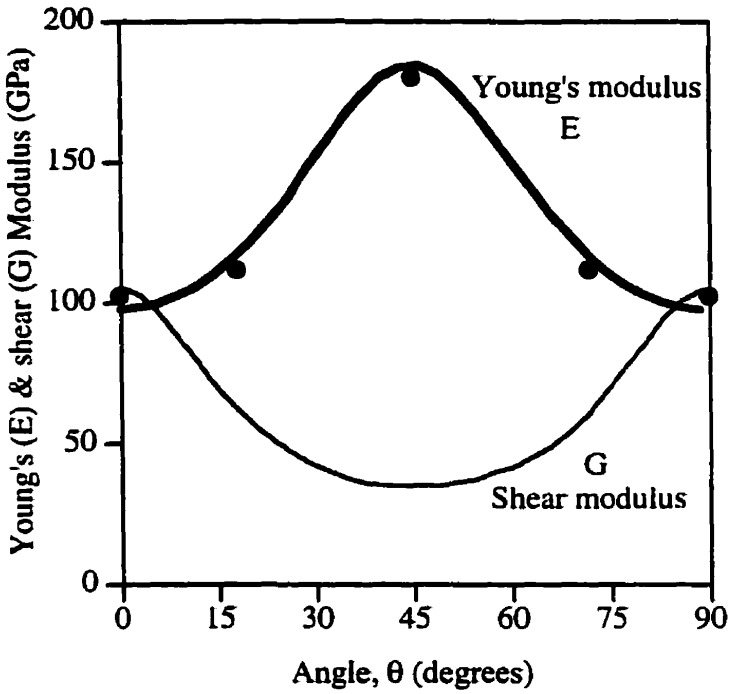

Figure 3.4 Orientation dependence of the Young's modulus (E) and the shear modulus (G) for Rene N4 VF 317 at 760° C. Data are from Sheh (1988).

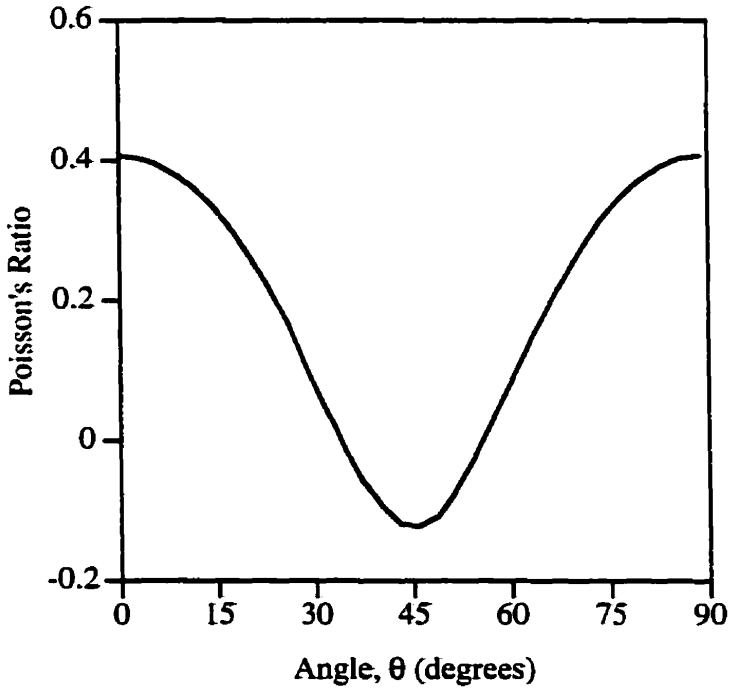

Figure 3.5 Orientation dependence of the Poisson's Ratio for Rene N4 VF317 at 760° C

3.2.2 – Temperature dependence of elastic constants

A more detailed study of temperature dependence of elastic constants for SC nickel base super-alloys is done in Li and Smith (1995a). In that study, the Young's modulus E (T) is normalized with respect to Young's modulus (E_0) at 20° C for MAR-M002 as a function of temperature, along the [0 0 1] orientation. In general, they found that the elastic modulus was higher for specimens near the $[\bar{1}\,1\,1]$ orientation and lower for specimens near the $[0\,0\,1]$ orientation over the temperature range studied. The elastic modulus decreased with increasing temperature. The observed variation in the elastic modulus of single crystal SRR99 showed a change in the slope dE/dT at about 650° C. This temperature appeared to be independent of crystal orientation. The decrease in elastic modulus above 650° C was greater than that below 650° C. A least squares regression fit to the normalized elastic modulus data yielded the following equations.

$$\frac{E(T)\mu(\theta,\psi)}{E_0} = \begin{cases} 0.515 - 0.14\times10^{-3}\,T & (0<T<650^{\circ}\,C) \\ 0.631 - 0.316\times10^{-3}\,T & (650^{\circ}\,C \le T < 1050^{\circ}\,C) \end{cases} \qquad (3.7.e)$$

where $\mu(\theta, \psi)$ is a rotation function and T the temperature.

They also found that $(dE/E_0)/dT$ is larger for the various polycrystalline alloys than for SC alloys for temperatures above and below the critical temperature, $T_c = 650°$ C (see Figure 3.6). After analysis, they attributed both the change in the slope (dE/dT) and the behavior of the elastic moduli with temperature to the major constituent phases of the material such as the γ, γ' phases and grain boundaries as shown in Figure 3.7.

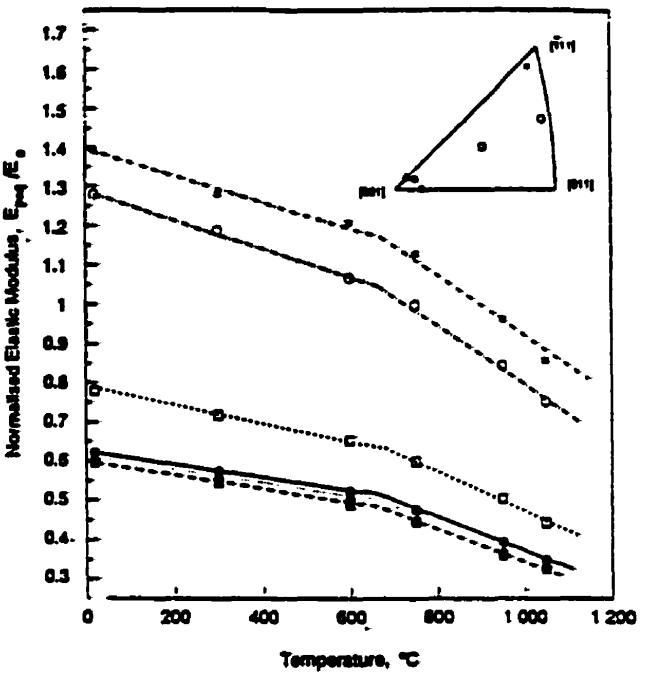

Figure 3.6 Temperature and orientation dependence of elastic modulus for single crystal super-alloys. From Li and Smith (1995.a).

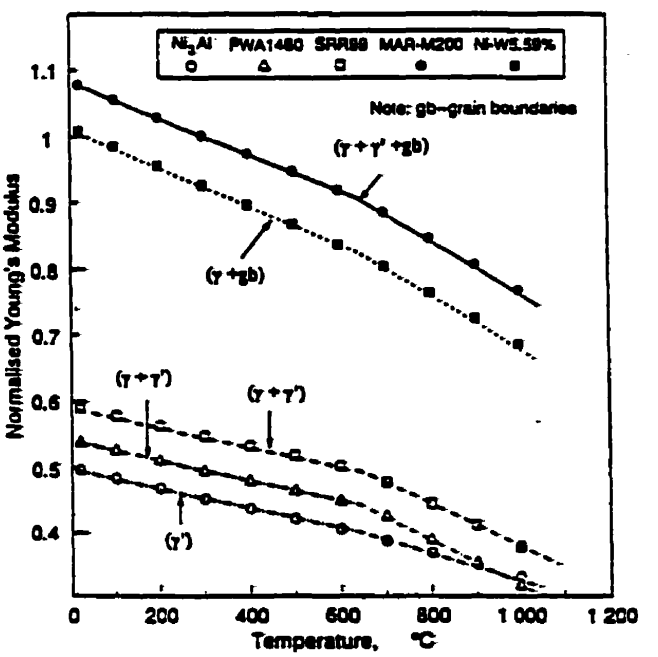

Figure 3.7 Variation in Young's modulus with temperature for nickel base alloys. From Li and Smith (1995.a).

3.3 – STRUCTURE OF THE COMBINED APPROACH

The principle of the **"combined approach"** is based on the extension of isotropic material behavior predicted models to anisotropic materials such as single crystals. The structure of this approach requires the establishment of two main elements: a macroscopic model that admits a yield function and a slip factor.

The macroscopic model describes the anisotropic effect in terms of bulk material properties and observed loading response. However, it accounts poorly for the initial anisotropy of SC material, which is attributed to the orientation-dependence of deformation mechanisms. The slip factor, in turn, accounts for the micro-mechanism deformation occurring within the crystal during the deformation process. Under a global state of stress defined by $\{\sigma$, yield is determined using an approach combining the phenomenological Lee and Zaverl (1979) yield function term, (f), and a crystallographic based factor, (Sf), called the slip factor. The initial yield stress, σ_y (value of σ that causes yield using the combined approach) is given by the relation,

$$\sigma_y = Sf\, \sigma_{LZ} \tag{3.8.a}$$

where,

- σ_{LZ} is the value of σ that results in yield using the Lee and Zaverl yield function (see section 3.3.1.1), and
- Sf is the slip factor, developed in section 3.3.2.

In the following sections, the theory of the CA is developed. Emphasis will be laid initially on the evaluation of the two terms σ_{LZ} and Sf as defined above, for the evaluation of the initial yield stress, σ_y. The extension of the theory to the plastic regime will be expounded in Chapter IV.

3.3.1 – Initial Yielding based on Lee and Zaverl's Theory

The macroscopic model retained in this work is Chaboche's unified viscoplastic model applied to anisotropic materials. This model, described in section 2.3 of Chapter II, has been used successfully for isotropic material analysis such as Inconel 718 at 1100° C and 1200° C, in Eftis et al.(1989) and Abdel-Kader et al. (1991). The choice of the Chaboche theory as the macroscopic model used for the purpose of the CA theory was motivated by the results obtained from its comparative studies with those of Bodner, Walker and Bodner-Partom in Eftis et al.(1989) and Abdel-Kader (1990). The authors conclude that all three theories appear to be capable of modeling the main features of the inelastic behavior of Inconel 718 at 1100° C, with varying degrees of acceptability. Chaboche's theory, however, seems to offer the greatest promise in this regard. In addition, Chaboche's model assumes a yield function, and for anisotropic material such as SC nickel base super-alloys, the von Mises criterion commonly used is changed by the generalized Hill's criteria. For the purpose of the CA developed in this work, the yield function proposed by Lee and Zaverl (1979) and defined in section 3.3.1.1 is adopted. That formulation is an extension of Hill's theory. In addition to modeling the initial anisotropic yield surface (the only feature that Hill's original theory allowed), it is also capable of modeling the translation and the expansion of the yield surface. It has been applied successfully to anisotropic hexagonal close packed (h.c.p) metals in Eleiche (1991), and was found to describe the yield surface of such materials more closely than the Hill theory. The same yield function has been used in Nouailhas (1990) for a cyclic viscoplastic model applicable to SC superalloys CMSX-2, (a trademark of Cannon Muskegon corporation) whose properties are very close to those of other SC superalloys such as PWA 1480, Rene N4, SRR99, developed for the same applications.

3.3.1.1 – The Yield Function

For anisotropic materials such as SC nickel base superalloys, the Lee and Zaverl yield function (using the vector form) may be expressed in the crystallographic coordinate system as follows,

The form of the yield function above has been used in Swanson et al. (1986), Eleiche (1991), and Nouailhas (1990). This type of formulation is readily adapted for use of the unified viscoplastic models whose employment will be required in the description of the time-dependent anisotropic material behavior of SC at elevated temperatures. In addition, it allows the yield surface to translate into stress space by means of the back stress, $\{ Y \}$, and to expand in stress space due to the presence of the drag stress, $\hat{R}$. To allow the yield surface to distort its shape and rotate in the stress space, an evolutionary form of the anisotropic tensor, M_{ij} is defined in Swanson et al. (1986) as follows

$$\dot{M}_{ij} = \alpha\left(M^{s}_{ij} - M^{0}_{ij}\right)\dot{p} \qquad (3.9.e)$$

Where, α is a material parameter M^{s}_{ij} is a stationary anisotropic state of the tensor M_{ij} under cumulative deformation, M^{0}_{ij} is the initial value of M_{ij}, and p is the cumulative inelastic strain rate.

A thermal recovery term may be added to Eq. (3.9.e) at high temperatures to allow recovery of the material to its original anisotropic state. In general, the choice of, M^{s}_{ij}, as a function of applied loading and the subsequent hardening, represents the main difficulty of this approach and does not seem to have been clearly defined yet. Thus, in this first attempt of the CA for predicting SC material behavior, the study will be restricted to the initial anisotropic state. Subsequent distortions of the yield surfaces are therefore beyond the scope of this work.

In order to describe the initial yield surface from a virgin state at a given temperature, one may set from Eq.(3.9.c), $f = 0$ and $Y = 0$. The components, M_{ij}, of the anisotropic matrix $[M]$ and the initial value of the internal variable, $\hat{R}$, need to be determined. In SC materials such as nickel base super-alloys with an f.c.c structure, properties along each of the crystallographic axes [1 0 0], [0 1 0] and [0 0 1] are assumed to be identical. Because of the symmetry of the structure, the components M_{ij} of the anisotropic matrix

[M] are such that: $M_{11} = M_{22} = M_{33}$ and $M_{44} = M_{55} = M_{66}$. Therefore, when specialized to the cubic symmetry appropriate for SC, the anisotropic matrix [M] may be reduced in [0 0 1] aligned crystallographic system to the form given in Eq. (3.10.a).

$$[M] = \begin{bmatrix} M_{11} & M_{12} & M_{12} & 0 & 0 & 0 \\ M_{12} & M_{11} & M_{12} & 0 & 0 & 0 \\ M_{12} & M_{12} & M_{11} & 0 & 0 & 0 \\ 0 & 0 & 0 & M_{44} & 0 & 0 \\ 0 & 0 & 0 & 0 & M_{44} & 0 \\ 0 & 0 & 0 & 0 & 0 & M_{44} \end{bmatrix} \qquad (3.10.a)$$

3.3.1.2 – Determination of M_{ij}

For the purpose of the determination of M_{11} , M_{12} and M_{44} , only one assumption is required and used in this work. It states that: the basic equations restore isotropic properties along the principal axes. Recall that the fulfillment of this assumption yields to incompressibility of the material. That assumption is further developed in Chapter IV, which deals with the plastic regime. Its application yields,

$$M_{11} - M_{12} = 2/3 \qquad (3.10.b)$$

However, the determination of M_{11} and M_{12} from the above equation gives an infinity of solutions. The optimum solution can be observed at the initial yield surface, where the yield function, $f = 0$, the back stress $Y = 0$ and the drag stress $\hat{R} = \hat{R}_0$, $\hat{R}_0$ being the initial value of the scalar, $\hat{R}$. From Eq.(3.9.c), the effective yield stress, $\bar{\sigma} = \hat{R}_0$ may be reduced to $\bar{\sigma} = \sigma\, \mu_1(\theta, \psi)$. Then, setting $\{X\} = [Q_e]^{-1}[N_0]\{e$, which may also be expressed as $\{X\}^t = \{x_1, x_2, x_3, x_4, x_5, x_6$, and substituting both the anisotropic matrix [M] and the vector { X } in the orientation function $\mu_1(\theta, \psi)$ defined in Eq. (3.9.d), the effective yield stress $\bar{\sigma}$ may be expressed as

- **For a uniaxial specimen oriented in the $[\bar{1}11]$ direction**

$\theta_0 = 45°$ and $\psi_0 = 35.26°$, so $x_1 = x_2 = x_3 = 0$ and $x_4 = x_5 = x_6 = 1/3$.

This implies that $g(\theta_0,\psi_0) = p(\theta_0,\psi_0) = 0$, and $h(\theta_0,\psi_0) = 1/3$. By substitution in Eq. (3.10.c), the effective stress becomes

$$\bar{\sigma} = \sigma_{[\bar{1}11]}\left(\frac{M_{44}}{2}\right)^{1/2} = \sqrt{2/3}\,\sigma_{+1} \qquad (3.11.c)$$

and after rearranging, one gets

$$M_{44} = \frac{4}{3}\left(\frac{\sigma_{+1}}{\sigma_{[\bar{1}11]}}\right)^2 \qquad (3.11.d)$$

- **For a uniaxial specimen oriented in the $[011]$ direction**

$\theta_0 = 45°$ and $\psi_0 = 0°$, so $x_1 = -1/3$, $x_2 = x_3 = 1/6$, $x_4 = 1/4$, and $x_5 = x_6 = 0$.

This implies that $g(\theta_0,\psi_0) = 1/6$, $p(\theta_0,\psi_0) = -1/12$, and $h(\theta_0,\psi_0) = 1/4$. By substitution in Eq. (3.10.c), the effective stress becomes

$$\bar{\sigma} = \sigma_{[011]}\left(1/6\,M_{11} - 1/12\,M_{12} + 1/4\,M_{44}\right)^{1/2} = \sqrt{2/3}\,\sigma_{+1} \qquad (3.11.e)$$

and substituting M_{44} in Eq. (3.11.e), by its value defined in Eq. (3.11.d), one gets after rearranging,

$$2M_{11} - M_{12} = 8\left(\frac{\sigma_{+1}}{\sigma_{[011]}}\right)^2 - 4\left(\frac{\sigma_{+1}}{\sigma_{[\bar{1}11]}}\right)^2 \qquad (3.11.f)$$

Equations (3.10.b) and (3.11.f) can be used for the determination of M_{11} and M_{12}. One obtains after calculation,

$$M_{11} = 8\left(\frac{\sigma_{+1}}{\sigma_{[011]}}\right)^2 - 4\left(\frac{\sigma_{+1}}{\sigma_{[\bar{1}11]}}\right)^2 - \frac{2}{3} \quad \text{(i)}$$

$$M_{12} = 8\left(\frac{\sigma_{+1}}{\sigma_{[011]}}\right)^2 - 4\left(\frac{\sigma_{+1}}{\sigma_{[\bar{1}11]}}\right)^2 - \frac{4}{3} \quad \text{(ii)} \qquad (3.11.g)$$

The anisotropic matrix [M] is therefore known. From the above results, it can be pointed out that the knowledge of the yield stresses σ_{+1}, $\sigma_{[011]}$ and $\sigma_{[\bar{1}11]}$ are sufficient for the determination of the initial anisotropic state in the material. Furthermore, since the initial yield stress is strain rate and temperature dependent, the anisotropic matrix [M] is implicitly strain rate and temperature dependent.

Now, before continuing with the investigation of the initial yielding, let us look at the variation of the orientation function, $\mu_1(\theta, \psi)$.

3.3.1.3 – Variation of the orientation function, $\mu_1(\theta, \psi)$

A brief review of the orientation function $\mu_1(\theta, \psi)$ defined in Eq. (3.9.d) shows that $\mu_1(\theta, \psi)$ depends on the initial anisotropic state by means of the matrix [M], the change of the base system by means of the rotation matrix [Q_c] and the applied stress direction by means of the unit vector, { **e** }. None of the terms above is explicitly function of the structure of the crystal. Consequently, the orientation function describes the material behavior only at the macroscopic level. A physical interpretation of $\mu_1(\theta, \psi)$ may be as follows: since $\hat{R}$ from Eq. (3.9.c) is constant, then, under any arbitrary global state of stress, $\mu_1(\theta, \psi)$ may be seen as the coefficient required to reach the yield surface. A plot of $\mu_1(\theta, \psi)$ versus θ along the $[0\,0\,1]$-$[0\,1\,1]$ orientation boundary is shown in Figure 3.8. From that graph, it emerges that $\mu_1(\theta, \psi)$ is orientation dependent and that it is minimum along the $[0\,0\,1]$ orientation and maximum along the $[0\,1\,1]$ orientation.

3.3.1.4 - Initial yielding

At the yield surface from the virgin state, Y= 0, and the yield function, f, defined in Eq.(3.9.c) is also zero. So, the initial yield stress, σ_{LZ} , based on Lee and Zaverl's theory for an arbitrary applied load is given to be

$$\sigma_{LZ} = \frac{\hat{R}_0}{\mu_1(\theta, \psi)} \tag{3.12.a}$$

where, $\hat{R}_0 = \sqrt{2/3}\,\sigma_{+1}$, defined in Eq.(3.11.b), is the initial value of the scalar $\hat{R}$, and $\mu_1(\theta, \psi)$ is the orientation function. Now, knowing the values of $\hat{R}_0$, the initial yield stress expression along any arbitrary [h k l] orientation becomes according to Lee and Zaverl's theory.

$$\sigma_{LZ} = \frac{\sqrt{2/3}\,\sigma_{+1}}{\mu_1(\theta, \psi)} \tag{3.12.b}$$

Since σ_{+1} is constant, the expression above shows that the predicted initial yield stress, σ_{LZ} is inversely proportional to the orientation function $\mu_1(\theta, \psi)$ studied in section 3.3.1.3. A graphic representation of σ_{LZ} is plotted and compared with experimental data for PWA 1480 at 593^0 C along the $[0\,0\,1]$-$[0\,1\,1]$ orientation boundary in Figure 3.9. Experimental data (σ_{+1} = 1220 MPa, and $\sigma_{[\bar{1}11]}$ = 1010 MPa) are taken from Sheh and Duhl (1984).

As observed in section 3.3.1.3 with the orientation function $\mu_1(\theta, \psi)$, it may be pointed out in Eq(3.12.b) that no element in that expression is related to the structure of the crystal, nor the deformation mechanisms. For this formulation, therefore, the yield strength is independent of the material's structure. In other words, the yield stress would

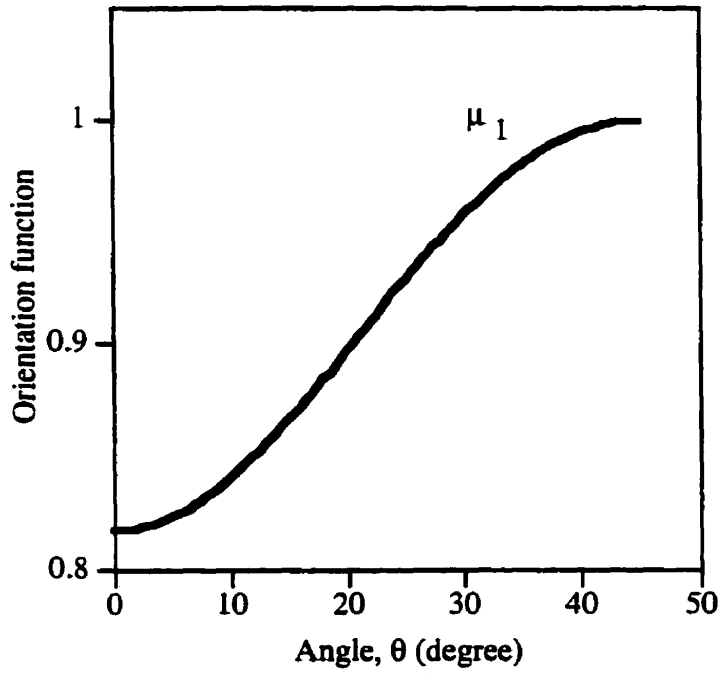

Figure 3.8 Orientation dependence of $\mu_1(\theta,\psi)$ for PWA 1480 at 593°C along the $[0\,0\,1]$-$[0\,1\,1]$ orientation boundary.

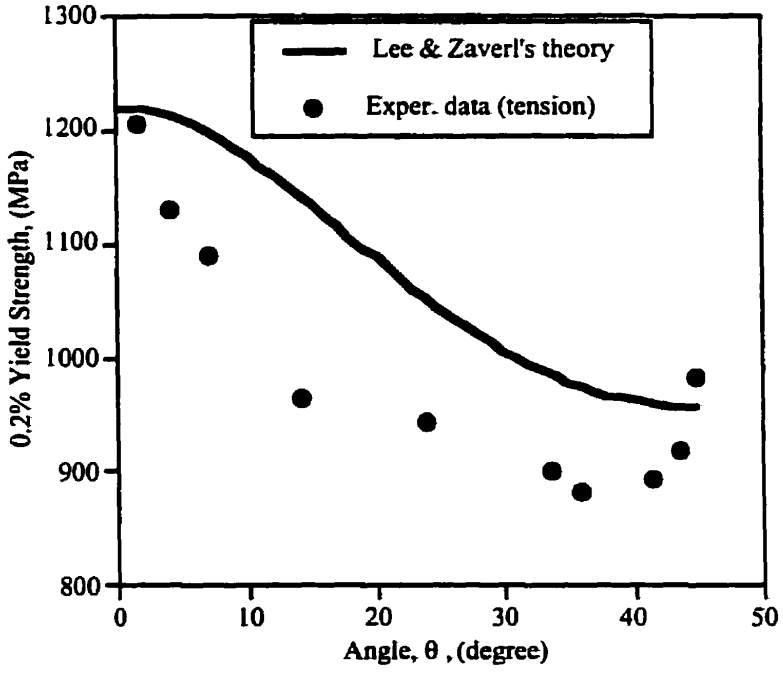

Figure 3.9 Comparison of the predicted yield strength based on Lee & Zaverl's theory with experimental data for PWA 1480 at 593° C along the $[0\,0\,1]$-$[0\,1\,1]$ boundary. From Sheh and Duhl (1986).

be the same whether the material's structure is faced centered cubic (f.c.c), body centered cubic (b.c.c) or hexagonal closed packet (h.c.p). Furthermore, that yield function is insensitive to the sign of the stress-state so that it cannot properly account for observed differences in tension and compression data, and the state of anisotropy does not change with deformation. Further limitations of this formulation have been identified in Swanson et al. (1986).

The first element required for the structure of the combined approach proposed in this work is therefore established. The slip factor, which is the second element of the theory, will be evaluated in the next section.

3.3.2 - Slip factor

As mentioned earlier in this chapter, the expression of the initial yield stress, based on Lee and Zaverl's theory and defined in Eq.(3.12.b), ignores the micro-mechanism effect that dominates the deformation process of single crystal materials. It goes without saying, for the same applied load, that the deformation should not be the same whatever the structure of the material is f.c.c, b.c.c or h.c.p. The omission of the micro-mechanism in Eq.(3.11.b) is the likely reason for the lack of correlation observed in Figure 3.9 between the predicted yield stress and the experimental data. It is therefore convenient to introduce a new parameter into the model that accounts for the micro-slip effect, which occurs within the crystal during the deformation process. Such a parameter should distinctly characterize the micro-mechanical slip within the sample due to the structure of the material, the intensity of the applied stress, its direction and its applied rate. In this study, such a parameter, denoted Sf and called **slip factor**, is evaluated. It is the second element required in order to completely establish the structure of the combined approach proposed in this work.

3.3.2.1 – Definition

Since, for a given stress state, the slip factor Sf accounts for the slip process which occur within the material during its deformation process, its evaluation would be based on the

crystallographic theory. Slip trace studies of SC materials such as nickel bases super-alloys with a faced centered cubic structure show that there exist two types of slip planes along which slip usually initiates. They consist of four octahedral slip planes and three cubic slip planes (see appendix A). Furthermore, when studying the temperature and orientation dependence of the yield stress in the SC alloys, Takeuchi and Kuramoto (1973) and Lal, Chin and Pope (1979) found that the activation of the slip process on the octahedral slip systems is strongly temperature and orientation dependent with respect to the applied stress direction. It is shown that loading near the $[0\,0\,1]$ orientation is thought to produce only octahedral slip at all temperatures since the RSS on the cube planes is zero. Conversely, near the $[\bar{1}\,1\,1]$ orientation, tests specimens exhibit cube slip at all temperatures. So, for a given applied load on a SC sample, one can define at each of its points, a pair of ratios $\left(\frac{\sigma}{\tau_{RT}}\right)_{oct}$ and $\left(\frac{\sigma}{\tau_{RT}}\right)_{cube}$, related respectively to the octahedral and cube slip systems. In the ratios above, σ represents the magnitude of the applied stress at the point considered, while τ_{RT} is the critical resolved shear stress (CRSS) of the same material at room temperature (RT) along the [0 0 1] orientation. The slip factor, Sf, is defined to be the minimum of the pair of ratios above. According to the applied stress orientation and the rate of deformation, it accounts for predominant active slip systems. It will be shown in this chapter that such a slip factor is, as the orientation function $\mu_1(\theta,\psi)$, a function of the applied load direction, the change of the base system, and the initial anisotropic state of the material. In addition, it is also a function of the structure of the crystal and the deformation mechanisms. The main emphasis of the following sections will be the evaluation of that slip factor.

3.3.2.2-Identification of the slip systems in the crystal

The application of an arbitrary load in a SC material sample gives rise to a stress field at any point of the sample. That stress field generates shear stresses, τ, along each potential slip system of the crystal and along each slip direction. These shear stresses may be positive, negative or zero. At a certain level of the applied load, one or several of these

where

- α defines a slip direction in the octahedral slip system,
- $\{ s \}^{(\alpha)}$ is the slip vector along the α^{th} slip direction,
- $\{ n \}^{(\alpha)}$ is the normal to the α^{th} slip direction,
- $s_i^{(\alpha)}$ and $n_j^{(\alpha)}$ are, respectively, the components of vectors $\{ s \}^{(\alpha)}$ and $\{ n \}^{(\alpha)}$,
- $\tau^{(\alpha)}$ and $\tau_c^{(\alpha)}$ are, respectively, the magnitude of the resolved shear stress (RSS), and the critical resolved shear stress (CRSS) in the α^{th} slip direction,
- σ^*_{ij} are the components of the second order stress tensor, σ^*, in the crystallographic system
- i and j are Cartesian indices that may be equal to 1, 2 or 3, where repeated indices imply summation.

a) - Structural matrices

Eq.(3.13.a) may be restated as

$$\tau^{(\alpha)} \equiv \pm m_i^{(\alpha)} \sigma_i^* \geq \tau_c^{(\alpha)} \qquad (3.13.b)$$

Where, $m_i^{(\alpha)}$, defined in Eq.(3.13.c), may be expressed as a function of $s_i^{(\alpha)}$ and $n_j^{(\alpha)}$.

$$\begin{bmatrix} m_1 \\ m_2 \\ m_3 \\ m_4 \\ m_5 \\ m_6 \end{bmatrix}^{(\alpha)} = \begin{bmatrix} s_1 n_1 \\ s_2 n_2 \\ s_3 n_3 \\ (s_2 n_3 + s_3 n_2) \\ (s_1 n_2 + s_2 n_1) \\ (s_1 n_3 + s_3 n_1) \end{bmatrix}^{(\alpha)} \qquad (3.13.c)$$

When α describes all the slip directions similar to $(111)[\bar{1}01]$ listed in Table 3.3, then one may generate from Eq.(3.13.c) a structural matrix $[X]$ (constant), related to the slip system of type i. Thus from Eq.(3.13.b), the corresponding RSS in the vector form $\{\tau\}_i$ may be expressed in the crystallographic coordinate system as

Table 3.3 - Octahedral slip systems

Slip system	Normal $[n_1, n_2, n_3]$	Slip system of type 1 Similar to $(111)[\bar{1}\,0\,\bar{1}]$ $\pm[s_1, s_2, s_3]$	Slip system of type 2 Similar to $(111)[\bar{1}\,2\,\bar{1}]$ $\pm[s_1, s_2, s_3]$
1	$n_1 = (-I+j+k)/\sqrt{3}$	$s_1 = (j-k)/\sqrt{2}$	$s_1 = (2i+j+k)/\sqrt{6}$
2		$s_2 = (-i-j)/\sqrt{2}$	$s_2 = (-i+j-2k)/\sqrt{6}$
3		$s_3 = (i+k)/\sqrt{2}$	$s_3 = (-i-2j+k)/\sqrt{6}$
4	$n_2 = (-I-j+k)/\sqrt{3}$	$s_4 = (-i-j)/\sqrt{2}$	$s_4 = (-i+2j+k)/\sqrt{6}$
5		$s_5 = (i-j)/\sqrt{2}$	$s_5 = (-i-j-2k)/\sqrt{6}$
6		$s_6 = (j+k)/\sqrt{2}$	$s_6 = (2i-j+k)/\sqrt{6}$
7	$n_3 = (i-j+k)/\sqrt{3}$	$s_7 = (-j-k)/\sqrt{2}$	$s_7 = (-2i-j+k)/\sqrt{6}$
8		$s_8 = (i+j)/\sqrt{2}$	$s_8 = (i+j-2k)/\sqrt{6}$
9		$s_9 = (-i+k)/\sqrt{2}$	$s_9 = (i+2j+k)/\sqrt{6}$
10	$n_4 = (i+j+k)/\sqrt{3}$	$s_{10} = (i-k)/\sqrt{2}$	$s_{10} = (i-2j+k)/\sqrt{6}$
11		$s_{11} = (-i+j)/\sqrt{2}$	$s_{11} = (i-2j+k)/\sqrt{6}$
12		$s_{12} = (-j+k)/\sqrt{2}$	$s_{12} = (i-2j+k)/\sqrt{6}$

Table 3.4 - Cube slip systems

Slip system	Normal $[n_1, n_2, n_3]$	Slip system of type 3 Similar to $(010)[\bar{1}\,0\,\bar{1}]$ $\pm[s_1, s_2, s_3]$
1	$n_1 = k$	$s_1 = (i+j)/\sqrt{2}$
2		$s_2 = (-i+j)/\sqrt{2}$
3	$n_2 = j$	$s_3 = (i+k)/\sqrt{2}$
4		$s_4 = (-i+k)/\sqrt{2}$
5	$n_3 = i$	$s_5 = (j+k)/\sqrt{2}$
6		$s_6 = (-j+k)/\sqrt{2}$

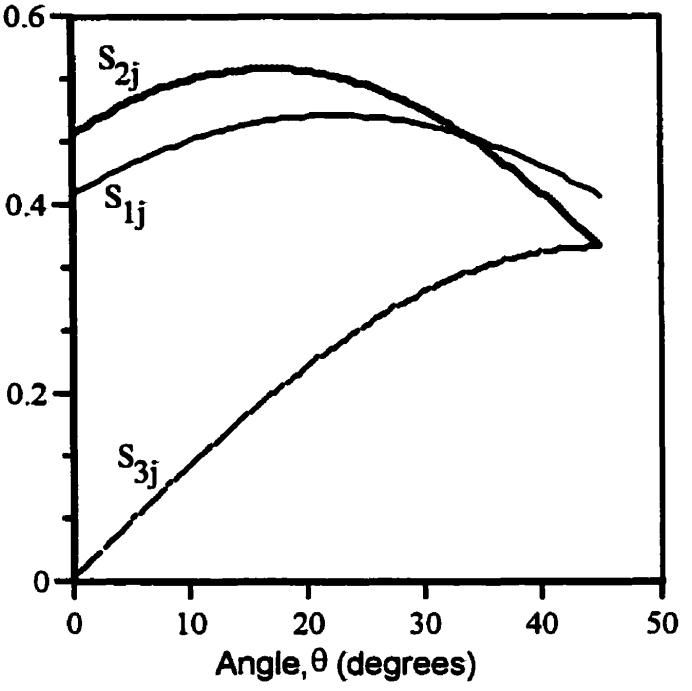

Figure 3.10 Orientation dependence of the structural coefficients S_{1j}, S_{2j} and S_{3j} along the $[0\,0\,1]$-$[0\,1\,1]$ orientation boundary.

3.3.2.4 – Expression of the RSS

A brief review of the coefficients S_{ij} reveals that they are function of the structure of the crystal, the change of the base system and the applied stress direction. Their orientation dependence is plotted in Figure 3.10 for the three slip system types defined previously. Now, combining Eqs.(3.14.b), (3.14.c) and (3.13.e), one obtains after rearranging,

$$\tau_i = \sigma S_{ij} \qquad (3.14.d)$$

τ_i is therefore proportional to the applied stress magnitude and the structural coefficient.

Since the structural matrices $[X]$ are constant and known for the f.c.c structure, then

from the above result it follows that, for a SC sample taken at a given temperature, the knowledge of the Euleurian angles θ and ψ defined previously and the applied stress indices $\{ e \}$, permits the evaluation of the structural coefficients S_{ij}.

Now, under the global state of stress $\{\sigma\}$, the value of stress, σ_y, that causes yield in the sample is reached when the maximum of the RSS τ_i defined in Eq.(3.14.d), reaches the minimum of the CRSS τ_c defined in Eq.(3.14.a). This may be expressed mathematically by the relation below,

$$\sigma S_{ij} = \tau_c \tag{3.15.a}$$

Normalizing both terms by the critical resolved shear stress (CRSS) τ_{RT} at room temperature (RT), one obtains after rearranging, the ratio.

$$\left(\frac{\sigma}{\tau_{RT}}\right)_{oct} = \frac{\tau_c}{\tau_{RT} S_{ij}} \tag{3.15.b}$$

At each point of the sample, the ratio above accounts for the state of the micro-mechanical slip (in the octahedral slip system) and its deformation mechanism. This ratio is proportional to the CRSS, τ_c, and inversely proportional to the structural coefficient S_{ij} and the CRSS, τ_{RT}. SC nickel base superalloys slip trace studies show that octahedral slip systems are active in both tension and creep tests. Their corresponding deformation mechanisms, however, are different. Consequently, many of the unified models are reasonable for modeling plasticity or creep but are not completely adequate for both. The common and easy way to characterize the effect of dislocation networks on both mechanisms is to couple two terms representing one mechanism each.

The origin of this approach is based on the physical motivation of many deformation mechanisms. A similar approach has been used in Dame (1985). The total flow rate was therefore taken to be the sum of two flow rates related to two distinct deformation mechanisms. In the present study, the same technique will be used, and a coupling parameter is the CRSS (τ_c). Thus τ_c, used in Eq.(3.15.b), must be decomposed into two terms coupled to characterize the effect of the dislocation network on both mechanisms so that Eq.(3.15.b) becomes

$$\left(\frac{\sigma}{\tau_{RT}}\right)_{oct} = \frac{(\tau_{oct})_1 + (\tau_{oct})_2}{\tau_{RT} S_{ij}} \qquad (3.16.a)$$

The first component $(\tau_{oct})_1$ is used to characterize dislocation cutting on the γ' particles while the second component $(\tau_{oct})_2$ is motivated by the interstitial emission and diffusion mechanism. In addition, $(\tau_{oct})_1$ is negligible at the low strain rates that correspond to the creep test and $(\tau_{oct})_2$ is negligible at the high strain rates that correspond to the tensile or compressive test. Recall that a sample is said to be in tension when the first invariant of the stress vector $\{\sigma\}$, $I_{\{\sigma\}}$, is positive and in compression when $I_{\{\sigma\}}$ is negative.

3.3.2.5 - Relationship between CRSS and deformation mechanisms

At elevated temperatures, the CRSS τ_c is usually associated with thermally activated processes and is presented in the form of an Arrhenius type relationship as

$$\tau_c = A_0 \exp\left(\frac{H(\tau_2, \tau_3)}{kT}\right) \qquad (3.16.b)$$

where A_0 is a material constant, T is the absolute temperature in (°K), k is Boltzmann's

constant, and H is a parameter function of the RSS τ_2 on the (1 1 1) plane in the $[\bar{1}\,2\,\bar{1}]$ direction and the RSS τ_3 on the (0 1 0) plane in the $[\bar{1}\,0\,1]$ direction.

In Eq. (2.2), H is extended in a Taylor series about the reference condition H_0. This form of the shear stress adds additional terms to Schmid's law. That formulation has been satisfactory developed and explained first by Takeuchi and Kuramoto (1973) and completed by Lall, Chin and Pope (1979). In the CA theory developed in this work, there exists a relationship between the CRSS and deformation mechanisms. As explained in section 3.3.2.2, there exist two distinct octahedral slip systems in the f.c.c crystal. The nature of slip systems activated depends on whether the sample is loaded in tension, or in compression, at high or low strain rate. For example, when the sample is loaded in tension the first invariant is positive and the slip system of type 1 is predominant. The structural matrix $[X]$, then, becomes the 12x6 matrix $[B_m]$ defined in Appendix A. When the sample is loaded in compression, the first invariant is negative. The slip system of type 2 is then predominant. The structural matrix $[X]$ becomes the 12x6 matrix $[C_m]$ defined in the appendix A.

a) – High strain rate

At the high strain rate under a j^{th} global stress state, the shear stress component $(\tau_{oct})_2$, shown in the Eq.(3.16.a), is negligible. Only the component $(\tau_{oct})_1$ is active. Its functional form has the form proposed by Lall, Chin and Pope expressed in Eq.(2.2). That form has been used with success to explain both the cross slip and the core width effects observed in a number of SC materials. However, since there exists two octahedral slip system types as mentioned previously, one of them or both may be active according to whether the sample is loaded in tension or in compression. Taking into account that fact, and setting $\delta = I_{\{\sigma\}}/\sigma$, where $I_{\{\sigma\}}$ is the first invariant of the stress vector $\{\sigma\}$, and σ is its magnitude, the shear stress component may be expressed as:

$$(\tau_{oct})_1 = \frac{|\delta+1|}{2}\left[A_{1t}\varphi_1(\dot{\varepsilon}) \exp\left(\frac{-H_0}{kT} + V_{11}S_{2j} + V_{12}S_{3j}\right)\right] + \frac{|\delta-1|}{2}\left[A_{1c}\varphi_1(\dot{\varepsilon}) \exp\left(\frac{-H_0}{kT} - V_{21}S_{2j} + V_{22}S_{3j}\right)\right] \quad (3.16.c)$$

where S_{2j} and S_{3j} are structural coefficients, related respectively to the core width and cross slip effects; A_{1t}, V_{11}, V_{12}, A_{1c}, V_{21} and V_{22} are material constants, δ is defined as above and $\varphi_1(\dot{\varepsilon})$ is a strain rate function (see section 3.3.2.7), defined such that it tends to 1 at the high strain rate and 0 at the low strain rate.

To motivate the functional form above, three one-dimensional cases will be considered as examples:

- For $\{\sigma\}^t = \{\sigma_1\ 0\ 0\ 0\ 0\ 0\}$, $\sigma = \sigma_1$ and $I_{\{\sigma\}} = \sigma_1 > 0$; then by definition $\delta = 1$, and therefore $\frac{|\delta-1|}{2} = 0$ and $\frac{|\delta+1|}{2} = 1$.

Substituting these results in Eq.(3.16.c), it follows that only the expression related to the slip system of type 1 is active in tension.

- For $\{\sigma\}^t = \{-\sigma_1\ 0\ 0\ 0\ 0\ 0\}$, $\sigma = \sigma_1$ and $I_{\{\sigma\}} = -\sigma_1 < 0$; then by definition $\delta = -1$, and therefore $\frac{|\delta-1|}{2} = 1$ and $\frac{|\delta+1|}{2} = 0$.

Substituting these results in Eq.(3.16.c), it follows that only the expression related to the slip system of type 2 is active in compression.

- For $\{\sigma\}^t = \{0\ 0\ 0\ \sigma_1\ 0\ 0\}$ then $\sigma = \sigma_1$ and $I_{\{\sigma\}} = 0$, then by definition $\delta = 0$, and therefore $\frac{|\delta-1|}{2} = \frac{1}{2}$ and $\frac{|\delta+1|}{2} = \frac{1}{2}$.

Again, substituting these results in Eq.(3.16.c), it allows that both slip system types are active in pure shear stress.

It can be observed that the functional form of both terms related to the slip system of type 1 and type 2 are similar, differing only by the material constants. That difference is therefore responsible for the tension compression asymmetry predicted by the model since, as discussed previously, Lee and Zaverl's yield function is unable to predict tension /compression asymmetry.

b) – Low strain rate

At low strain rates under a j^{th} global stress state, the shear stress component $(\tau_{oct})_1$, shown in the Eq.(3.16.a), is negligible. Only the component $(\tau_{oct})_2$ is active. Its functional form is taken to be similar in structure to the form above. The form adopted in this work is very close to the one used in Dame (1985) to model creep behavior for Rene N4. However, as mentioned above, there exist two octahedral slip system types. One of them or both may be active according to whether the sample is loaded in tension or in compression. The shear stress component may be expressed as:

$$(\tau_{oct})_2 = \frac{|\delta+1|}{2}\left[A_{1\alpha}\varphi_2(\dot{\varepsilon})\exp\left(\frac{-H_0}{kT}-\frac{V_{13}}{\sqrt{J_2}}\sigma_{+1}S_{2j}+\frac{V_{14}}{\sqrt{J_2}}\sigma_{+1}S_{3j}\right)\right] + \frac{|\delta-1|}{2}\left[A_{2\alpha}\varphi_2(\dot{\varepsilon})\exp\left(\frac{-H_0}{kT}-\frac{V_{23}}{\sqrt{J_2}}\sigma_{+1}S_{2j}+\frac{V_{24}}{\sqrt{J_2}}\sigma_{+1}S_{3j}\right)\right] \quad (3.16.d)$$

Where, $A_{1\alpha}$, V_{13} , V_{14} , $A_{2\alpha}$, V_{23} and V_{24} are material parameters, J_2 is the second invariant of the deviatoric stress tensor, and $\varphi_2(\dot{\varepsilon})$ is another strain rate function defined in section 3.3.2.7 such that it tends to 1 at the low strain rate and 0 at the high strain rate.

The first term $(\tau_{cube})_1$ and the second term $(\tau_{cube})_2$ are similar to those defined for octahedral slip except that the coefficient of S_{2j} and S_{3j} are excluded. A similar formulation has been used in Dame (1985).

Thus, at the high strain rate, the functional form of $(\tau_{cube})_1$ has the form defined in Eq. (3.17.b).

$$(\tau_{cube})_1 = \frac{|\delta+1|}{2}\left[A_{3t}\varphi_1(\dot{\varepsilon})\exp\left(\frac{-H_0}{kT}+V_{31}\right)\right] + \frac{|\delta-1|}{2}\left[A_{3c}\varphi_1(\dot{\varepsilon})\exp\left(\frac{-H_0}{kT}+V_{31}\right)\right] \tag{3.17.b}$$

where A_{3t}, A_{3c} and V_{31} are material constants.

At the low strain rate, the functional form of $(\tau_{cube})_2$ has the form below,

$$(\tau_{cube})_2 = \frac{|\delta+1|}{2}\left[A_{3cr}\varphi_2(\dot{\varepsilon})\exp\left(\frac{-H_0}{kT}+V_{32}\right)\right] + \frac{|\delta-1|}{2}\left[A_{4cr}\varphi_2(\dot{\varepsilon})\exp\left(\frac{-H_0}{kT}+V_{32}\right)\right] \tag{3.17.c}$$

where A_{3cr}, A_{4cr} and V_{32} are material constants.

For any given global stress state, the determination of the shear strain components $(\tau_{oct})_1$, $(\tau_{oct})_2$, $(\tau_{cube})_1$ and $(\tau_{cube})_2$, allows the determination of the ratios $\left(\frac{\sigma}{\tau_{RT}}\right)_{oct}$ and $\left(\frac{\sigma}{\tau_{RT}}\right)_{cube}$ defined in Eqs.(3.16.a) and (3.17.a) respectively. Since the slip factor Sf is defined to be the minimum of the above ratios, therefore knowledge of

these implies the knowledge of the slip factor Sf. Once Sf is known, the determination of the initial yield stress, for any arbitrary global stress state, is given from Eq.(3.8.a). These results are evaluated and compared with experimental data (when available) in Chapter VI for three SC nickel base superalloys.

3.3.2.7 – Definition of the strain rate functions $\varphi_1(\dot{\varepsilon})$ and $\varphi_2(\dot{\varepsilon})$

In the present work, the strain rate function $\varphi_1(\dot{\varepsilon})$ is defined as follows.

$$\varphi_1(\dot{\varepsilon}) = \tanh\left(r_0\left(\dot{\varepsilon} - \dot{\varepsilon}_0\right)\right) \tag{3.18.d}$$

where, r_0 and $\dot{\varepsilon}_0$ are material constants, and $\dot{\varepsilon}$ is a current strain rate.

The determination of the material constants above at the temperature of interest requires a set of initial yield stresses evaluated at different strain rates within the range covering low strain rate and high strain rate as well as intermediate strain rate. Because the lack of experimental data these constants will not be fully studied in this thesis. However, for the purpose of the present work, one will consider $r_0 = 4 .10^5$ and $\dot{\varepsilon}_0 = 10^{-8}\,s^{-1}$. The strain rate function $\varphi_2(\dot{\varepsilon})$ is defined as follows,

$$\varphi_2(\dot{\varepsilon}) = 1 - \varphi_2(\dot{\varepsilon}) \tag{3.18.e}$$

The representation of both strain rate functions $\varphi_1(\dot{\varepsilon})$ and $\varphi_2(\dot{\varepsilon})$ versus the strain rate $\dot{\varepsilon}$ is shown in Figure 3.11. From that graph, it can be seen that when $\dot{\varepsilon} > 10^{-5}\,s^{-1}$, $\varphi_1(\dot{\varepsilon})$ tends to +1 and $\varphi_2(\dot{\varepsilon})$ tends to 0. Inversely, when $\dot{\varepsilon} < 10^{-7}\,s^{-1}$, $\varphi_1(\dot{\varepsilon})$ tends to 0 and $\varphi_2(\dot{\varepsilon})$ tends to 1. In this work, emphasize is given on two main cases: the high strain rate ($\dot{\varepsilon} > 10^{-5}\,s^{-1}$) and the low strain rate ($\dot{\varepsilon} < 5\times10^{-7}\,s^{-1}$).

There are a total of twenty material constants required in the determination of slip factors. Because the lack of experimental data used at the temperatures of interest, only fourteen of them are evaluated in Chapter V, using independent parameters. For PWA 1480 at 593° C, the material constants for Sf at the high strain rate ($\dot{\varepsilon} = 8.33 \times 10^{-4} s^{-1}$) are evaluated in Chapter V. In the octahedral slip systems, one has $A_{1t} = 6.5682.10^3$ MPa, $V_{11} = 0.1498$ and $V_{12} = -0.0088$. The corresponding slip factor, Sf is plotted in Figure 3.12 along the [0 0 1]-[0 1 1] orientation boundary. Along that boundary, Sf is seen to be orientation dependent and that it reaches the minimum value around $\theta = 22.5°$.

Table 3.5 Material constants required in the determination of the slip factor for a f.c.c crystal.

Slip systems	Strain rate	First Invariant $I_{\{\sigma\}}$	Material Constants	
Octahedral	High	$I_{\{\sigma\}} > 0$	A_{1t}, V_{11}, V_{12}	
		$I_{\{\sigma\}} < 0$	A_{1c}, V_{21}, V_{22}	
	Low	$I_{\{\sigma\}} > 0$	A_{1cr}, V_{13}, V_{14}	
		$I_{\{\sigma\}} < 0$	A_{2cr}, V_{23}, V_{24}	
Cube	High	$I_{\{\sigma\}} > 0$	A_{3t}	V_{31}
		$I_{\{\sigma\}} < 0$	A_{3c}	
	Low	$I_{\{\sigma\}} > 0$	A_{3cr}	V_{32}
		$I_{\{\sigma\}} < 0$	A_{4cr}	
			r_0 $\dot{\varepsilon}_0$	

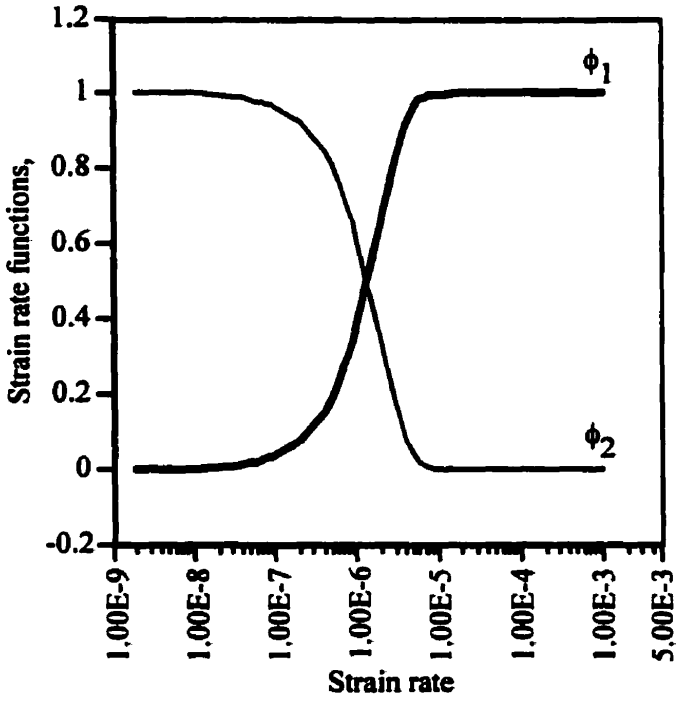

Figure 3.11 Variation of $\varphi_1(\dot{\varepsilon})$ and $\varphi_2(\dot{\varepsilon})$ with the strain rate.

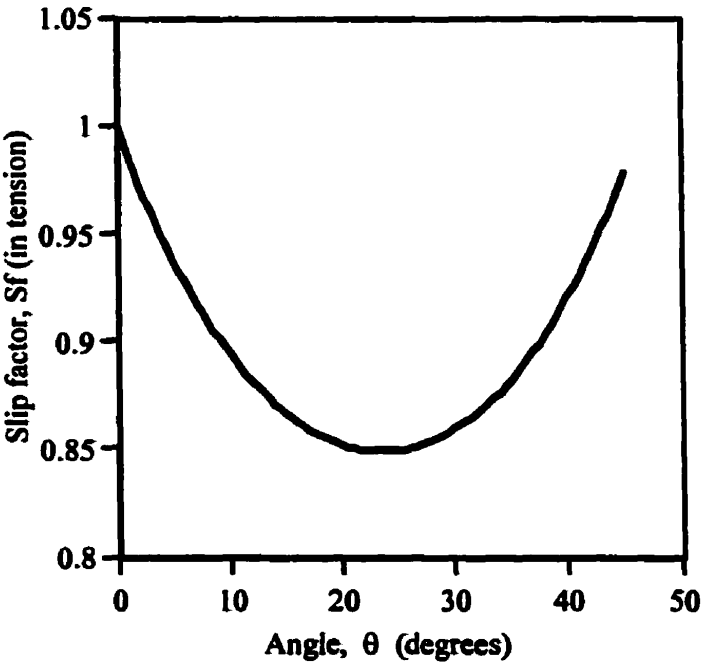

Figure 3.12 Orientation dependence of the slip factor, Sf (tension) in the octahedral slip system along the [0 0 1] – [0 1 1] orientation boundary.

CHAPTER IV

EXTENSION OF THE COMBINED APPROACH TO THE PLASTIC REGIME

In Chapter III, the theory of the combined approach (CA) was developed in 3D and applied to the determination of the initial yield stress in the SC nickel base superalloys. The predicted results, shown in Chapter VI, confirm that, the initial yield stress depends to the orientation as well as their crystal's structure. Also, using the equations developed in Leknitskii (1962), the orientation dependence of elastic constants has been confirmed. The initial values taken by the yield stress and elastic constants for a given applied load are determinant to the material responses beyond the yield surface. For such materials, the present chapter emphasizes two main points: (i) - the extension of the CA beyond the elastic regime, and (ii) - the general analysis of the behaviour of such materials. For that reason, the general formulation of the basic equations is first presented in the crystallographic co-ordinate system, and transformed after into the global co-ordinate system (system in which the applied stress is given). In order to determine the material constants of the model, the 3D form of the basic equations is reduced to one-dimensional form. The chapter starts with some useful definitions and transformation relations, and concludes with the one-dimensional form used for the determination of the material parameters of the model. This is done in Chapter IV.

4.1 – DEFINITIONS AND TRANSFORMATION RELATIONS

All the symbols used in this chapter remain the same as those used in Chapter III.

4.1.1 - Definitions

- Recall that the deviatoric stress vector, $\{\sigma'\}$, was defined in Eq.(3.2.a) as

$$\begin{cases} \{\sigma'\} = [N_0]\{\sigma\} = \sigma[N_0]\{e\} \\ \{\sigma'\} = \sigma\{u\} \quad \text{for } \{u\} = [N_0]\{e\} \end{cases} \tag{4.1.a}$$

where $[N_0]$ is a constant matrix, defined in Eq.(3.2.d), and $\{e\}$ is the cosine direction of the applied stress. Thus, using the same relation, the deviatoric back stress and the over-stress vectors may be expressed respectively as follows,

$$\{Y'\} = [N_0]\{Y\} = Y\{u\} \tag{4.1.b}$$

and,

$$\{\sigma' - Y'\} = [N_0]\{\sigma - Y\} = (\sigma - Y)\{u\} \tag{4.1.c}$$

4.1.2 – Transformation relations

- The stress and strain transformation relations from the crystallographic co-ordinate system (with * symbol) to the global co-ordinate system (without symbol) have been defined in Eq.(3.5.e) and Eq.(3.5.f) respectively as,

$$\{\sigma^*\} = [Q_c]\{\sigma\} = \sigma[Q_c]\{e\} \tag{4.1.d}$$

$$\{\varepsilon^*\} = [Q_d]\{\varepsilon\} = \varepsilon[Q_d]\{v\} \tag{4.1.e}$$

where $\{v$ and $\{e$ are unit vectors, and $[Q_c]$ and $[Q_d]$ are two orientation matrices defined in Eqs.(3.5.c) and (3.5.d).

- Let us set, $\{V\}$ to be a vector defined as

$$\{V\} = [Q_d]^{-1}[M][Q_c]\{u\} \tag{4.2.a}$$

Then its cosine director $\{v_0\}$ is given by the relation

$$\{v_0\} = \frac{[Q_d]^{-1}[M][Q_c]\{u\}}{\left\|[Q_d]^{-1}[M][Q_c]\{u\}\right\|} \tag{4.2.b}$$

A non unit vector, $\{w\}$ can be defined as,

$$\{w\} = \sqrt{3/2}\{v_0\} \tag{4.2.c}$$

- Three terms, $\mu_1(\theta,\psi)$, $\mu_2(\theta,\psi)$ and $\mu_3(\theta,\psi)$, termed orientation functions, are defined as follows,

$$\mu_1(\theta,\psi) = \sqrt{\frac{3}{2}([Q_c]\{u\})^t[M]([Q_c]\{u\})} \tag{4.3.a}$$

$$\mu_2(\theta,\psi) = \left\|[Q_d]^{-1}[M][Q_c]\{u\}\right\| \tag{4.3.b}$$

and,

$$\mu_3(\theta,\psi) = \sqrt{([Q_d]\{w\})^t[M]^{-1}[Q_d]\{w\}} \tag{4.3.c}$$

As observed in section 3.3.1.3 with $\mu_1(\theta,\psi)$, a brief review of the three orientation functions above shows that $\mu_2(\theta,\psi)$ and $\mu_3(\theta,\psi)$ depend also on the following three elements: the initial anisotropic state by means of the anisotropic matrix [M], the

change of the base system by means of the rotation matrices [Q_c] and [Q_d], and the applied stress direction by means of the unit vector { e }. None of the terms in these functions is related to the structure of the crystal. Consequently, these functions can be used to describe the behavior of the material at the macroscopic level. A graphic representation of $\mu_1(\theta, \psi)$, $\mu_2(\theta, \psi)$, and, $\mu_3(\theta, \psi)$ is shown in Figure 4.1 for PWA 1480 at 593° C along the [0 0 1]-[0 1 1] orientation boundary. These results confirm the orientation dependence of $\mu_1(\theta, \psi)$, $\mu_2(\theta, \psi)$, and, $\mu_3(\theta, \psi)$. Since the three orientation functions above are initial anisotropic state dependent (not shown in the graph), they are therefore temperature dependent.

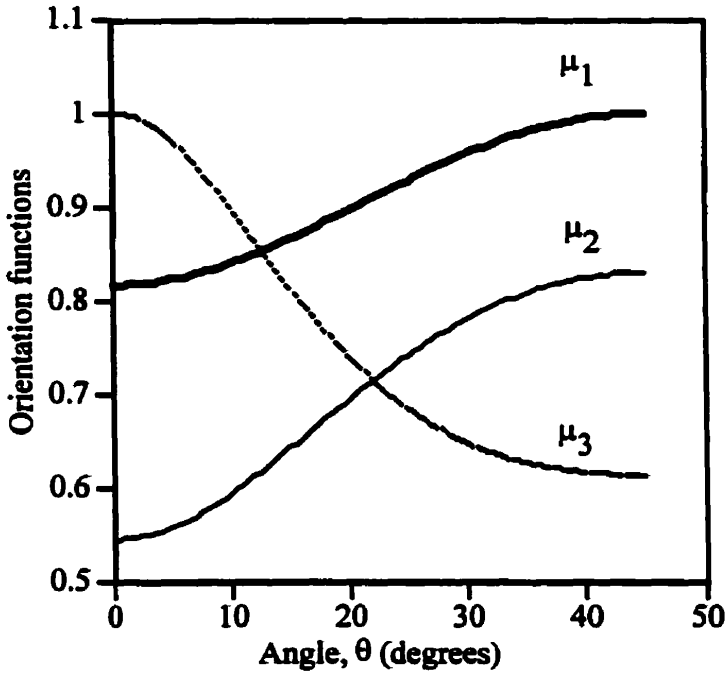

Figure 4.1 Orientation dependence of μ_1, μ_2 and μ_3 for $M_{11} = 5.25$, $M_{12} = 4.58$ and $M_{44} = 2.25$, along the [0 0 1] - [0 1 1] boundary of the stereographic triangle.

4.2 – MODELING OF SC MATERIALS

The principle of the CA has been defined in Chapter III as the extension of predictive models of isotropic material behavior to anisotropic materials such as single crystals. It has been shown in the same chapter that the structure of the CA requires two main elements: a viscoplastic model (assuming a yield function), and a slip factor. The viscoplastic model, usually based on the Continuum Mechanics Approach (CMA), describes the behavior on the macroscopic level and accounts for the viscous nature of the material. On the other hand, the slip factor based on the crystallographic approach, accounts for the micro-slip effect occurring within the crystal during the deformation process. Although the present study is principally devoted to SC nickel based super-alloys for gas turbine engines, a general presentation of the model will be nevertheless presented. Since the problem of the anisotropic formulation is very common for a variety of materials, it is the convenient to keep the general character for such studies.

For the purpose of the CA theory proposed in the present work, the unified Chaboche model has been retained, as the viscoplastic model required for its structure. The formulation of the basic equations used in the present model is similar to that developed in Nouailhas (1990), while its thermodynamic formulation is developed in Nouailhas and Freed (1990). In this work, the model is limited to small deformations, and, only two anisotropy types are taken into account. These are the initial anisotropy and that introduced by the flow stress (characterized by the Bauschinger effect). The present study is therefore limited to a brief presentation of the anisotropic constitutive equations and the evolutionary equations of the internal variables. The basic equations of Chaboche's model are expressed in the crystallographic co-ordinate system. Since the applied stress is usually given in the global co-ordinate system, however, it is convenient to express these basic equations in the global co-ordinate system. This can be done using the stress-strain transformation relations defined in Eqs.(3.5). The assumption made in this study is that the theory is unified and thus the total strain rate, $\{\dot{\varepsilon}^*\}$, may be

decomposed into two components: the elastic strain rate $\{\dot{\varepsilon}^{e*}\}$ and the inelastic strain rate $\{\dot{\varepsilon}^{i*}\}$. That may be expressed in the vector form as

$$\{\dot{\varepsilon}^{*}\} = \{\dot{\varepsilon}^{e*}\} + \{\dot{\varepsilon}^{i*}\} \tag{4.4}$$

4.2.1 - The elasticity law

The elasticity law is generally known. It is governed in the crystallographic co-ordinate system defined in Chapter III, by the constitutive equation

$$\{\dot{\varepsilon}^{e*}\} = [D]^{-1}\{\dot{\sigma}^{*}\} \tag{4.5.a}$$

where $[D]^{-1}$ is the stiffness matrix inverse, and $\{\dot{\sigma}^{*}\}$ is the applied stress rate vector. Using the transformation relationships defined in Eqs.(4.1.e) and (4.1.f), then Eq.(4.5.a) may be rewritten in the global coordinate system as

$$\{\dot{\varepsilon}^{*}\} = \dot{\sigma}\,[Q_d]^{-1}[D]^{-1}[Q_c]\{e\} \tag{4.5.b}$$

4.2.2 - The yield function

The yield function F, used in the CA theory, is a modified form of the Lee and Zaverl yield function f defined in Eq.(3.9.c). F differs to f only by the slip factor Sf, defined in Chapter III. Since it has been shown previously that Sf accounts for micro-slip in the crystal, then conversely to f the yield function F takes into account the properties of the crystal's structure. Similarly as the Lee and Zaverl's yield function f, F defines a yield surface within which material responses are elastic. Furthermore, it is parameterized by the isotropic variable $\hat{R}$ and the kinematic variable $\{Y\}$. For SC material, the von Mises criterion commonly used is replaced by the yield function F that may be seen as the generalization of Hill's criteria. In the vector form, one obtains

$$F = \left[\frac{3}{2} \{\sigma^{*'} - Y^{*'}\}^t [M] \{\sigma^{*'} - Y^{*'}\} \right]^{1/2} - Sf(\theta, \varphi) \hat{R}(p) \qquad (4.6.a)$$

Where $\{\sigma'^*\}$ and $\{Y'^*\}$ are respectively the deviatoric and the back stress in the crystallographic coordinate system, $Sf(\theta, \varphi)$ is the slip factor, $\hat{R}(p)$ is the isotropic hardening /softening variable and $[M]$ is a fourth order tensor defined in Eq.(3.10.a). Recall that, $[M]$ is introduced to describe the initial anisotropy and eventually an induced anisotropy of the material according to whether their components are constant or variable. At this level, different possibilities may be observed for the induced anisotropy. For example in Lee and Zaverl's formulation, the anisotropic tensor $[M]$ is introduced as a new internal variable with an associate evolutionary equation, whereas in Baltov and Sawezuk's (1961) model, tensor components are defined as functions of elastic deformation. In short, whatever the formulation above, $[M]$ allows the distortion of the yield surface. For purpose of the present work, $[M]$ is not associated to any evolutionary equation. Therefore, the present model cannot predict the distortion of the yield surfaces usually observed experimentally. Eq.(4.6.b) can be reduced in the global coordinate system to the simple form:

$$F = |\sigma - Y| \, \mu_t(\theta, \psi) - Sf(\theta, \psi) \hat{R}(p) \qquad (4.6.b)$$

This formulation confirms the statement wording earlier stating that both the yield functions f and F differ only by the slip factor $Sf(\theta, \varphi)$.

4.2.3 - The flow law

The yield surface tells us the combination of stresses that initiate plastic flow. To mathematically describe the subsequent plastic behavior of the material requires specification of the flow law. For many materials, the flow law is given in terms of a plastic-potential function of the stress components, such that the increment of plastic

strain is proportional to the gradient of the potential. i.e. the direction of plastic strain is normal to the potential function. Taking the potential function to be a convex surface in stress space, convexity a priori satisfies requirement for positive dissipative from viscoplastic flow. In many cases, the potential function is taken to be the yield surface itself. The flow law is then said to be associative. Most of the viscoplastic theories found in the literature (such as Lee and Zaverl's defined in Chapter III) use that assumption and the normality condition is written as,

$$\left\{\dot{\varepsilon}^{i*}\right\}=\dot{\lambda}\left\{\frac{\partial f}{\partial \sigma^{*}}\right\} \tag{4.7.a}$$

where $\left\{\dot{\varepsilon}^{i*}\right\}$ is the inelastic strain rate vector, $\dot{\lambda}$ is a scalar, f is the yield function, and $\left\{\sigma^{*}\right\}$ is a stress vector.

However, for some theories such as those used to describe rocks, concrete, and soils, the normality is violated and the basis of convexity is destroyed. The non-associative flow rule provides a better representation of their plastic deformation. Given the anisotropic properties observed in SC materials, and the shape of the subsequent yield surface, the non-associative flow law is used in this work. The Lee and Zaverl yield function is used as the potential function. Therefore, the flow law can be written in the crystallographic co-ordinate system as,

$$\left\{\dot{\varepsilon}^{i*}\right\}=\begin{cases}\dfrac{3}{2}\left\langle\dfrac{F}{K}\right\rangle^{n}\dfrac{[M]\{\sigma'^{*}-Y'^{*}\}}{\sqrt{\dfrac{3}{2}(\{\sigma'^{*}-Y'^{*}\})^{t}[M](\{\sigma'^{*}-Y'^{*}\})}} & \text{if } F>0\\ 0 & \text{if } F\le 0\end{cases} \tag{4.7.b}$$

where F is the yield function defined in Eq.(4.6.b). Transforming the over stress vector $\{\sigma'^{*}-Y'^{*}\}$ and using the transformation relations and the deviatoric properties presented previously, Eq.(4.7.b) may be expressed in the global coordinate system as,

$$\{\dot{\varepsilon}^{i}\}=\frac{3}{2}\left\langle\frac{F}{K}\right\rangle^{n}\frac{(\sigma-Y)[Q_d]^{-1}[M][Q_e]\{u\}}{|\sigma-Y|\sqrt{\frac{3}{2}([Q_e]\{u\})^{t}[M]([Q_e]\{u\})}} \qquad (4.7.c)$$

Combining Eqs.(4.2.b), (4.2.c), (4.3.a), (4.3.b), (4.6.b) and (4.7.c), then the flow law may be rewritten in the form,

$$\{\dot{\varepsilon}^{i}\}=\left\langle\frac{\mu_1|\sigma-Y|-Sf\hat{R}}{K}\right\rangle^{n}\left(\sqrt{\frac{3}{2}}\frac{\mu_2}{\mu_1}\right)\left(\frac{\sigma-Y}{|\sigma-Y|}\right)\left(\sqrt{\frac{3}{2}}\{v_0\}\right) \qquad (4.7.d)$$

Furthermore, setting

$$\operatorname{sgn}(\sigma-Y)=\frac{(\sigma-Y)}{\|\sigma-Y\|}=\pm 1 \qquad (4.7.e)$$

and

$$\dot{\bar{\varepsilon}}^{i}=\left\langle\frac{|\sigma-Y|-\frac{Sf}{\mu_1}\hat{R}}{\frac{K}{\left(\sqrt{\frac{3}{2}}\mu_2\mu_1^{\,n-1}\right)^{1/n}}}\right\rangle^{n} \qquad (4.7.f)$$

After rearranging Eq.(4.7.d), the flow law can be expressed as

$$\left\{\dot{\varepsilon}^{i}\right\}=\begin{cases}\dot{\bar{\varepsilon}}^{i}\{w\}\operatorname{sgn}(\sigma-Y) & \text{if} \quad F>0\\ 0 & \text{if} \quad F>0\end{cases} \tag{4.7.g}$$

where $\dot{\bar{\varepsilon}}$ is the effective inelastic strain rate, and $\{w\}$ is the vector defined in Eq.(4.2.c).

4.2.4 - The Accumulated inelastic strain

The accumulated inelastic strain rate, $\dot{p}$, is governed in the crystallographic co-ordinate system by the equation,

$$\dot{p}=\left[\frac{4}{9}\left\{\dot{\varepsilon}^{i}*\right\}^{t}[M]^{-1}\left\{\dot{\varepsilon}^{i}*\right\}\right]^{1/2} \tag{4.8.a}$$

Using Eq.(4.7.g) and the transformation relations defined previously, one may have after substitution,

$$\begin{aligned}\dot{p}&=\sqrt{\left(\dot{\bar{\varepsilon}}^{i}\{w\}\right)^{t}[Q_d]^{t}[M]^{-1}[Q_c]\left(\dot{\bar{\varepsilon}}^{i}\{w\}\right)} \qquad \text{(i)}\\ &=\left|\dot{\bar{\varepsilon}}^{i}\right|\sqrt{\left([Q_d]\{w\}\right)^{t}[M]^{-1}[Q_d]\{w\}} \qquad \text{(ii)}\end{aligned} \tag{4.8.b}$$

Combining Eqs.(4.3.c) and (4.8.b), one obtains, after rearranging, the simple form

$$\dot{p}=\left|\dot{\bar{\varepsilon}}^{i}\right|\mu_3(\theta,\psi) \tag{4.8.c}$$

where μ_3 is the orientation function defined in Eq.(4.3.c).

4.2.5 - The evolutionary equations

4.2.5.1 - The back stress

The evolution of the yield surface centre is given by the non-linear kinematic hardening equation. In the 3D form, the anisotropy is introduced in the back stress variable by two fourth order tensors $[N_a]$ and $[N_b]$. The same formulation has been used in Nouailhas (1990). In the crystallographic co-ordinate system, these two matrices are similar to the anisotropic matrix $[M]$, defined in Eq.(3.10.a). In the vector form, the kinematic evolutionary equation used in this work, without the recovery term, is expressed in the crystallographic coordinate system by the equation,

$$\{\dot{Y}'^*\}=\frac{2}{3}[N_a]\{\dot{\varepsilon}^{i}{}^*\}-[N_b]\{Y'^*\}\dot{p} \qquad (4.9.a)$$

Since the matrices $[N_a]$ and $[N_b]$ are unknown, it is possible to express their components as a function of the material constants A and C used in the back stress evolutionary equation of Chaboche's model defined in Eq.(2.20.f). The 3D form of that equation in terms of the material constants may be expressed in vector form as,

$$\{\dot{Y}'^*\}=CA\{\dot{\varepsilon}^{i}{}^*\}-C\{Y'^*\}\dot{p} \qquad (4.9.b)$$

Using the deviatoric back stress properties defined in Eq.(4.1.b) and the transformation relation given in Eq.(4.1.d), then, after transformation and reduction, both Eqs.(4.9.a) and (4.9.b) can be written in the global coordinate system respectively as follows,

$$\dot{Y}\{u\}=\frac{2}{3}\left([Q_c]^{-1}[N_a][Q_d]\{w\}\right)\dot{\bar{\varepsilon}}^{i}-\left([Q_c]^{-1}[N_b][Q_c]\{u\}\right)Y\dot{p} \qquad (4.9.c)$$

$$\dot{Y}\{u\}=CA\left([Q_c]^{-1}[Q_d]\{w\}\right)\dot{\bar{\varepsilon}}^{i}-C\left([Q_c]^{-1}[Q_c]\{u\}\right)Y\dot{p} \qquad (4.9.d)$$

$$b_{11} - b_{12} = C, \text{ and } a_{11} - a_{12} = \frac{3}{2}AC \tag{4.10.d}$$

- **Tension test along $[\bar{1}\,1\,1]$ orientation**

Along the $[\bar{1}\,1\,1]$ orientation, $\theta_0 = 45°$ and $\psi_0 = 35.26°$. The corresponding rotation matrices $[Q_c]$ and $[Q_d]$ are populated. Vectors $\{\sigma\}$, $\{Y\}$, $\{e\}$ and $\{w\}$ remain unchanged as noted along the $[0\,0\,1]$ orientation.

Performing the same calculation as in the previous case, one obtains after rearranging,

$$a_{44} = \frac{3}{2}AC, \quad \text{and} \quad b_{44} = C \tag{4.11.a}$$

All of the components are therefore known. The anisotropic matrices $[N_a]$ and $[N_b]$ may be expressed as follows:

$$[N_a] = AC[N_{a0}] \text{ and } [N_b] = C[N_{b0}] \tag{4.11.b}$$

where $[N_{a0}]$ and $[N_{b0}]$ are constant matrices defined as follows,

$$[N_{a0}] = \begin{bmatrix} 1 & -\frac{1}{2} & -\frac{1}{2} & 0 & 0 & 0 \\ -\frac{1}{2} & 1 & -\frac{1}{2} & 0 & 0 & 0 \\ -\frac{1}{2} & -\frac{1}{2} & 1 & 0 & 0 & 0 \\ 0 & 0 & 0 & 3/2 & 0 & 0 \\ 0 & 0 & 0 & 0 & 3/2 & 0 \\ 0 & 0 & 0 & 0 & 0 & 3/2 \end{bmatrix} \tag{4.11.c}$$

and

4.3 – BASIC EQUATIONS

From the foregoing results, the basic equations of the Chaboche's model based on the CA theory may be summarized as follows

$$\{\dot{\varepsilon}\} = \{\dot{\varepsilon}^e\} + \{\dot{\varepsilon}^i\} \tag{4.13.a}$$

$$\{\dot{\varepsilon}^e\} = [Q_d][D]^{-1}[Q_c]\{\dot{\sigma}\} \tag{4.13.b}$$

$$F = |\sigma - Y|\,\mu_1 - Sf\hat{R}(p) \tag{4.13.c}$$

$$\{\dot{\varepsilon}^i\} = \begin{cases} \left\langle \dfrac{|\sigma - Y| - \left(\dfrac{Sf}{\mu_1}\right)\hat{R}}{K\left(\sqrt{\dfrac{3}{2}}\,\mu_2\,\mu_1^{\,n-1}\right)^{1/n}} \right\rangle^n \{w\}\,\mathrm{sgn}(\sigma - Y) & \text{if } F > 0 \\ 0 & \text{if } F \le 0 \end{cases} \tag{4.13.d}$$

$$\dot{p} = \left|\dot{\bar{\varepsilon}}^i\right|\mu_3 \tag{4.13.e}$$

$$\{\dot{Y}^i\} = \frac{2}{3}AC\left([N_{a0}][Q_d]\{w\}\right)\dot{\bar{\varepsilon}}^i - \mu_3\, C\left([N_{b0}][Q_c]\{u\}\right)Y\left|\dot{\bar{\varepsilon}}^i\right| \tag{4.13.f}$$

$$\dot{\hat{R}} = B(Q - \hat{R})\,\mu_3\left|\dot{\bar{\varepsilon}}^i\right| \tag{4.13.g}$$

where K is the over stress parameter, n is a strain rate sensitivity exponent, A is the back stress parameter, C is the back stress coefficient, B is the drag stress coefficient, and Q is the saturated value of $\hat{R}$.

The six material constants above used in the basic equations of Chaboche's viscoplastic model based on the CA theory are similar to those for isotropic materials obtained in Eqs.(2.20). Similarly as in that case, these material constants are temperature dependent. In addition to the three elastic constants (E, G, v), the six material constants above are to be determined. As mentioned in section 2.4.2 in Chapter II, these material constants (capital letters) used in the 3D form of the model can be determined using simple tests along the [0 0 1] orientation. In the following sections, a major effort is made in order to reduce the 3D basic equations of the model listed in Eqs.(4.13) into a one-dimensional form, and to relate their corresponding material parameters with the material constants.

4.3.1 – Reduction of the basic equations.

As mentioned previously, the determination of the material constants used in the present model required a set of simple tests experimental data. Since the set of the experimental data required can be generated easily using simple tests such as tensile test, the stabilized fully reversed cyclic test, the creep test and so on, it is therefore convenient to reduce the 3D form of the basic equations to a one-dimensional form. To do so let us consider an arbitrary direction (D) with the director cosines $\{e_0\}$, the reduction of the 3D basic equations onto the one dimension form can be done by projection of the basic equations along the direction (D). By multiplying the left hand side of both part of each equation with a transpose of $\{e_0\}$, one obtains

$$\{e_0\}^t\{\dot{\varepsilon}\}=\{e_0\}^t\left(\{\dot{\varepsilon}^e\}+\{\dot{\varepsilon}^i\}\right)=\dot{\varepsilon} \tag{4.14.a}$$

$$\{e_0\}^t\{\dot{\varepsilon}^e\}=\{e_0\}^t[Q_d][D]^{-1}[Q_c]^{-1}\{\dot{\sigma}\}=\dot{\varepsilon}^e \tag{4.14.b}$$

And for $F > 0$,

$$\{e_0\}^t\{\dot{\varepsilon}^i\} = \begin{cases} \dot{\bar{\varepsilon}}^i \{e_0\}^t\{w\}\mathrm{sgn}(\sigma - Y) & \text{if } F > 0 \\ 0 & \text{if } F \le 0 \end{cases} \tag{4.14.c}$$

$$\{e_0\}^t\{u\}\dot{Y} = \frac{2}{3} A C \left(\{e_0\}^t [Q_c]^{-1} [N_{a0}] [Q_d] \{w\}\right) \dot{\bar{\varepsilon}}^i - \mu_3 C \left(\{e_0\}^t [Q_c]^{-1} [N_{b0}] [Q_c] \{u\}\right) Y |\dot{\bar{\varepsilon}}^i| \tag{4.14.d}$$

And setting

$$R = \frac{S_f}{\mu_1} \hat{R} \tag{4.15.a}$$

$$k = \frac{K}{\left(\sqrt{\frac{3}{2}} \mu_2 \mu_1^{\,n-1}\right)^{1/n}} \tag{4.15.b}$$

$$a = \frac{2}{3} \frac{A}{\mu_3} \left(\frac{\{e_0\}^t [Q_c]^{-1} [N_{a0}] [Q_d] \{w\}}{\{e_0\}^t [Q_c]^{-1} [N_{b0}] [Q_c] \{u\}} \right) \tag{4.15.c}$$

$$c = \mu_3 C \left(\frac{\{e_0\}^t [Q_c]^{-1} [N_{b0}] [Q_c] \{u\}}{\{e_0\}^t \{u\}} \right) \tag{4.15.d}$$

$$b = \mu_3 B \tag{4.15.e}$$

and

$$q = \frac{Sf}{\mu_1} Q \tag{4.15.f}$$

Eqs.(4.15) define the relationship between the material parameters a, b, c, k, and q and the material constants A, B, C, K, and Q respectively along the direction $\{\mathbf{e}_0\}$. As an example, along the principal orientation [0 0 1], $\theta = 0$ and $\psi = 0$. The relations above may be reduced to:

$$a = \frac{3}{2}A \quad , \quad k = \left(\frac{3}{2}\right)^{\frac{n+1}{2n}} K, \quad q = \sqrt{\frac{3}{2}}\,Q$$
$$b = B, \qquad c = C, \qquad R = \sqrt{\frac{3}{2}}\,\hat{R} \tag{4.15.g}$$

4.3.2 – One-dimensional form of the basic equations

The relations above are similar to those presented in Eqs.(2.26) for an isotropic material. The combination of Eqs.(4.13), Eqs.(4.14) and Eqs.(4.15) gives after rearranging the reduced form of the basic equation of the model along the unit vector $\{\mathbf{e}_0\}$. One obtains, after simplification,

$$\dot{\varepsilon} = \dot{\varepsilon}^{e} + \dot{\varepsilon}^{i} \tag{4.16.a}$$

$$\dot{\varepsilon}^{e} = \dot{\sigma}\left(\{\mathbf{e}_0\}^{t}[Q_d]^{-1}[D]^{-1}[Q_c]\{\mathbf{e}\}\right) \tag{4.16.b}$$

$$f = |\sigma - Y| - R \tag{4.16.c}$$

$$\dot{\varepsilon}^{i} = \begin{cases} \left\langle \frac{F}{k} \right\rangle^{n} \operatorname{sign}(\sigma - Y) & \text{if } F > 0 \\ 0 & \text{if } F \le 0 \end{cases} \tag{4.16.d}$$

$$\dot{p} = \left|\dot{\bar{\varepsilon}}\right| \mu_3(\theta, \psi) \tag{4.16.e}$$

$$\dot{Y} = c\left(a\dot{\bar{\varepsilon}}^{i} - Y\left|\dot{\bar{\varepsilon}}^{i}\right|\right) \tag{4.16.f}$$

$$\dot{R} = b(q - R)\left|\dot{\bar{\varepsilon}}^{i}\right| \tag{4.16.g}$$

where k is the over stress parameter, n is the strain rate sensitivity exponent, a is the back stress parameter, c is the back stress coefficient, b is the drag stress coefficient, and q is the saturated value of R .

From Eqs.(4.16) it is seen that the 3D form of the basic equations of the model for a SC material can be reduced to one-dimensional form as in the case of isotropic materials as, defined in Eqs.(2.27) in Chapter II. However, there are some particularities in this case that must be pointed out.

As for isotropic material, the material parameters are all temperature dependent. In addition, the material parameters a, b, c, k and q can be related to the constants A, B, C, K and Q respectively. Also, in the present case, aside from the exponent n, all of the parameters are orientation dependent, and that according to Eqs.(4.15), that orientation dependence is based essentially on the orientation functions μ_1, μ_2 and μ_3. Since A, B, C, K, Q and n are constants, then from the relations above, it can be seen that b and c are proportional to μ_3, a is inversely proportional to μ_3, while k is inversely function of μ_1 and μ_2, and q is inversely proportional to μ_1. The orientation dependence of the ratios a/A, b/B, c/C, k/K and q/Q are shown in Figures 4.2 (a) and (b).

It is important to note that q is the only parameter which is explicitly function to the structure of the crystal by means of the slip factor Sf, q being the saturated value of the drag stress R (which is corrected by Sf) then that result should be expected.

4.3.3 – Relationship between M_{11} and M_{12}

Another important remark concerns the relationship between the components of the anisotropic matrix [M] defined in Chapter III. In the present work, the material is assumed to have equal properties along the principal axis in the stereographic co-ordinate system. This is equivalent to saying that, along the principal axis, the basic equations of the model based on the CA must be similar to those obtained for the isotropic material. In order to reach that condition, Eq.(4.14.b) should be identical to Eq.(2.26.d).

$$\frac{K}{\left(\sqrt{\frac{3}{2}}\,\mu_2\,\mu_1^{\,n-1}\right)^{1/n}} = \frac{K}{\left(\frac{2}{3}\right)^{\frac{n+1}{2n}}} \tag{4.17.a}$$

Along the [0 0 1] orientation, the orientation functions $\mu_1(\theta, \psi)$ and $\mu_2(\theta, \psi)$, defined previously, may be evaluated as a function of M_{ij}. That gives, after rearranging,

$$\begin{aligned} \mu_1(0,0) &= \sqrt{\frac{3}{2}\left(\left[I_D\right]\frac{2}{3}\{w\}\right)^t [M]\left(\left[I_D\right]\frac{2}{3}\{w\}\right)} \\ &= \sqrt{M_{11} - M_{12}} \end{aligned} \tag{4.17.b}$$

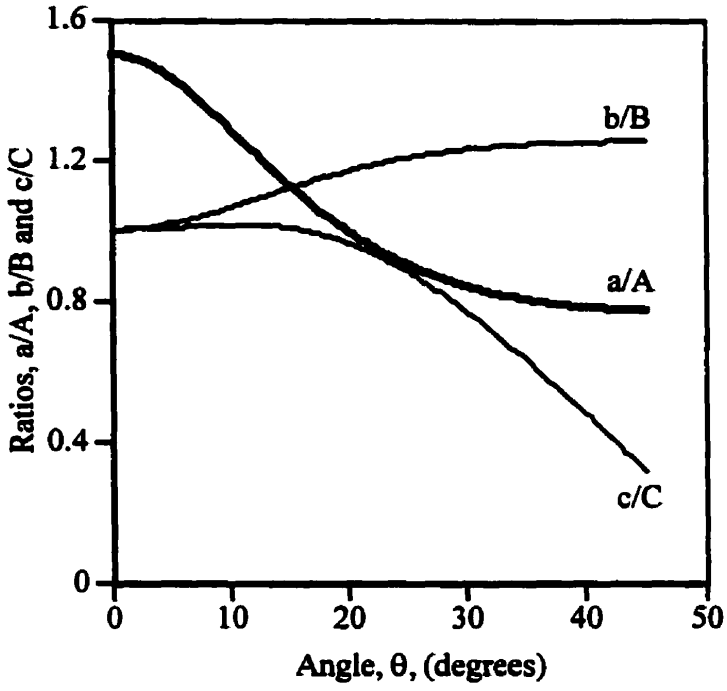

(a)

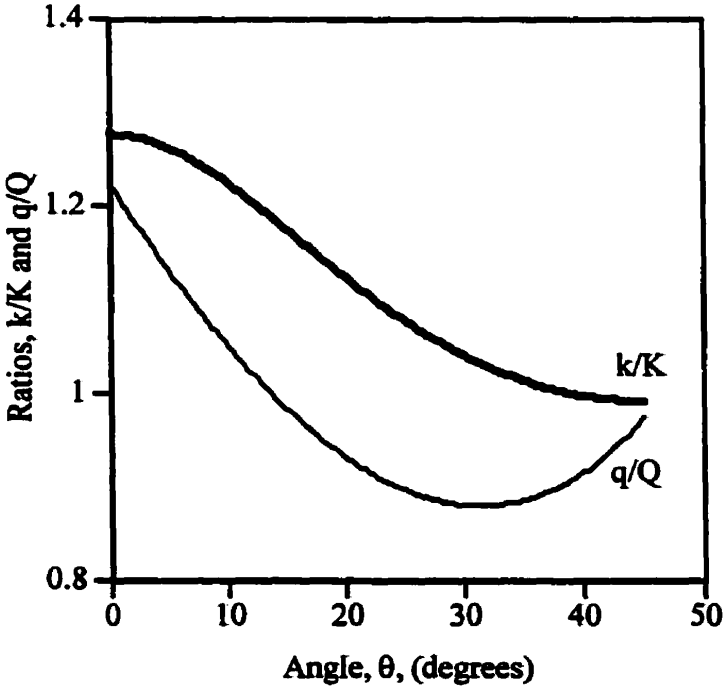

(b)

Figure 4.2 Orientation dependence of the material parameters a, b, c in (a) and k and q in (b) used in the CA for SC material along the [0 0 1] - [0 1 1] orientation boundary of the stereographic triangle.

similarities observed between the reduced uniaxial forms of the basic equations obtained with the CA (for SC materials) and the original theory (for isotropic materials) are noteworthy. The only exception is the orientation dependence of the material parameters a, b, c, k, q in the case of the CA. The readers may observe that, if one assumes the material to be isotropic, the relationships between material parameters (small letters) and material constants (capital letters) in Eqs.(4.15) will be identical to those defined in Eqs.(2.26). The next section will focus on the determination of the material parameters a, b, c, k, n and q, using available experimental data of nickel base super-alloys along the [0 0 1] orientation.

CHAPTER V

EXPERIMENTAL DATA AND MATERIAL CONSTANTS

The determination of most of the material parameters identified so far requires a series of simple tests (at the temperature of interest) to create a sufficient database from which to be evaluated. In the present work, these constants can be evaluated into three distinct groups: (i) - independent parameters, (ii) – parameters related to the slip factor, and (iii) the material parameters of the model.

- The first group deals with parameters such as elastic constants and the initial yield stress (in tension/compression) along some orientations, such as $[0\,0\,1]$, $[0\,1\,1]$ and $[\bar{1}\,1\,1]$. All parameters used in that group are taken from the literature and will be used in the evaluation of some parameters of the two other groups.
- In the second group, constants are related to the slip factor Sf, defined in Chapter III and are evaluated using principally independent parameters; and finally,
- In the third group the material constants, related to the model are developed using simple tests and specific assumptions.

In general, approaches used are not unique; rather, it could simply be considered appropriate for the kind of data available. Because of the lack of experimental data available in the literature, three single crystal nickel base superalloys are widely used in this work. These are Rene N4, PWA 1480, and an earlier version of Rene N4, designated as Rene N4 VF317. No experimental tests were conducted with these materials. A fully detailed study of chemical and heat treatment of these superalloys will be referred to the original references.

This chapter is divided into three main parts: the first part deals with the presentation of the material used. The second part deals with the evaluation of the material constants related to the slip factor and the third part presents the evaluation of the material parameter used in the basic equations of the model.

5.1 – EXPERIMENTAL DATA

5.1.1 – PWA 1480

For the purpose of the present work, the experimental data available for PWA 1480 at 593° C are used for orientation dependence of the initial yielding and tension compression asymmetry. At that temperature, the orientation dependence of the initial yielding and the asymmetry between tension and compression are important, and the repeatability of the data is better as well. In addition, elasticity components D_{ij} of the same material are available in a wide range of temperatures and therefore are used for the determination of elastic constants for all of the other superalloys used in this work. Experimental data come from Milligan and Antolovich (1987), Jordan and Walker (1992), and Swanson et al. (1986). A summary of its chemical composition and heat treatment was given in Tables 1.1 and 1.2 in Chapter I.

5.1.2 – Rene N4

Most of the experimental data available for Rene N4 are from tension and creep tests, performed with the specimens oriented in the [0 0 1] material direction. The two temperatures at which the best database for Rene N4 is currently available are 760° C and

980° C. For Rene N4 at 760 °C, the cyclic response, as well as the stress-strain response for several orientations in both tension and compression, were determined by Miner, Voigt, Gayda and Gabb (1986.a), Miner, Gabb, Gayda and Hemker (1986.b), and Gabb, Gayda and Miner (1986).

These results were drawn from seven tests in three different orientations. The specimens had a cylindrical gage section 19 mm long by 4.7 mm in diameter. The tests were run at a constant cross head rate with an initial strain rate of about $2x10^{-4}$/sec. Data recorded were load and crosshead displacement. Plastic strain was estimated using the offset from the elastic loading line, as well as the specimen gage length.

It was confirmed by TEM analysis that slip in the specimen oriented along the [0 0 1] and [0 1 1] directions was in the octahedral system, while cube slip was observed with orientations near the $[\bar{1}\,1\,1]$ orientation. Tensile axis rotation was observed in the specimens tested to failure. The variability of results between crystals was as large as 23%. The discrepancy, which is attributed to the orientation and tension/compression asymmetry is typical of other single crystals near this temperature; however, at 980° C the orientation and asymmetry properties are much less important and Schmid's law appears to be applicable as shown in Nouailhas (1990). Stresses beyond yield increased initially and then flattened out for the [0 0 1] and $[\bar{1}\,1\,2]$ specimens. The serrated yielding that is observed in PWA 1480 and MAR M200, is attributed to the operation of a small number of slip planes.

The fatigue response at 760° C, reported in part II of the work of Miner, Voigt, Gayda, and Gabb (1986.a), consisted of the monotonic yield points for specimens at six orientations in tension and compression and first cyclic hysteresis loops for three orientations. The specimens had a cylindrical gage section 15 mm long by 5mm in diameter.

The tensile and compressive yield stresses at several orientations are shown in Table 5.1.

The [0 0 1] specimen had the greatest initial yield in tension and the [0 1 1] specimen was strongest in compression. Both of these specimens displayed significant tension /compression asymmetry while $[\bar{1}\,1\,1]$, [0 2 3] and $[\bar{2}\,3\,6]$ specimens displayed very little or none. The initial hysteresis loops for [0 0 1], $[\bar{1}\,4\,5]$, $[\bar{2}\,3\,6]$ and [0 2 3] specimens had serrated flow characteristics. All specimens displayed slight hardening with continued cycling, which increased with increasing strain range but was generally less than 10%. For all tests, the response stabilized well before the half-life. A summary of chemical composition and heat treatment of Rene N4 is also given in Table 1.1 in Chapter I.

Table 5.1 Monotonic yield strength (0.02 % offset) of Rene N4 at 760° C. From Gabb et al. (1986.a).

Orientation	Tensile Yield MPa	Compressive Yield MPa
$[0\,0\,1]$	956	818
$[0\,1\,1]$	748	905
$[0\,2\,3]$	695	747
$[\bar{1}\,1\,1]$	817	842
$[\bar{2}\,3\,6]$	716	714
$[\bar{1}\,4\,5]$	656	792

5.1.3 – Rene N4 VF317

Most of the experimental data available for Rene N4 VF317 at 760 °C are tensile stress-strain and creep data at three distinct orientations. These data, determined in Wukusick (1980) have been used respectively by Dame (1985), Dame and Stouffer (1986) and Sheh (1988). As observed in Table 1.1 in Chapter I, there is a slight chemical difference between Rene N4 and Rene N4 VF 317. That chemical difference may be the source of the differences in the observed response. The tensile response reported in Miner, Voigt, Gayda and Gabb (1986) for a specimen oriented along [0 0 1] direction was about 30 % weaker than VF 317 in tension. Since the response characteristics are significantly different for the two data sets, it was not possible to develop a single set of material constants for the constitutive model. In this work the Miner, Voigt, Gayda and Gabb data are used to develop constants and test the model for octahedral and cube slip at high strain rates in tension, compression and cyclic. The Rene N4 VF 317 data are used to develop the constants for octahedral slip at high strain rates (in tension) and low strain rates (in creep). A summary of structural, chemical and heat treatment studies of these super-alloys is presented in Chapter I. Their mechanical properties are also reviewed in that chapter.

5.2 - DERIVATION OF MATERIAL CONSTANTS USED IN THE SLIP FACTOR

It was shown in Chapter III that the constitutive slip factor, Sf, is developed on the individual slip systems. That was essential in order to establish the relationship between the applied stress tensor and local shear stresses and the relationship between local slip rates and the global strain rate tensor. As an example, all of the RSS components observed in the whole crystal are evaluated for an applied stress of 100 MPa and listed in Table 5.2 for four distinct directions. From the same table, one may understand why octahedral slip alone is found near the $[0\,0\,1]$ orientation (no stress on the cube planes) while cube slip alone is found near the $[\bar{1}\,1\,1]$ direction (dominant stress on the cube planes). The local stress in every slip direction on each of the octahedral and cube planes

Table 5.2 Local stress for an applied stress of 100 MPa in four distinct directions.

Orientation	Slip System	[0 0 1]	[0 1 1]	[$\bar{1}$ 1 1]	[$\bar{1}$ 2 3]
(1 1 1)[$\bar{1}$ 0 1]	1	- 40.82	- 40.82	- 27.22	- 46.66
	2	0	40.82	27.22	29.16
	3	40.82	0	0	17.50
	4	- 40.82	0	0	- 27.50
	5	0	- 40.82	0	- 9.16
	6	40.82	40.82	0	36.66
	7	- 40.82	0	0	- 16.67
	8	0	0	- 27.21	- 20.83
	9	40.82	0	27.22	37.50
	10	- 40.82	0	27.22	- 7.51
	11	0	0	0	0.83
	12	40.82	0	- 22.22	6.67
(1 1 1)[$\bar{1}$ 2 1]	13	- 23.57	23.57	15.72	6.67
	14	- 23.57	- 11.79	15.72	- 9.14
	15	47.14	- 11.79	- 31.43	2.41
	16	- 23.57	0	15.71	- 4.81
	17	47.14	35.36	15.72	42.81
	18	- 23.57	- 35.36	- 31.43	- 38.00
	19	47.14	35.36	15.72	48.59
	20	- 23.57	- 35.36	15.71	- 14.91
	21	- 23.57	0	- 31.42	- 33.67
	22	- 23.57	- 11.79	0	- 9.14
	23	- 23.57	23.57	0	- 10.59
	24	47.14	- 11.79	0	19.73
(0 1 0)[$\bar{1}$ 0 1]	25	0	35.36	0	8.66
	26	0	35.36	47.14	43.29
	27	0	35.36	0	17.32
	28	0	35.36	47.14	34.36
	29	0	35.36	- 47.14	- 25.97
	30	0	35.36	0	- 8.66

$$\{\tau\} = \pm [X][Q_c]\{\sigma\} \tag{5.1.c}$$

where [X] is the structural (12×6) matrix, defined in Eq.(3.13.c). Combining Eqs.(5.1.b) and (5.1.c) gives after rearranging

$$\{\tau\} = [X][D][Q_d]\{\varepsilon\} \tag{5.1.d}$$

Under the same global stress state, $\{\sigma\}$, the RSS (12×1) vector $\{\tau\}$ can be related to the shear strain (12×1) vector $\{\gamma\}$ by the relation

$$\{\tau\} = G\{\gamma\} \tag{5.1.e}$$

where G is the shear modulus defined in Eq.(3.7.b). Combining Eqs.(5.1.d) and (5.1.e), one gets

$$G\{\gamma\} = \pm [X][D][Q_d]\{\varepsilon\} \tag{5.1.f}$$

that may be rewritten as,

$$\gamma\{s_0\} = \pm \frac{\varepsilon}{G}[X][D][Q_d]\{v\} \tag{5.1.g}$$

where γ and ε are, respectively, the shear stress and the strain magnitudes, and $\{s_0\} = \frac{\{\gamma\}}{\|\gamma\|}$ and $\{\varepsilon\} = \frac{\{\varepsilon\}}{\|\varepsilon\|}$ are their corresponding unit director cosines. From Eq.(5.1.b), the strain vector may be expressed as,

$$\{\varepsilon\} = \sigma [Q_d]^{-1}[D]^{-1}[Q_c]\{e\} \tag{5.1.h}$$

where $\{e\}$ is the applied stress unit vector. Since all the terms in that equation are known, thus the cosines director, $\{v\}$ of the strain vector $\{\varepsilon\}$ is:

$$\{v\}=\frac{[Q_d]^{-1}[D]^{-1}[Q_e]\{e\}}{\|[Q_d]^{-1}[D]^{-1}[Q_e]\{e\}\|} \tag{5.1.i}$$

Once $\{v\}$ is known, Eq.(5.1.g) may be rewritten as

$$\gamma\{s_0\}=\pm\frac{\varepsilon}{G}\|[X][D][Q_d]\{v\}\|\frac{[X][D][Q_d]\{v\}}{\|[X][D][Q_d]\{v\}\|} \tag{5.1.j}$$

and setting

$$\rho=\frac{\|[X][D][Q_d]\{v\}\|}{G} \tag{5.1.k}$$

then by identification, one gets,

$$\begin{cases} \gamma=\dfrac{\|[X][D][Q_d]\{v\}\|}{G}\varepsilon=\rho\,\varepsilon & \text{(i)} \\ \{s_0\}=\pm\dfrac{[X][D][Q_d]\{v\}}{\|[X][D][Q_d]\{v\}\|} & \text{(ii)} \end{cases} \tag{5.1.l}$$

If one assumes that only the shear strain and the total strain are time dependent, then from Eq.(5.1.l), one may therefore obtain

$$\dot{\gamma}=\frac{\|[X][D][Q_d]\{v\}\|}{G}\dot{\varepsilon}=\rho\dot{\varepsilon} \tag{5.1.m}$$

which gives the relationship between the shear strain rate $\dot{\gamma}$ and the strain rate $\dot{\varepsilon}$. The orientation dependence of the ratio $\left(\frac{\dot{\gamma}}{\dot{\varepsilon}}\right)$ is plotted in Figure 5.1. Eq.(5.1.m) is valid in the elastic range as well as in the plastic range with the difference that in the later case, the matrix [D], and consequently the shear modulus, change as the plastic strain increases. The derivation of the tangent stiffness of the matrix [D] is done in Swanson et al. (1986).

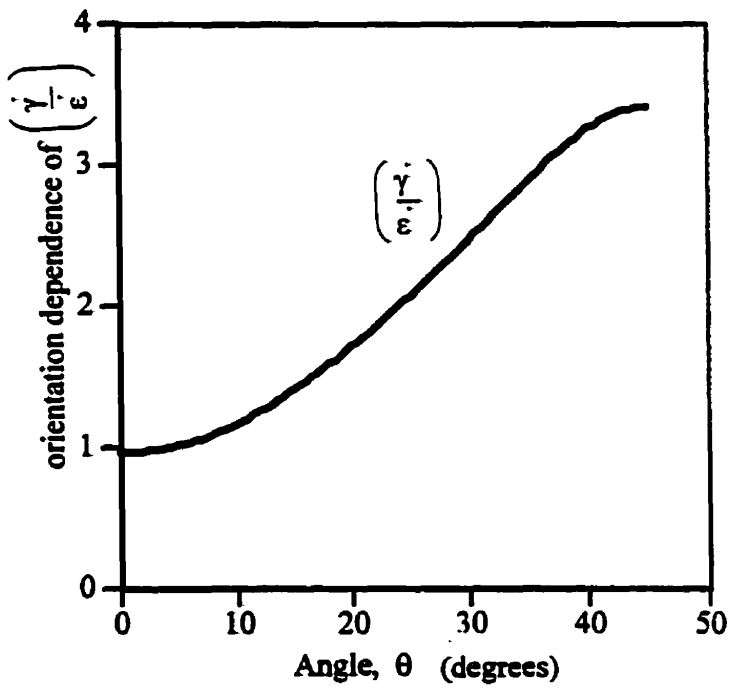

Figure 5.1 Orientation dependence between the shear strain rate, $\dot{\gamma}$ and the strain rate $\dot{\varepsilon}$ along the [0 0 1]-[0 1 1] orientation boundary.

5.2.2 – Octahedral slip systems

It has been shown in Chapter III, Eq.(3.16.a) that in SC materials, the critical resolved shear stress (CRSS) in the octahedral slip systems can be decomposed into two terms, each representing a specific deformation mechanism. The two terms are defined so that when the first one is predominant (at the high strain rate), the second one is negligible, and when the second term is predominant (at the low strain rate), the first term becomes negligible.

5.2.2.1 - At the high strain rate

The orientation dependence of the CRSS in the octahedral slip systems, defined in Eq.(3.16.c), is characterized in tension and compression by constants A_{1t}, V_{11}, V_{12}, and A_{1c}, V_{21}, V_{22} respectively. According the slip trace studies of SC materials developed in Chapter II, the octahedral slip constants may derived from tests where cube slip is not present, as in, for example, the [0 0 1] and [0 1 1] orientations. Cube slip constants on the other hand are derived from tests where octahedral slip is not present i.e., in the $[\bar{1}\,1\,1]$ orientation. The constants A_{1t}, V_{11}, V_{12}, can be evaluated from any three tensile tests at constant strain rate as long as their orientations are different and cube slip is not involved. Best results, however, are obtained if the orientations are not close. Tests close together tend to magnify the experimental variability. An optimum set of tests is probably $[0\,0\,1]$, $[0\,1\,1]$ and another orientation [h k l] where cube slip is not present. The choice of the third orientation should be well away from the cube slip regime. When a choice of orientation is available for developing constants, the data from the [0 0 1] orientation is often the primary loading direction.

During the tension test ($I_{\{\sigma\}} > 0$), under the j^{th} global applied stress state, only the first component of the ratio $\left(\frac{\sigma_y}{\tau_{RT}}\right)_{oct}$ given in Eq.(3.16.a) is active, the second component being negligible. By substitution of Eq.(3.16.c) in Eq.(3.16.a), one may get, after rearranging,

$$Sf = \left(\frac{\sigma_y}{\tau_{RT}} \right)_{oct1} \frac{A_{1t}\,\varphi_1 \exp\left(\frac{-H_0}{kT} + V_{11}\,S_{2j} + V_{12}\,S_{3j} \right)}{\tau_{RT}\,S_{1j}} \qquad (5.2.a)$$

Since the effective yield stress expression (σ_y), defined in Eq.(3.8.a), has the form,

$$\sigma_y = Sf\,\sigma_{LZ} \qquad (5.2.b)$$

where σ_{LZ} is the initial yield stress generated by the Lee and Zaverl yield stress defined in Eq.(3.12.b), then substituting Sf and σ_{LZ} in Eq.(5.2.b) by their values gives,

$$\sigma_y = \frac{\varphi_1 A_{1t}}{\tau_{RT} S_{1j}} \exp\left(\frac{-H_0}{kT} + \delta V_{11} S_{2j} + V_{12} S_{3j} \right) \left(\frac{\sqrt{2/3}\,\sigma_{+1}}{\mu_{1j}} \right) \qquad (5.2.c)$$

and setting,

$$r_{1j} = \frac{\sigma_y \tau_{RT} S_{1j} \mu_{1j}}{\sqrt{2/3}\,\sigma_{+1}\,\varphi_1} \qquad (5.2.d)$$

Eq.(5.2.c) may then be reduced to the form

$$V_{11} S_{2j} + V_{12} S_{3j} + \ln\left(A_{1t}\right) = \frac{H_0}{kT} + \ln\left(r_{1j}\right) \qquad (5.2.e)$$

where, S_{2j} and S_{3j} are structural coefficients in the octahedral and cube slip systems respectively, σ_y is the yield stress, μ_{1j} is an orientation function defined in Eq.(3.9.d), and all the other terms were defined previously.

Setting j = 1, 2 and 3, respectively, for tension tests along the orientations [0 0 1], [0 1 1] and [h k l] where cube slip is not involved, and applying these three tests above on the Eq.(5.2.e) yields

$$\begin{cases} V_{11} S_{21} + V_{12} S_{31} + \ln(A_{1t}) = \dfrac{H_0}{kT} + \ln(r_{11}) \\ V_{11} S_{22} + V_{12} S_{32} + \ln(A_{1t}) = \dfrac{H_0}{kT} + \ln(r_{12}) \\ V_{11} S_{23} + V_{12} S_{33} + \ln(A_{1t}) = \dfrac{H_0}{kT} + \ln(r_{13}) \end{cases} \qquad (5.2.f)$$

Since S_{2j} , S_{3j} and r_{1j} can be computed from Eqs.(3.14.c) and (5.2.d), therefore, constants A_{1t}, V_{11} and V_{12} can be determined.

The determination of constants A_{1c}, V_{21} and V_{22} defined in Eq.(3.16.c) is done in a similar way as above, except that compression tests ($I_{\{\sigma\}} \leq 0$) must be used instead of tension tests. The summary of these constants for the SC nickel base superalloys Rene N4 at 760° C is given in Table 5.7.

5.2.2.2 - At the low strain rate

During the creep test in the octahedral slip systems, the orientation dependence of the CRSS, defined in Eq.(3.16.d), is characterized by the constants A_{1cr} , V_{13} , and V_{14}. These constants can be evaluated by using the primary and secondary regime for three creep tests from distinct orientations along which cube slip is not involved. As in the previous case, best results are obtained if the orientations are not close together. However, the evaluation of the material constants A_{1cr} , V_{13} and V_{14} for the creep regime proposed in the present work is based on the following approximate technique.

Based on the experimental studies on aluminum crystals, Taylor and Elam (1936) found that the resolved shear stress-shear strain curves of f.c.c crystals can be approximately represented by the parabolic equation,

$$\tau_c = \lambda (\gamma)^{1/2} \tag{5.3.a}$$

where τ_c is the CRSS, γ is shear strain and λ is a proportionality parameter. That observation shows that the CRSS τ_c is a function of plastic strain and will usually increase due to the material hardening caused by plastic deformation. This hardening behavior is described by $\tau_c - \gamma$ curves for different materials. More recently, other studies have shown that the $\tau_c - \gamma$ curve can be represented as illustrated in Figure 5.2. That representation is quite different from what Taylor and Elam (1936) observed and cannot be described completely by Eq.(5.3.a). In the deformation process of f.c.c metal crystals, there are, in general, three distinct regions of the $\tau_c - \gamma$ curve. The first region (stage I) is usually called the easy glide region, as there the hardening rate is low. This region is followed by stage II, which represents a much higher linear hardening process. The third region hardening (stage III) is characterizing by a decreased hardening rate. That region can be approximated by Taylor and Elam's parabolic Eq.(5.3.a). It should be pointed out that it is not necessary that all three stages always be present. There are several conditions that decide whether a particular stage will occur, and its relative importance to the others stages. These include the orientation of the crystals, their purity, the temperature during deformation, the material, the grain size, the surface condition and the strain rate.

For the purpose of this work, the resolved shear stress-shear strain curve used with f.c.c crystals has the form

$$\tau_c = G(\gamma)^{1/2} \tag{5.3.b}$$

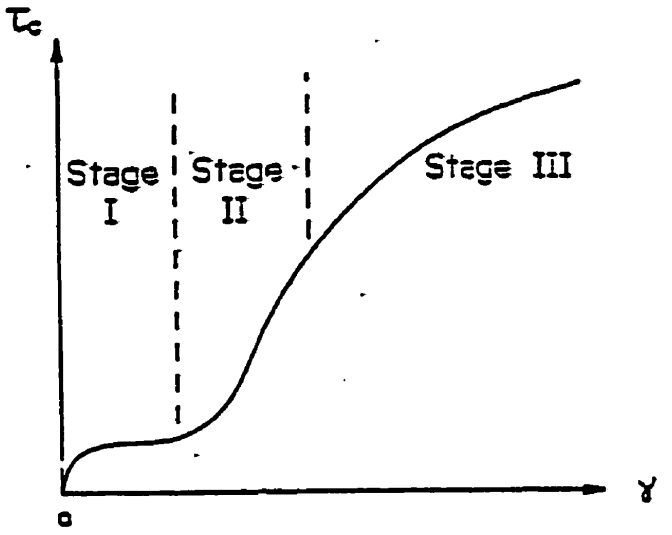

Figure 5.2 - $\tau_c - \gamma$ curves for SC material. From Khan (1995)

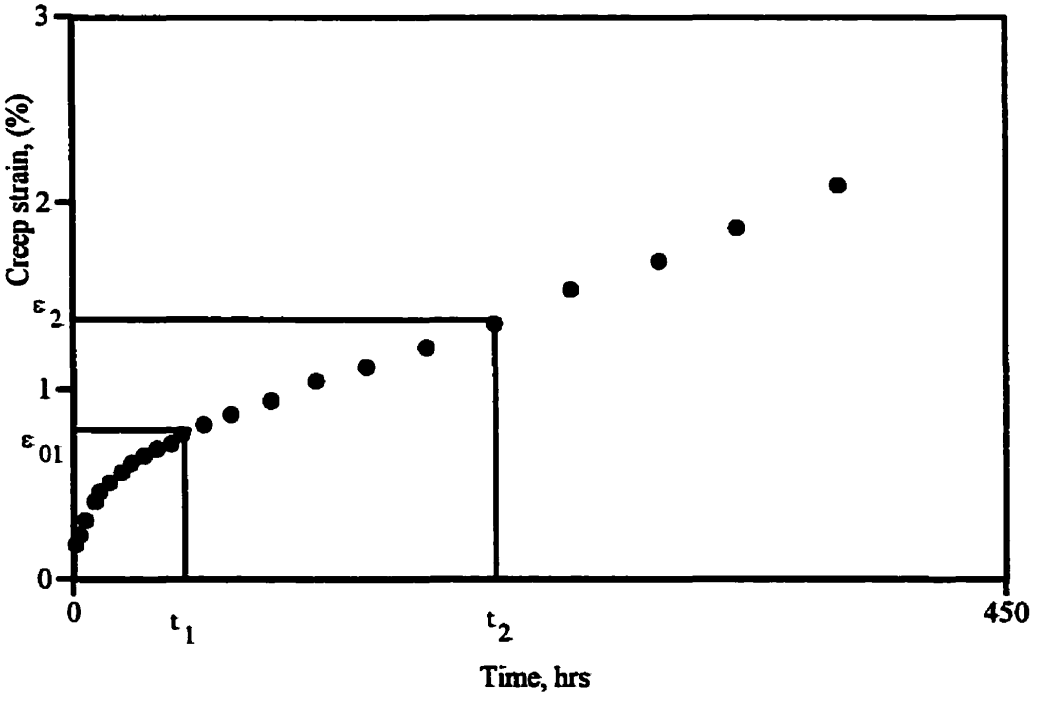

Figure 5.3 Experimental creep test response for a given SC material along the [0 0 1] orientation. From Dame (1985)

where the shear modulus G defined in Eq.(3.7.b) is used as the proportionality parameter. Under the j^{th}- global state of stress on the SC sample, the corresponding strain rate $\dot{\varepsilon}_j$ during the creep test can be integrated over the primary and the secondary creep stages using experimental data as shown in Figure 5.3. One obtains

$$\varepsilon_j = \int_0^{t_1} \dot{\varepsilon}_j \, dt + \int_{t_1}^{t_2} \dot{\varepsilon}_j \, dt \qquad (5.3.c)$$

where t_1 is the time at the end of the primary stage, and t_2 is the time at the end of the test. Recall that t_2 should be chosen within the secondary creep stage and has the same value for all the three creep tests. After integrating, one gets

$$\varepsilon_j = \varepsilon_{0j} + \dot{\varepsilon}_j (t_2 - t_1) \qquad (5.3.d)$$

where ε_{0j} is the creep strain at the end of the primary creep. Since the relationship between the total strain (ε) and the shear strain (γ) is known, then combining Eqs.(5.1.l), (5.3.b) and (5.3.d), one obtains after rearranging

$$\tau_c = G\rho^{1/2}\left[\varepsilon_{0j} + \dot{\varepsilon}_j (t_2 - t_1)\right]^{1/2} \qquad (5.3.e)$$

The CRSS τ_c above must be equal to the CRSS component defined in Eq.(3.16.e). Equating both equations, one may have

$$A_{1\alpha}\,\varphi_2 \exp\left(\frac{-H_0}{kT} - \frac{V_{13}}{\mu_{1j}} S_{2j} + \frac{V_{14}}{\mu_{1j}} S_{3j}\right) = G_j \rho^{1/2}\left(\varepsilon_{0j} + \dot{\varepsilon}_j (t_2 - t_1)\right)^{1/2} \qquad (5.4.a)$$

Setting,

$$p_{1j} = G\rho^{1/2}\left(\varepsilon_{0j} + \dot{\varepsilon}_j\left(t_2 - t_1\right)\right)^{1/2} \qquad (5.4.b)$$

Recall that at a given orientation j, φ_2 tends to 1, thus ln(φ_2) tends to 0. Given that G and ρ can be computed from Eqs.(3.7.b) and (5.1.k), while ε_{0j}, $\dot{\varepsilon}_j$ and $\Delta t = \left(t_2 - t_1\right)$ can be determined from creep experimental data, then p_{ij} can be calculated. Taking the natural log of both sides gives

$$-V_{13}\left(\frac{S_{2j}}{\mu_{1j}}\right) + V_{14}\left(\frac{S_{3j}}{\mu_{1j}}\right) + \ln\left(A_{1cr}\right) = \frac{H_0}{kT} + \ln\left(p_{1j}\right) \qquad (5.4.c)$$

Since S_{2j} , S_{3j} , μ_{1j} , and p_{1j} can be computed from Eqs.(3.14.c), (4.3.a) and (5.4.b), then using creep tests along three distinct orientations in which cube slip is not involved, therefore, the constants A_{1cr} , V_{13} , and, V_{14} can be determined. Because of the availability of the experimental data, the creep tests was performed along the orientations [0 0 1], [0 321 940] and [0 1 1]. Eq.(5.4.c) may be rewritten for each of the three tests as,

$$\begin{cases} -V_{13}\left(\frac{S_{21}}{\mu_{11}}\right) + V_{14}\left(\frac{S_{31}}{\mu_{11}}\right) + \ln\left(A_{1cr}\right) = \frac{H_0}{kT} + \ln\left(p_{11}\right) \\ -V_{13}\left(\frac{S_{22}}{\mu_{12}}\right) + V_{14}\left(\frac{S_{32}}{\mu_{12}}\right) + \ln\left(A_{1cr}\right) = \frac{H_0}{kT} + \ln\left(p_{12}\right) \\ -V_{13}\left(\frac{S_{23}}{\mu_{13}}\right) + V_{14}\left(\frac{S_{33}}{\mu_{13}}\right) + \ln\left(A_{1cr}\right) = \frac{H_0}{kT} + \ln\left(p_{13}\right) \end{cases} \qquad (5.4.d)$$

The summary of these constants is listed in Table 5.7.

5.2.3 – Cube slip systems

The orientation dependence of the CRSS in the cube slip systems is defined in Eq.(3.17.c). The determination of all these constants, at the high strain rate as well as the

low strain rate, can be done in the same way as in the octahedral slip system. Except that in this case, only two tests (tension and compression) are required along the $[\bar{1}11]$ orientation. Because of the lack of experimental data, constants for low strain rate compression are not evaluated. All the others constants are evaluated and summarized in Table 5.7.

Table 5.3 Identification of material constants and tests or calculations required for their evaluation.

Constants	Tests or calculations required
E, G, ν	• **Elastic constants:** Eqs.(3.7). Crystal orientation and elasticity components D_{11}, D_{12}, and D_{44}. D_{ij} (see Table 3.1) were measured by ultrasonic wave velocity at different temperatures. *From Swanson et al. (1986)*
$M_{11}-M_{12}=2/3$ $M_{44}=\frac{4}{3}\left(\frac{Y_{+1}}{Y_{[\bar{1}11]}}\right)^2$	• **The components** M_{ij} Eqs.(3.11) (d) and (g). Their evaluation requires two tensile tests along the $[001]$ and $[\bar{1}11]$ orientations.
A_{1t}, V_{11}, V_{12} (A_{1c}, V_{22}, V_{23})	• **Orientation parameters** (at the high strain rate tests) Their evaluation requires 3 tensile (or compressive) tests at a constant strain rate, along 3 distinct orientations in which octahedral slip is predominant.
A_{1cr}, V_{13}, V_{14} $(A_{2cr}, V_{23}, V_{24})$	• **Orientation parameters** (at the low strain rate tests) Their evaluation requires 3 creep tests, along 3 distinct orientations in which octahedral slip is predominant.
τ_{RT}	• **The CRSS** of the material at room temperature (RT), along the $[001]$ orientation. Its determination requires a tensile test. The sample is deformed to about 2 % plastic strain. The slip system is confirmed by either slip trace analysis, or tensile axis rotation. *From Miner et al.(1986.a); Miner et al.(1986.b); Li et al. (1995).*
H_0	• **Activation enthalpy of cross slip:** from Eq.(3.16.b), it can be determined using a tension (or a compression) test along the $[\bar{1}11]$ orientation at two distinct temperatures.

5.3 – DETERMINATION OF THE MATERIAL PARAMETERS OF THE MODEL

In this section, a method will be presented to evaluate the material constants A, B, C, K, Q, and n used in the 3D form of the basic equation of the model defined in Eqs.(4.13). To do so, the one-dimensional form of the basic equations defined in Eqs.(4.16) will be used. The corresponding material parameters a, b, c, k, q (that are orientation dependent in this case), and n will first be evaluated along the [0 0 1] orientation using experimental data from a series of simple tests on the SC samples. After that, knowing the relationship between the material parameters a, b, c, k, and q, and the material constants A, B, C, K, and Q, the latter constants can therefore be deduced. The method of determination of the set of the material parameters a, b, c, k, q, and n for SC materials proposed in the present work, are similar to those used for isotropic materials. The difference is that in this case, the series of tests must be done along the [0 0 1] orientation. As mentioned previously, this approach is not unique; rather, it is appropriate for the kind of data available. The parameter values will be determined in pairs, and some approximations and judicious assumptions will have to be made and discussed as they are introduced. Similar studies have been done in Abdel-Kader (1986), and Chiu (1988).

5.3.1 – Determination of a and c

The material parameters a and c, defined in Eq.(4.16.f), represent the kinematic hardening behavior. In order to calculate their values, one must assume that cyclic stabilization occurs and that the isotropic hardening variable, R, remains constant at its saturation value. A number of authors such as Lee and Zaverl (1978), Abdel-Kader (1986), Chiu (1988), Li and Smith (1995.b) and others have used those same assumptions for the purpose of their work. Therefore, in the stabilized strain controlled cyclic test, the isotropic hardening variable R approaches its saturated value q asymptotically. Any additional hardening is modeled by the kinematic variable, Y. The constants a and c, which describe Y, may be determined by using the power law function or the stabilized stress-strain curve. Upon inversion, the flow law Eq.(4.16.d) takes the form

$$\sigma = Y + R + k\left(\dot{\varepsilon}^{i}\right)^{1/n} \qquad (5.5.a)$$

For the uniaxial tensile load, the derivative of Eq.(5.5.a), with respect to the inelastic strain ε^i, gives

$$\frac{d\sigma}{d\varepsilon^i}=\frac{dY}{d\varepsilon^i}+\frac{dR}{d\varepsilon^i}+\frac{k}{n}\left(\frac{d\dot{\varepsilon}^i}{d\varepsilon^i}\right)\left(\dot{\varepsilon}^i\right)^{\frac{1}{n}-1} \tag{5.5.b}$$

Since the isotropic hardening is in a cyclically stable state, R is constant (R = q), and

$$\frac{dR}{d\varepsilon^i}=\frac{dq}{d\varepsilon^i}=0 \tag{5.5.c}$$

In addition, if the load cycling is assumed to be perform at a constant strain rate, then

$$\frac{d\dot{\varepsilon}^i}{d\varepsilon^i}=0 \tag{5.5.d}$$

Combining Eqs.(5.5.b), (5.5.c) and (5.5.d), one may obtain

$$\frac{d\sigma}{d\varepsilon^i}=\frac{dY}{d\varepsilon^i}=\frac{d\dot{Y}}{d\dot{\varepsilon}^i} \tag{5.5.e}$$

Substituting the expression for $\dot{Y}$ given in Eq.(4.16.f), into Eq.(5.5.e) yields

$$\frac{d\sigma}{d\varepsilon^i}=\frac{d}{d\varepsilon^i}\left[c\left(a\dot{\varepsilon}^i-Y\left|\varepsilon^i\right|\right)\right]=c\left(a-Y\right) \tag{5.5.f}$$

For $\dot{\varepsilon}^i>0$ at $Y=0$, Eq.(5.5.f) gives

$$\frac{d\sigma}{d\varepsilon^i}=ca \tag{5.5.g}$$

It has been demonstrated in Chiu (1988) that Eqs.(5.5.f) and (5.5.g) represent the slopes of the stabilized cyclic stress inelastic–strain curve. Thus, as Y approaches the limiting value, a, $d\sigma/d\varepsilon^i$ approaches 0. According to Eq.(5.5.f), the strain-hardening behavior of a stabilized cyclic stress-inelastic strain curve is modeled only by the kinematic hardening variable, Y. Using the initial values of Y = 0, Eq.(5.5.f) gives an expression for Y as

$$Y = a\left[1 - \exp\left(-c\varepsilon^i\right)\right] \tag{5.6.a}$$

Substituting Eq.(5.6.a) into Eq.(5.5.f) gives

$$\begin{aligned} \frac{d\sigma}{d\varepsilon^i} &= c\left\{a - a\left[1 - \exp\left(-c\varepsilon^i\right)\right]\right\} \\ &= ac\exp\left(-c\varepsilon^i\right) \end{aligned} \tag{5.6.b}$$

Using the natural log of both sides of Eq.(5.6.b), one obtains

$$\ln\left(\frac{d\sigma}{d\varepsilon^i}\right) = \ln(ac) - c\varepsilon^i \tag{5.6.c}$$

Eq.(5.6.c) represents a straight line on the log plot, where c represents the value of the slope and ln(ac) the y intercept.

Now, using the experimental data obtained from the stabilized strain controlled cyclic test, the stable cyclic stress amplitude, $\Delta\sigma/2$, can be related to the cyclic plastic strain amplitude $\Delta\varepsilon/2$ by the power law function defined as

$$\frac{\Delta\sigma}{2} = \bar{k}\left(\frac{\Delta\varepsilon^i}{2}\right)^{\bar{n}} \tag{5.6.d}$$

where, $\bar{n}$, is the cyclic strain hardening exponent and $\bar{k}$ is the cyclic strength coefficient in MPa. Eq.(5.6.d) may also be expressed as

$$\sigma = \bar{k}\left(\varepsilon^{i}\right)^{\bar{n}} \tag{5.6.e}$$

Now, using the derivative of Eq.(5.6.e) with respect to ε^{i} one has

$$\frac{d\sigma}{d\varepsilon^{i}} = \bar{k}\bar{n}\left(\varepsilon^{i}\right)^{\bar{n}-1} \tag{5.6.f}$$

In addition, using the natural log on both side of Eq.(5.6.f), one obtains Eq.(5.7.a), from which one can get a straight line that represents the best least square of the corresponding data.

$$\ln\left(\frac{d\sigma}{d\varepsilon^{i}}\right) = \ln\left(\bar{k}\bar{n}\right) + \left(\bar{n}-1\right)\ln\left(\varepsilon^{i}\right) \tag{5.7.a}$$

Through use of Eq.(5.6.c), that empirical equation provides, in a specific inelastic strain range, the necessary information on $\ln\left(\frac{d\sigma}{d\varepsilon^{i}}\right)$ and $\ln\left(\dot{\varepsilon}^{i}\right)$ to determine a and, c. From Eq.(5.6.d), after rearranging the cyclic strength coefficient, one obtains

$$\bar{k} = \frac{\left(\Delta\sigma/2\right)}{\left(\Delta\varepsilon/2\right)^{\bar{n}}} \tag{5.7.b}$$

Such stabilized cyclic stress-strain tests have been performed in Gabb et al. (1986) for Rene N4 measured at half life. The corresponding results are plotted in the log-log scale in Figures 5.4.a and 5.4.b for two temperatures; 760° C and 980° C, respectively. According to the authors, the cyclic strain hardening exponent $\bar{n}$ for Rene N4 at 760° C was found to be equal 0.20 for all the orientations shown on the graph, while at 980° C $\bar{n}$ was found to be equal 0.13 along the $\left[\bar{1}\,1\,1\right]$ orientation and 0.28 along all the others orientations. Since $\Delta\sigma/2$ and $\Delta\varepsilon/2$ can be evaluated, then the knowledge of $\bar{n}$ allows the calculation of the cyclic strength coefficient $\bar{k}$ from Eq.(5.7.b). The corresponding results of $\bar{n}$ and $\bar{k}$ along the [0 0 1] orientation are summarized in Table 5.4 for both

(a)

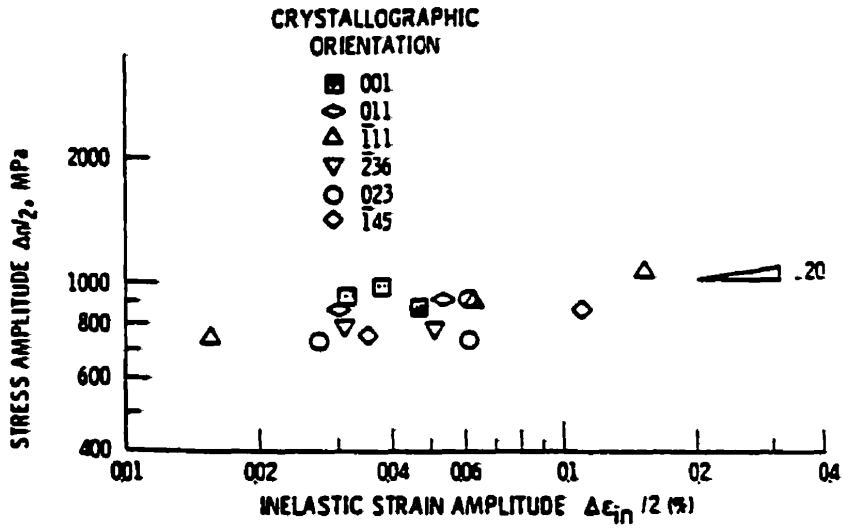

(b)

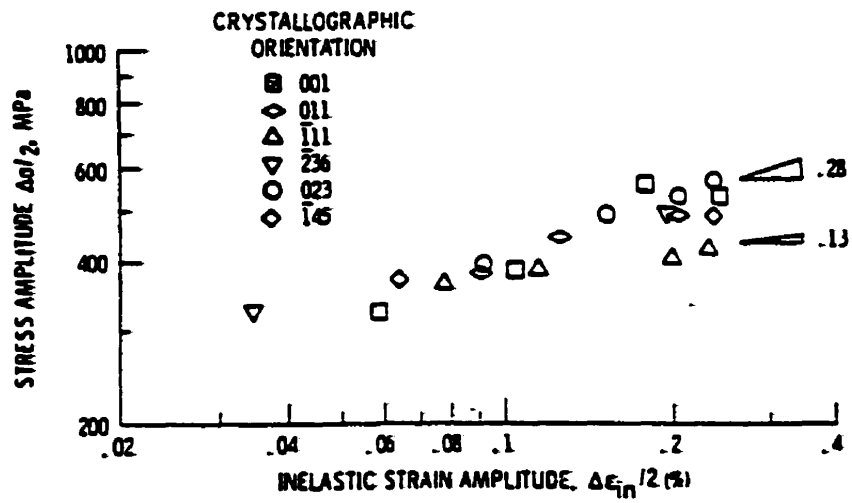

Figure 5.4 Cyclic stress-strain curves for Rene N4 at (a) 760° C and (b) 980° C. From Gabb et al. (1986).

temperatures. Thus, combining both the analytical equation Eq.(5.6.c), and the empirical equation Eq.(5.7.a), one obtains the system of two equations below, which provides within an appropriate range of inelastic strain, necessary information so that a and c may be determined.

$$\begin{cases} \mathrm{Ln}\left(\dfrac{d\sigma}{d\varepsilon^i}\right) = \mathrm{Ln}(ac) - c\,\varepsilon^i \\ \mathrm{Ln}\left(\dfrac{d\sigma}{d\varepsilon^i}\right) = 5.196 - 0.8\,\mathrm{Ln}\left(\varepsilon^i\right) \end{cases} \tag{5.7.c}$$

The following data are tabulated according to Eqs.(5.6.f) and (5.7.a) for various values of inelastic strain. Now, fitting the system of Eq.(5.7.c) through the five points in Table 5.5, one obtains the straight line defining the best least-square plotted in Figure 5.5. By identification, that straight line can be used to determine the slope of the line c = 171.7, while the parameter a = 173.16 can be deduced in the same equation. A comparison of the plots derived from Eqs.(5.6.b) and (5.6.f) over the appropriate strain range is shown in Figure 5.6. For an elastic strain of 0.35 to 0.75 percent, reasonable agreement is observed between the empirical experimental approximation and the analytical Chaboche's approximation.

Table 5.4 – Stabilized cyclic stress strain tests data

Temperature	$\frac{\Delta\sigma}{2}$ (MPa)	$\frac{\Delta\varepsilon^{i}}{2}$ (mm/mm)	$\bar{n}$	$\bar{k}$ (MPa)
T = 760°C	700	0.28	0.20	903.00
T = 980°C	400	0.20	0.28	627.73

Table 5.5 – Evaluation of the quantities $d\varepsilon^{i}$ and $Ln\left(d\sigma/d\varepsilon^{i}\right)$ for various inelastic strain

ε^{i}	$d\sigma/d\varepsilon^{i}$		$\ln\left(d\sigma/d\varepsilon^{i}\right)$
	Eq(5.6.c)	Eq(5.7.a)	
0.0025	19355.83	21795.44	9.8703
0.0035	16302.10	16651.88	9.6986
0.0045	13730.15	13619.07	9.5269
0.0055	11563.96	11599.18	9.3552
0.0065	9739.54	10148.15	9.1835

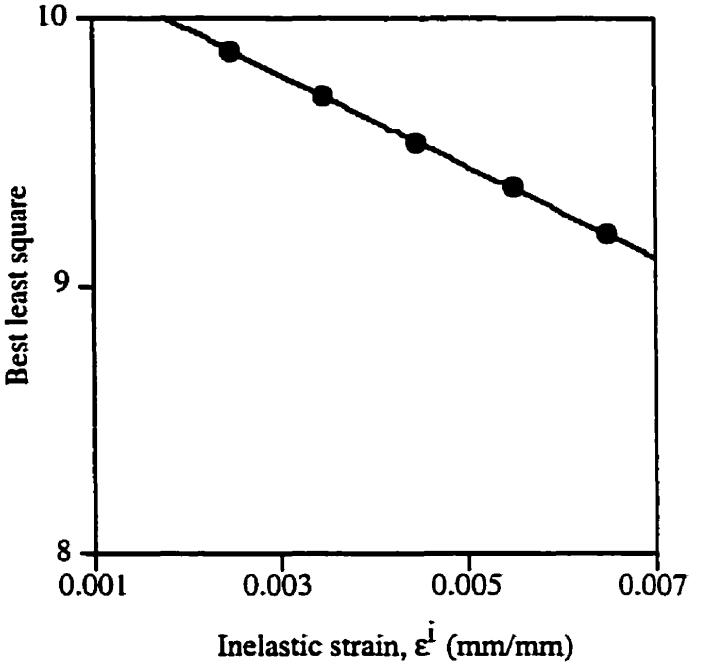

Figure 5.5 – Best least-square plotted from Eq.(5.7.a)

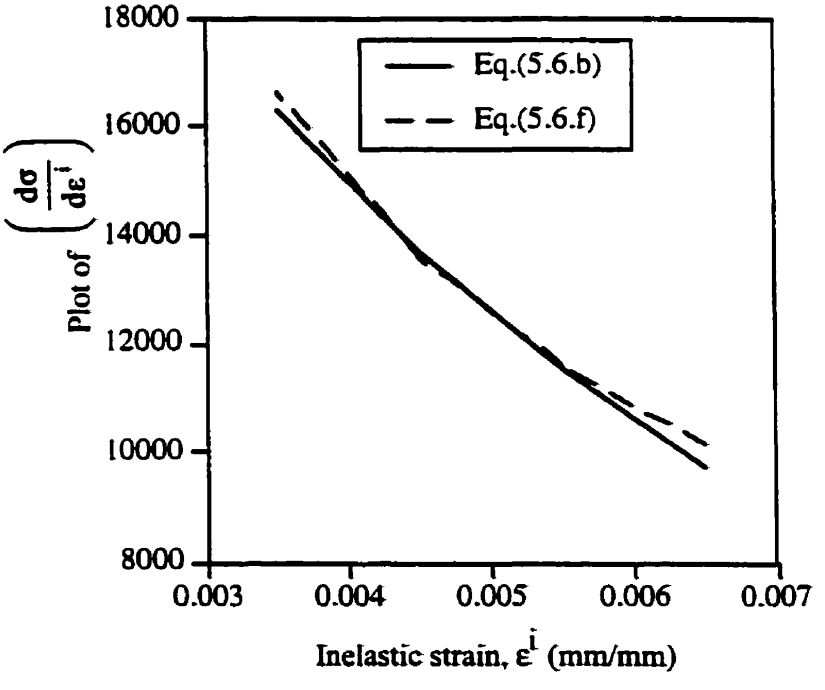

Figure 5.6 Plot of $\left(\frac{d\sigma}{d\varepsilon^i}\right)$ versus ε^i for a cyclic stress-strain curve according Eq.(5.6.b) and Eq.(5.6.f)

5.3.2 - Determination of n and k

The material parameters k and n, defined in Eq.(4.16.d), represent the flow law behavior. At a hold stress level σ_h, the primary creep-strain rate represented by Chaboche's theory has the form below; the values of k and n can therefore be calculated using the creep tests.

$$\dot{\varepsilon}^i = \left(\frac{\sigma_h - Y - R}{k} \right)^n \tag{5.8.a}$$

In order to make use of Eq.(5.8.a) further simplification is needed. During the primary creep deformation, where the inelastic strain accumulation is small, the isotropic hardening can in a first approximation, be assumed to be negligible. All of the creep hardening behavior is therefore assumed to be primarily kinematic. A similar assumption has been used in Abder-Kader (1986), and Chiu (1988). In that case, the isotropic hardening variable R, defined in Eq.(4.16.g), may keep its initial value $R_0 = \frac{Sf}{\mu_1(\theta,\psi)}\hat{R}_0$. Using the natural log on both sides of Eq.(5.8.a) yields:

$$\ln(\dot{\varepsilon}^i) = n\ln(\sigma_h - Y - R) - n\ln(k) \tag{5.8.b}$$

From the foregoing results, it is observed for the SC nickel base super-alloys Rene N4 VF317 at 760 °C along the [0 0 1] orientation that:

- the kinematic variable Y may be expressed as

$$\begin{aligned} Y &= a\left[1 - \exp(-c\varepsilon^i)\right] \\ &= 173.16\left[1 - \exp(-171.7\varepsilon^i)\right] \end{aligned} \tag{5.8.c}$$

- The yield stress is $\sigma_{+1} = 956$ MPa, $\mu_1(0,0) = \sqrt{2/3}$, $\hat{R}_0 = \sqrt{2/3}\,\sigma_{+1}$, and the slip factor (Sf) corresponding to the creep test is equal to 0.4. Therefore, one obtains

$$R \cong \frac{Sf}{\mu_1(\theta,\psi)}\hat{R}_0 = 382.72 \text{ MPa} \qquad (5.8.d)$$

For $\sigma_h = 655$ MPa, one can substitute R and Y, into Eq.(5.8.b). This equation is not enough to determine the constants n and k. For that reason, the Bailey-Norton empirical equation is used.

It has been observed by a number of authors that the primary creep behavior of structural material is in good agreement with the Bailey-Norton creep law defined in Eq.(5.9.a). For that reason, the creep experimental data for Rene N4 VF317 at 760°C along the [0 0 1] orientation, shown in Figure 5.7, is used to obtain approximate values of n and k.

$$\varepsilon^i = \left(\frac{\sigma_h}{\overline{T}}\right)^{m_1} t^{m_2} \qquad (5.9.a)$$

where

ε^i is the creep strain (in percent),

t is time (in hours),

$\overline{T}$, m_1 and m_2 are material parameters to be determined from creep data,

and σ_h is the hold stress level (in MPa) at which the creep test was conducted

An expression for the primary creep strain rate $\dot{\varepsilon}^i$ (in percent per hour) can be obtained by using the time derivative of Eq.(5.9.a), thus

$$\dot{\varepsilon}^i = m_2\left(\frac{\sigma_h}{\overline{T}}\right)^{m_1} t^{m_2-1} \qquad (5.9.b)$$

Eq.(5.9.b) shows that the creep rate is a function of both stress and time and it is commonly referred to as the time-hardening formulation. As reported by Chiu (1988), $\overline{T}$ is close to the yield strength of the material along [0 0 1] orientation. Fitting the primary creep experimental data given in Figure 5.7 with Eq.(5.9.a) leads to

$$m_2 = \frac{\ln\left(\varepsilon_1^i / \varepsilon_2^i\right)}{\ln\left(t_1 / t_2\right)} \tag{5.9.c}$$

$$m_1 = \frac{\ln\left(\varepsilon_1^i / t_1'^{m_2}\right)}{\ln\left(\sigma_h / \overline{T}\right)} \tag{5.9.d}$$

For $\varepsilon_1^i = 0.0037$, $\varepsilon_2^i = 0.007$, $t_1 = 5.55$ h, $t_2 = 42.6$ h,

$\sigma_h = 655$ MPa, $\overline{T} = 0.8 \times 956 = 765$ MPa.

After calculating, one obtains

$$m_2 \approx 0.32 \qquad \text{and} \qquad m_1 \approx 10 \tag{5.9.e}$$

When Eq.(5.9.a) is solved for t and the resulting expression substituted into Eq.(5.9.b), the creep rate becomes a function of the applied hold stress and the creep strain. Thus,

$$\dot{\varepsilon}^i = m_2 \left(\frac{\sigma_h}{\overline{T}}\right)^{\frac{m_1}{m_2}} \left(\varepsilon^i\right)^{1-\frac{1}{m_2}}$$

$$\dot{\varepsilon}^i = 0.32 \left(\frac{655}{765}\right)^{\frac{10}{0.32}} \left(\varepsilon^i\right)^{-2.125} \tag{5.9.f}$$

Eq.(5.9.f) represents the so-called strain-hardening formulation. This formulation generally leads to more accurate predictions than the time-hardening formulation. Taking the natural log of both sides of Eq.(5.9.a) gives, after calculating, the empirical equation

$$\ln\left(\dot{\varepsilon}^{i}\right) = -5.99 - 2.125\ln\left(\varepsilon^{i}\right) \tag{5.9.g}$$

Thus, combining both the analytical equation (5.8.b) and the empirical equation (5.9.g), one derives the system of two equations, which provides the necessary information to determine k and n.

$$\begin{cases} \ln\left(\dot{\varepsilon}^{i}\right) = -5.99 - 2.125\ln\left(\varepsilon^{i}\right) \\ \ln\left(\dot{\varepsilon}^{i}\right) = n\ln\left(\sigma_{h} - Y - R\right) - n\ln(k) \end{cases} \tag{5.10.a}$$

The experimental data given in Figure 5.7 shows that for a hold stress level σ_h = 655 MPa, the higher bound for the primary creep strain can be taken at approximately 0.8 %. Thus for creep strains of 0.01% and 0.8 %, the corresponding empirical creep strain rates computed by Eq.(5.9.f) are,

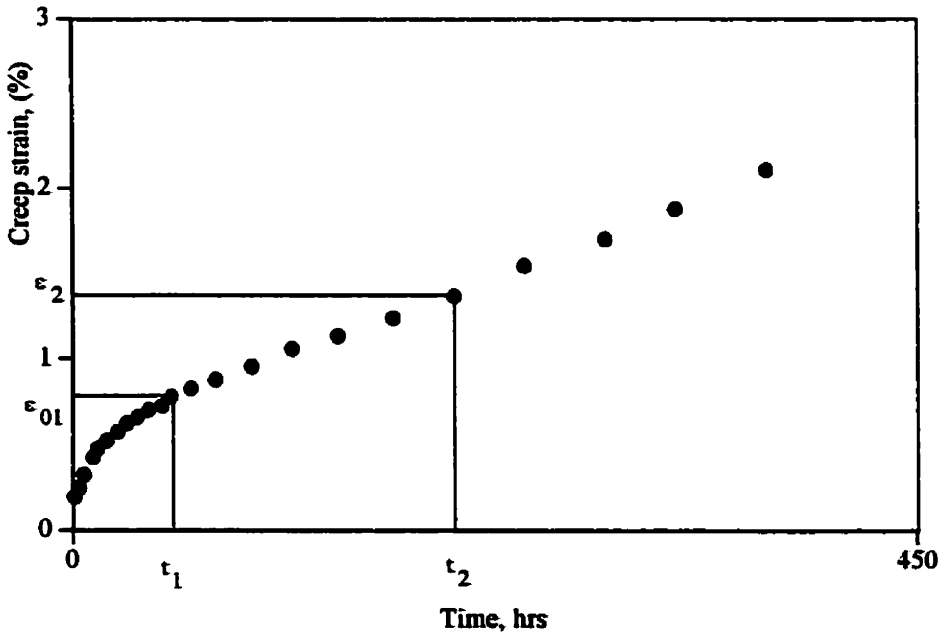

Figure 5.7 Creep test experimental data for Rene N4 VF317 at 760°C along the [0 0 1] orientation. From Dame (1985).

$$\begin{cases} \varepsilon^i = 0.0001 & \dot{\varepsilon}^i = 1.235\times10^{-4}\ \text{mm/mm/s} \\ \varepsilon^i = 0.008 & \dot{\varepsilon}^i = 4.463\times10^{-6}\ \text{mm/mm/s} \end{cases} \tag{5.10.b}$$

Substituting each of the above sets of creep strain and creep strain rates into Eq.(5.10.a) gives two equations for the unknown constants n and k. Solving the resulting equations gives n = 5.07 and k = 1667 MPa.

5.3.3 - Determination of b and q

The isotropic variable R, in Eq.(4.16.g) below describes the transient cyclic behavior of a given material,

$$\dot{R} = b(q-R)\left|\dot{\varepsilon}^i\right| \tag{5.10.c}$$

According to Chiu (1988), the initial cyclic hardening or softening data obtained from cyclic tests provides the necessary information to evaluate b and q. The determination of constants b and q thus requires a series of selected cyclic hysteresis loop data from a constant strain amplitude cyclic test at a constant strain range and strain rate. In order to evaluate b (the isotropic hardening) and q (the saturation value of the isotropic hardening variable), a plot of R versus the accumulated inelastic strain p is required. However, because of the lack of such experimental data available in the literature for SC nickel base alloys, the initial values of b and q used in Eftis et al.(1989) for Inconel 718 at 1200 °F will be used in this work as the initial values. That yields b = 3.75 and q = 400 MPa.

Through this judicious use of limited data, it was possible to determine an initial set of values for the material constants, so they may undergo changes of varying degree. Therefore, the values for the material constants determined thus far should be treated as a first approximation. In the present work, the modification of the initial set of the material parameters determined above is done as in Chiu (1988), by comparing the predicted responses with experimental data, to determine the sensitivity of each parameter. The

the modified material parameters as well as the corresponding material constants are listed in Table (5.7).

Table 5.6 Independent parameters. Data are respectively from Shah and Dhul (1984), and, Sheh (1988).

Independent constants	PWA 1480 T = 593° C	Rene NA VF317 T = 760° C	Rene N4 T = 982° C
Y_{+1} (MPa)	1200	956	240
Y_{-1} (MPa)	1020	818	---
$Y_{[011]}$ (MPa)	970	748	240
$Y_{[\bar{1}11]}$ (MPa)	900	817	280
$Y_{-[\bar{1}11]}$ (MPa)	960	842	---
D_{11} (GPa)	227.58	219.31*	206.20*
D_{12} (GPa)	152.41	150.34*	146.20*
D_{44} (GPa)	111.03	104.82*	94.48*
H_0	0.466e-19. (the natural activation energy)		
K	1.38e-23 (J/K.mol) (the Boltzmann's constant)		
τ_{RT}	380 MPa, (the CRSS at the room temperature)		

The D_{ij} with the symbol * are those for a SC PWA 1480 used for other SC materials.

CHAPTER VI

COMPARISON OF THE MODEL'S RESULTS AND EXPERIMENTAL DATA

The basic equations of the Chaboche's model based on the CA theory and defined in Eqs.(4.16) were used in this work to simulate the behavior of some single crystal (SC) nickel base superalloys. Numerical calculation responses were performed using a Matlab program. The results will now be presented and compared with those from other theories and from experimental data available in the literature. All of the material parameters used in the model were determined in Chapter V. Because of the assumptions required in the derivation of the material constants of the model, however, most of the applications for this data set are intended to demonstrate features of the constitutive model rather than exact correlation with experimental data. The results are presented in two parts:

- the first part deals with the orientation dependence of the initial yield stress, the tension compression asymmetry, and the yield loci;
- the second part deals with the prediction of some simple test responses.

In each of these parts, the correlation between model calculations and experimental data used for evaluating material constants is presented first. Comparisons between the model predictions and other experimental results are then given. The constitutive model

6.1 – YIELD STRESS

It has been shown in a number of studies that mechanical properties of anisotropic materials in general and SC nickel base super-alloys in particular are orientation dependent. This is true for elastic constants as well as their initial yielding. As observed by Li and Smith (1995.d), although elastic constants and the initial yield stress are based on the behavior of such materials within and over their elastic ranges, not many studies in the literature are devoted to their orientation dependence.

Concerning elastic constants, the theory developed in Lekhnitskii (1962) and presented in section 3.2.1 of Chapter III was used. The orientation dependence of the Young's modulus and the shear modulus for SC nickel base superalloys for Rene N4 at 760° C were plotted in Figure 3.4, while the corresponding Poisson's ratio was plotted in Figure 3.5. These results are in agreement with those observed in Dame (1985.d), and Li and Smith (1995). This portion of the theory can therefore be assumed valid.

The technique used by the CA theory for the determination of initial yield stress in SC nickel base superalloys was developed in Chapter III. Recall that, in the CA theory, the effective yield stress under a global state of stress is determined by combining the yield stress derived from Lee and Zaverl's yield function with a factor that accounts for the micro-slip state in the material. The results are presented in this section.

6.1.1 – Orientation dependence of the initial yielding

6.1.1.1 – Along the $[0\,0\,1]$–$[0\,1\,1]$ boundary

In order to illustrate the importance of using the CA theory, two predicted phenomenological yield stresses from Lee and Zaverl (with and without correction) are plotted and compared with experimental data. In Figure 6.1, the predicted yield stress without correction is compared with experimental data for PWA 1480 at 593° C. The difference observed in the shape of both curves is significant and may be

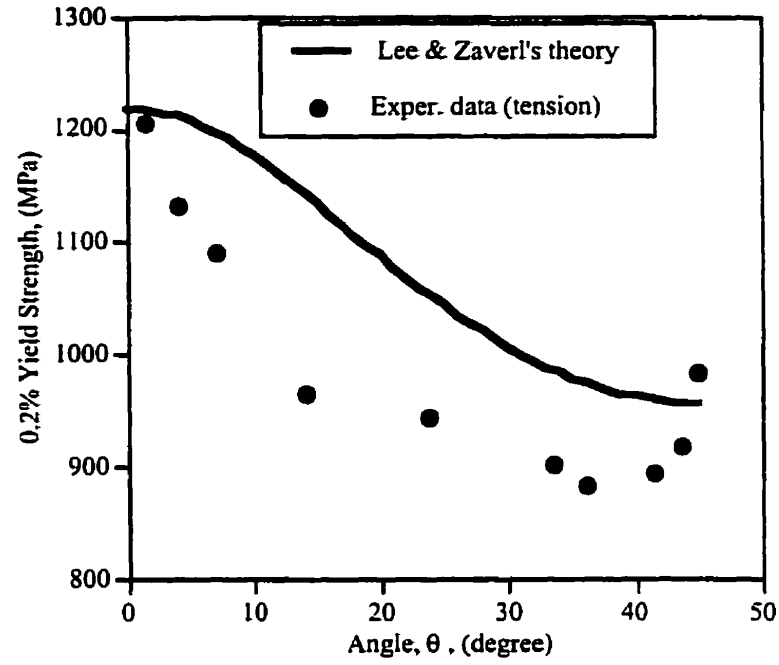

(a)

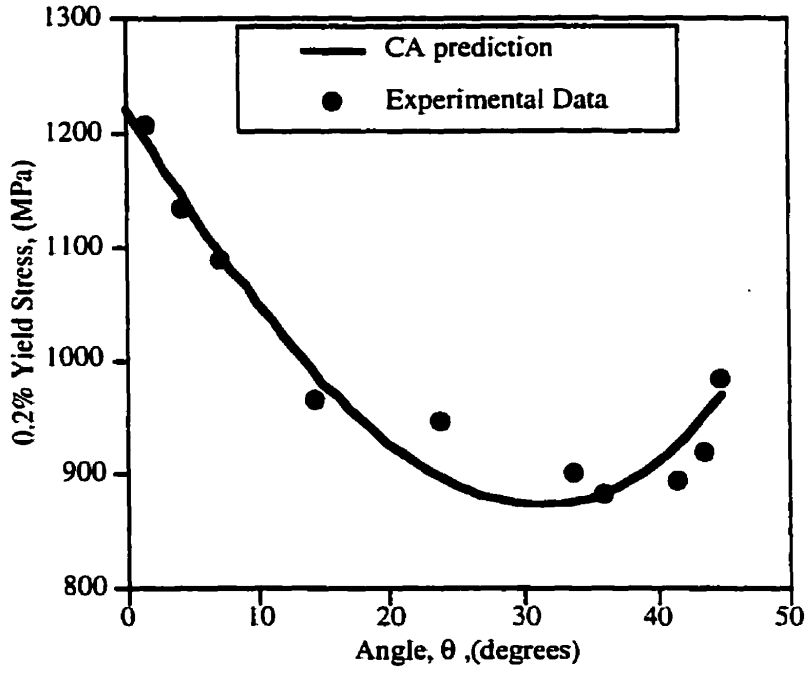

(b)

Figure 6.1 Comparison of the initial yielding for PWA 1480 at 593° C along the [0 0 1] - [0 1 1] orientation boundary, between experimental data and the Lee and Zaverl's yield function: (a) before correction (b) after correction (CA). Data are from Shah and Duhl (1984).

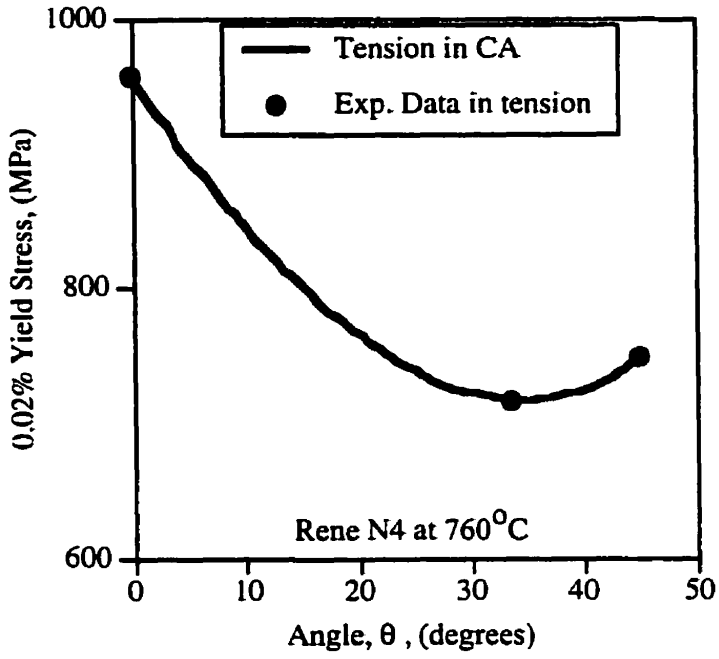

(a)

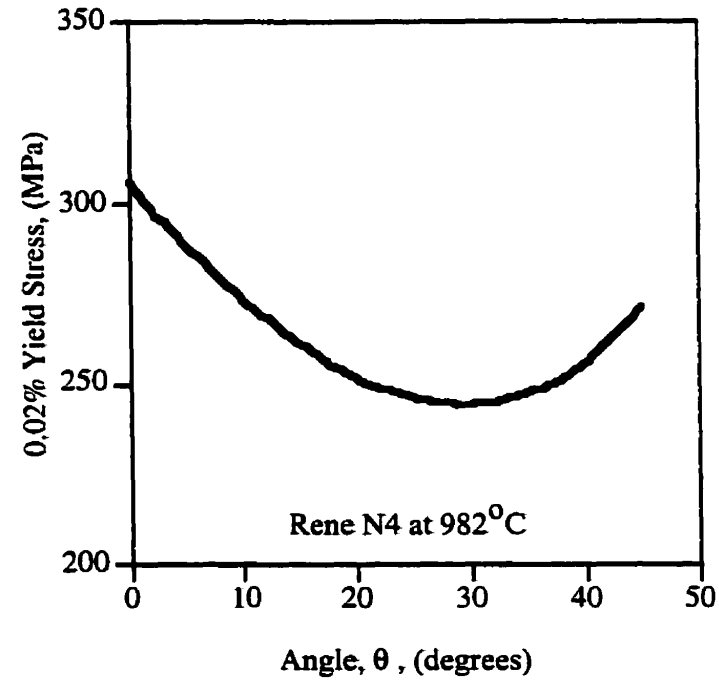

(b)

Figure 6.2 Orientation dependence of the initial yielding between experimental data and the CA theory for: a) Rene N4 VF317 at 760° C and b) Rene N4 at 982° C along the [0 0 1] –[0 1 1] orientation boundary.

attributed to the lack of micro-slip that is predominant in the deformation of such materials. In Figure 6.1.(b), the predicted yield stress after correction is compared with experimental data for the same material at the same temperature. From these results, it can be observed that the CA theory predicts well the orientation dependence of the initial yielding in the octahedral slip along the $[0\,0\,1]$–$[0\,1\,1]$ boundary. Two other predicted initial yield stresses along the $[0\,0\,1]$- $[0\,1\,1]$ boundary are plotted in Figures 6.2.(a) and 6.2.(b), for Rene N4 VF317 at 760° C and Rene N4 at 982° C respectively.

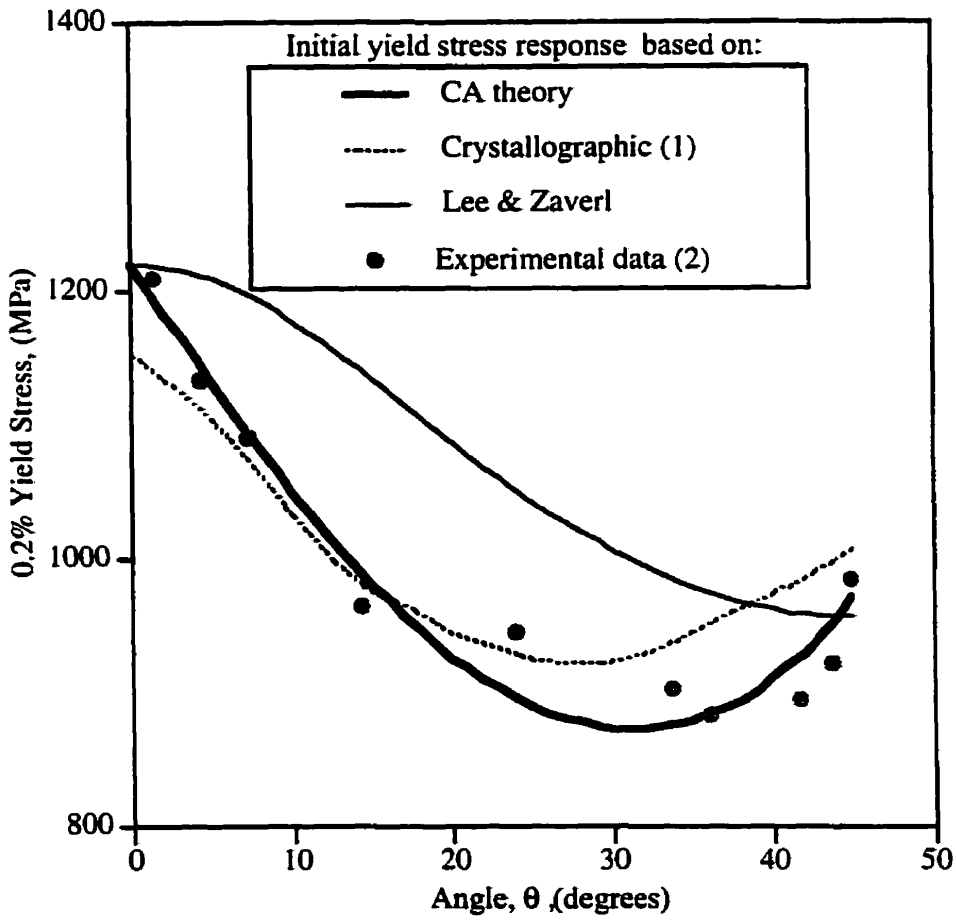

Figure 6.3 Comparison between three predicted yield stress theories with experimental data for PWA 1480 at 593° C along the [0 0 1]-[0 1 1] boundary. Data are from: (1) Jordan and Walker (1991) and (2) Shah and Duhl (1984).

Once again, it can be observed from these results that the CA theory successfully predicts the initial yielding of these SC materials for the three temperatures above. In Figure 6.3, the orientation dependence of the initial yielding for three predicted theories is compared with experimental data for PWA 1480 at 593° C along the [0 0 1]-[0 1 1] boundary. Once again, the CA seems to predict that feature better than the two other theories. It is therefore evident that the way micro-slip is introduced in the evaluation of the yielding along the [0 0 1]-[0 1 1] boundary is consistent with the results.
In order to validate the theory for orientation other than the [0 0 1]-[0 1 1] boundary, the yield contours are plotted in the stereographic triangle, defined in Appendix B.

6.1.1.2 – In the stereographic triangle

Figures 6.4. (a), (b) and (c) show the yield contour plots for PWA 1480 at 593° C in the stereographic triangle. Those plots are derived respectively from experimental data, the CA theory and Lee and Zaverl's theory. Although the experimental data do not show cube slip predominance near the [1 1 1] orientation, it can be seen from Figures 6.4.a and 6.4.b that the trend of the yield contour predicted by the CA theory, using the octahedral slip system, is similar to those obtained experimentally. Furthermore, the yield contours generated by the CA theory predicts very well the octahedral and cube slip systems predominance, respectively near the [0 0 1] and [1 1 1] orientations. As noted by Sheh (1988), for the SC response of Rene N4, the observed difference between the predicted yield contour in Figure 6.4.b, and the experimental data in Figure 6.4.a is thought to be caused by inaccurate reproduction of the experimental data.

One of the arguments in favor of that idea is illustrated in Figure 6.5, where two experimental data sets representing the initial yield stress for PWA 1480 at 593° C along the [0 0 1]-[0 1 1] boundary are plotted. Recall that the set (data N°1) comes from Sheh and Duhl (1984), while the set (data N°2) is derived from the experimental yield contour plotted in Figure 6.4.(a). Although both sets of data are from the same material at the same temperature along the same boundary, it is seen that the set (data N°2) is shifted up comparatively to the set (data N°1). Therefore, one of the data set should be wrong.

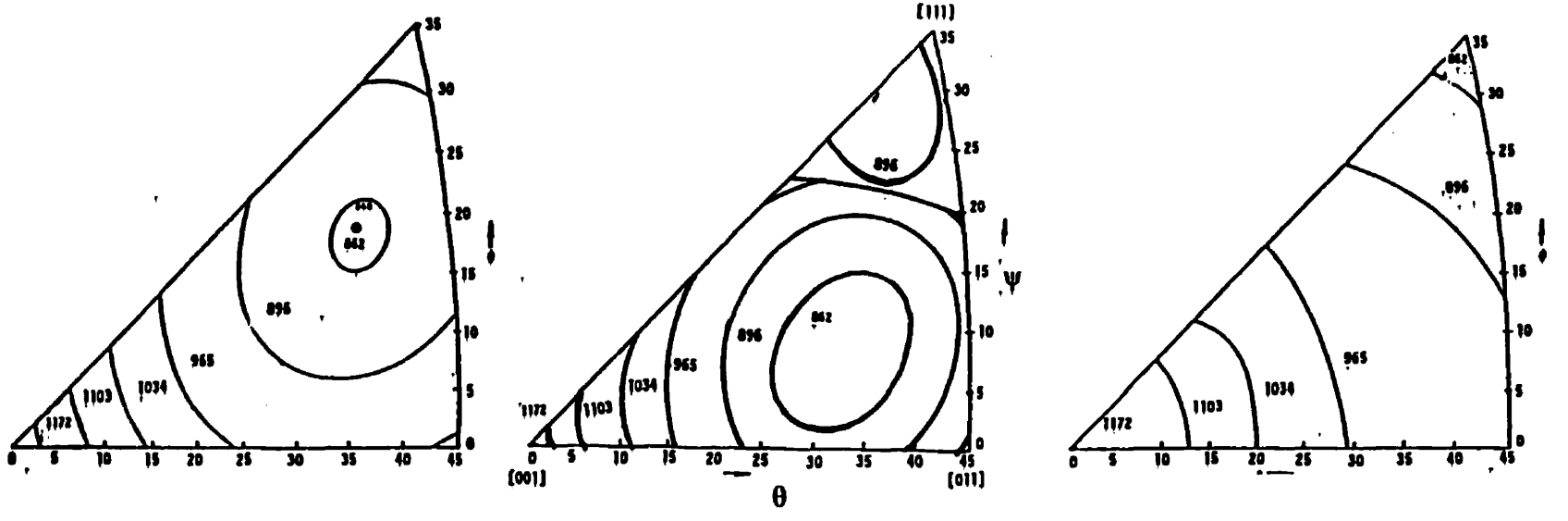

(a) (b) (c)

Figure 6.4 Representation of the yield contour in the stereographic triangle for PWA 1480 at 593° C, using: (a) the experimental data, (b) the CA theory and (c) the Lee and Zaverl's theory. Data are from Swanson et al. (1986).

There is another argument in favor of the idea that the yield contour plotted in Figure 6.4.(a) is shifted up: in that graph, only the octahedral slip systems are active even around the $[\bar{1}11]$ orientation, where cube slip systems are supposed to be predominant. According to the slip trace studies summarized in Chapter II, cube slip systems are predominant around the $[\bar{1}11]$ orientation, while octahedral slip systems are predominant around the [0 0 1] orientation regardless of temperature. This feature, observed in several SC slip trace studies such as Takeuchi and Kuramoto (1973) and Lal, Chin and Pope (1979), is predicted by the CA theory, as shown in Figure 6.4.(b). In any case, the best way to validate these results is to perform new tests.

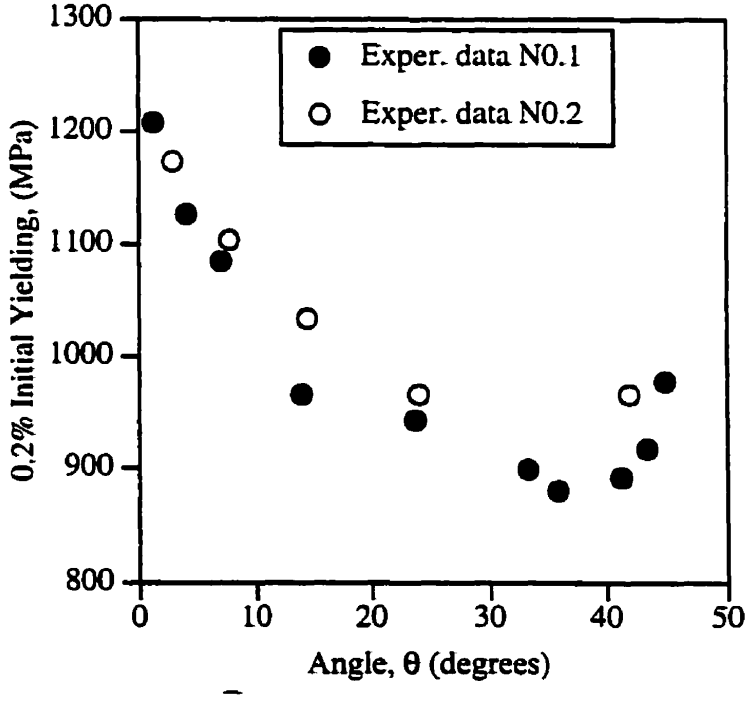

Figure 6.5 Comparison between two sets of experimental yield stress data for PWA 1480 at 593° C along the [0 0 1]-[0 1 1] boundary. Data N° 1 comes from Sheh and Duhl (1984), while N° 2 comes from Swanson et al (1986).

6.1.1.2 – Tension/compression asymmetry

Tension/compression asymmetry is one of the features observed in SC materials that the classical Lee and Zaverl yield function cannot predict. This feature, however, can be predicted satisfactorily by the CA theory. Two distinct slip factors are required to exhibit that phenomenon, according to whether the sample is loaded in tension or in compression. For example during tension tests, slip systems similar to $(1\,1\,1)[\bar{1}\,0\,1]$ are predominant, while during compression tests, slip systems similar to $(1\,1\,1)[\bar{1}\,2\,1]$ are predominant. Figure 6.6 shows the orientation dependence of tension/compression asymmetry between the predicted and experimental data for the SC nickel base superalloys PWA 1480 at 593° C. Good correlation is observed between the predicted curves and experimental data in tension as well as in compression (see Table 6.1). The biggest error in the predicted yield stress (8%) appears along the $[\bar{2}\,3\,6]$ orientation.

In the regions where cube slip systems are predominant, the difference on the slip factors comes from the material constants.

Recall that, in the CA theory, the slip systems of type 1 are predominant in tension while the slip systems of type 2 are predominant in compression. There may therefore exist two distinct regions within any SC sample where the yield stress in tension (T) is higher or lower than the yield stress in compression (C). Figure 6.7 shows the tension/ compression predominance regions in the stereographic triangle for PWA 1480 at 593° C. These results are in agreement with those obtained by Li and Smith (1995.d) for the SC nickel base superalloys SRR99.

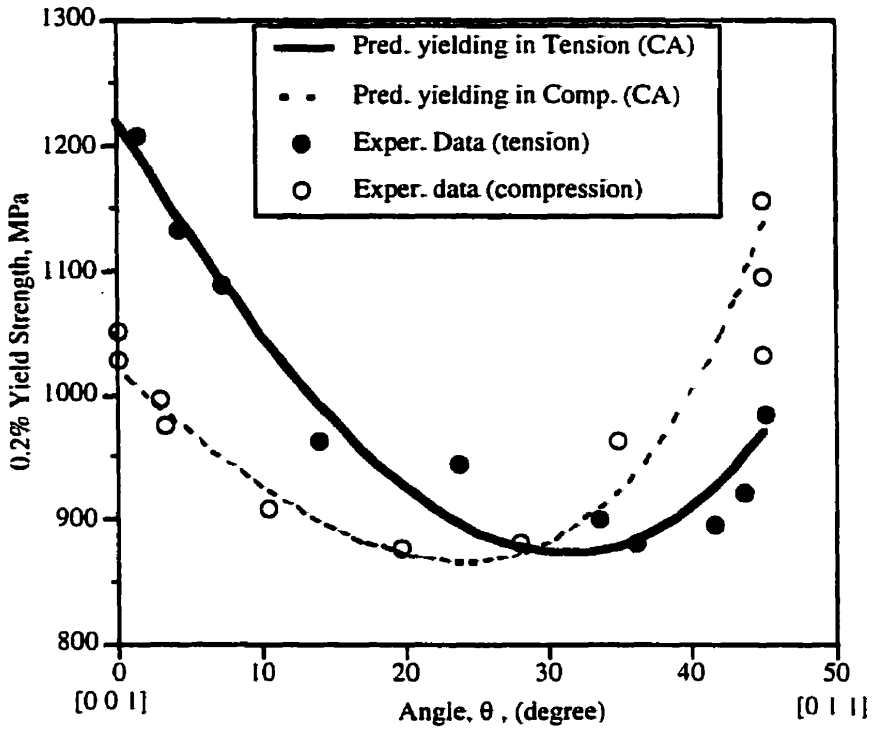

Figure 6.6 Comparison of tension/compression asymmetry between the CA theory and experimental data for PWA 1480 at 593° C along the [0 0 1]-[0 1 1] boundary. Data are from Sheh and Duhl (1984).

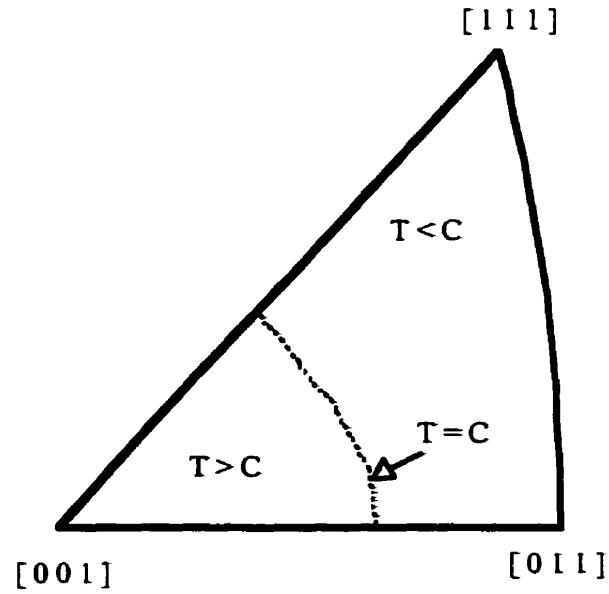

Figure 6.7 Tension/compression predominance regions in the stereographic triangle for PWA 1480 at 593° C.

Table 6.1 Comparison of the monotonic yield strength between the predicted CA theory and data for Rene N4 at 760° C. From Gabb et al. (1986).

Orientation MPa	Tensile Yield (MPa)	Error %	Compressive Yield (MPa)	Error %
[0 0 1]	956 (956.0)	0.00	818 (818.0)	0.00
[0 1 1]	748 (748.0)	0.00	905 (911.1)	0.67
[0 2 3]	695 (714.0)	2.73	747 (741.0)	0.80
$[\bar{1}\,1\,1]$	817 (815.6)	0.17	842 (840.6)	0.16
$[\bar{2}\,3\,6]$	716 (683.5)	4.53	714 (771.2)	8.01
$[\bar{1}\,4\,5]$	656 (676.0)	3.04	792 (802.0)	1.26

Values in parenthesis derived from the CA theory

6.1.3 – Temperature dependence on the initial yielding

Temperature dependence of the initial yielding for SC materials shows that these materials respond differently as they work at low temperatures (under 750° C), high temperatures (above 850° C) and at intermediate temperatures. It is therefore convenient, when developing a new theory for SC material analysis, to make sure that it adequately predicts the material behavior within each of the three ranges mentioned above.

The combined approach theory developed in the present work is essentially isothermal. However, in order to check how it predicts cube slip system expansion with increasing temperature, three distinct temperatures (T_1=593° C, T_2=760° C and T_3=982°) were chosen within each of the three temperature ranges mentioned above. At each of the temperatures, the limit between octahedral slip systems and cube slip systems was plotted in the stereographic triangle. The results are plotted in Figures 6.8 (a), (b) and (c) for three distinct SC nickel base superalloys. From these figures, it is seen that with the exception of Rene N4 at 760° C, the results are as expected. Cube slip system expands with increasing temperature. Contrary to the octahedral slip system, it is seen that the range of orientations exhibiting cube slip or slip system of type 3 expands with increasing test temperature. That feature has been observed in many SC nickel base superalloys slip trace studies such as Takeuchi and Kuramoto (1973), Lal, Chin and Pope (1977) and others. Although the trend of cube slip expansion is in the agreement with testing, it is conceivable that its actual area (of cube slip system expansion) is higher than the predicted area. This is observed in Miner et al. (1986.a), where cube slip traces were observed on the [0 2 3] orientation for Rene N4 at 875° C, indicating the great extent of the orientations exhibiting cube slip at that temperature. It is evident that the predicted cube slip area for Rene N4 should be far away from that orientation at that temperature.

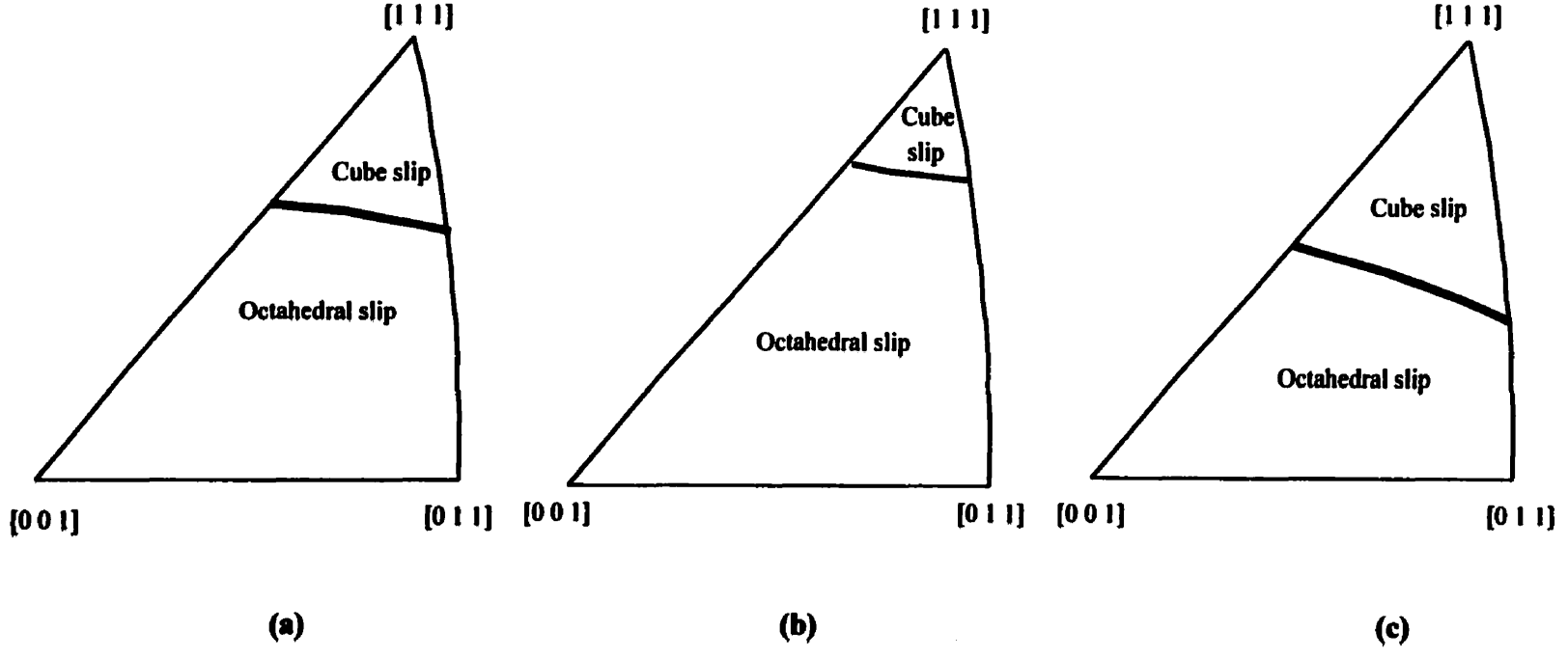

Figure 6.8 Predominance limit representation in the stereographic triangle between octahedral and cube slip systems for 3 SC nickel base superalloys: (a) PWA 1480 at 593° C, (b) Rene N4 VF317 at 760° C and (c) Rene N4 at 982° C.

6.1.4 – Predicted Yield Loci

The yield loci for SC nickel base superalloys in the octahedral slip system have been evaluated considering: (i) the slip system similar to $(111)[\bar{1}01]$ (type 1) and (ii) both of the slip systems similar to $(111)[\bar{1}01]$ and $(111)[\bar{1}21]$ (type 2) respectively.

In Figures 6.9 (a) and (d), two yield loci based on Lee and Zaverl's yield function (ellipse), and the slip factor Sf using only the octahedral slip systems of type 1 (solid straight line) are presented in each plot respectively. From these graphs, it is seen that the yield loci generated by the slip factor alone using only slip systems of type 1 are similar to those shown in Figures 6.10 (c) and (d). These yield loci, performed by Piehler and Backofen (1969), are based on the crystallographic slip analysis and use both upper and lower bound predictions.

In Figures 6.9 (b) and (e), two yield loci based on Lee and Zaverl's yield function (ellipse), and the CA theory using only octahedral slip systems of type 1 (solid line) are presented in each plot respectively. From these graphs, it is seen that the yield loci based on the CA theory and shown in Figures 6.9.(b) and (e) are somewhat the combination of both yield loci represented in Figures 6.9.(a) and (d) respectively. As the yield loci generated by the CA are symmetric to the origin, therefore the tension compression cannot be described using that formulation.

Finally, Figures 6.9.(c) and (f) represent the yield loci based on the CA theory in the cases where the slip factor use the slip systems of type 1 in tension, and the slip systems of type 2 in compression. The corresponding yield loci present asymmetry behavior to the origin and therefore, they can describe tension compression asymmetry.

From the results above, it is evident that, only the slip factor is responsible for tension compression symmetry.

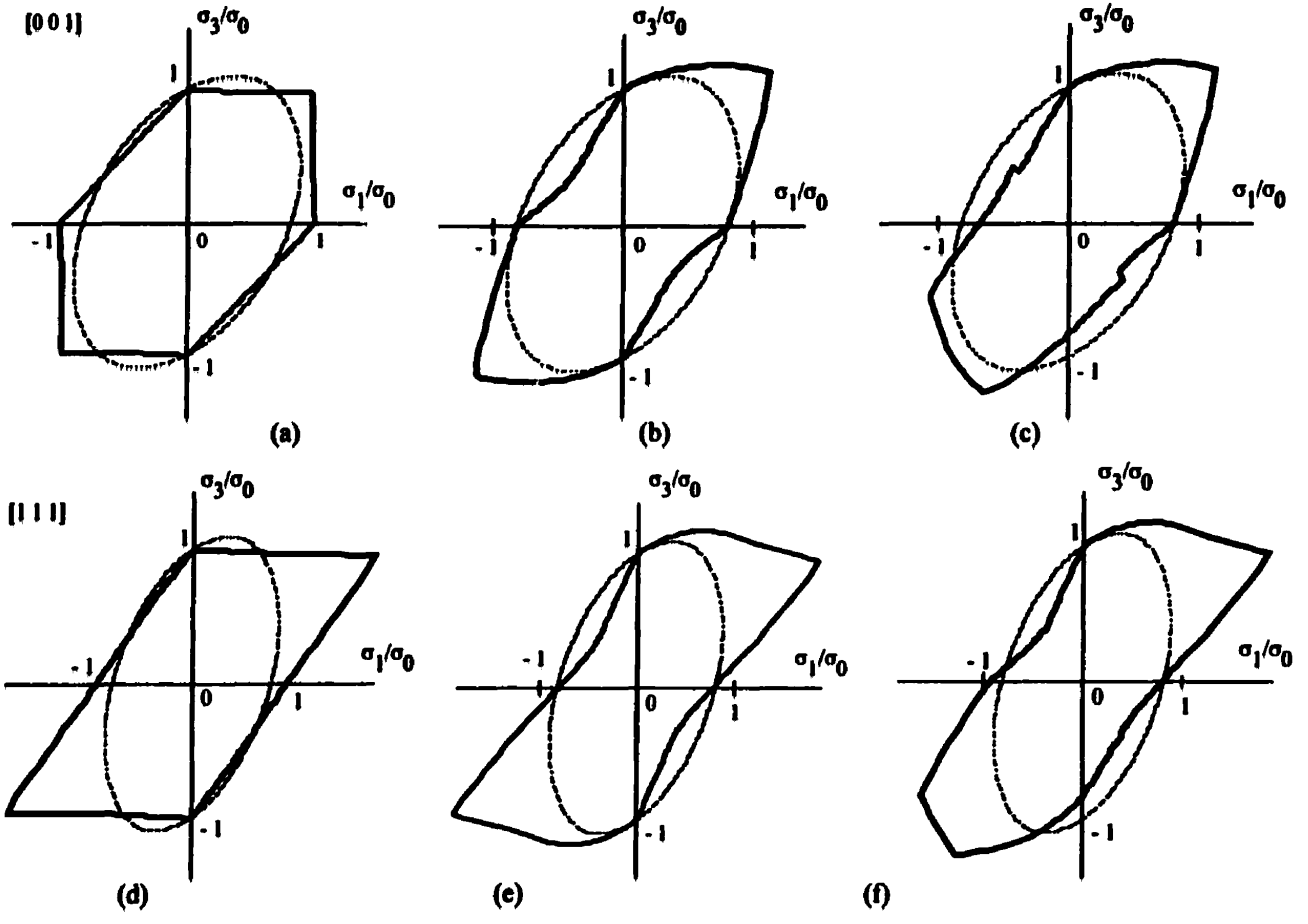

Sf1 is the slip system similar to (1 1 1)[1 0 1] while SF2 is the slip system similar to (1 1 1)[1 2 1].

Figure 6.9 Comparison between yield loci based on the Lee and Zaverl theory (ellipse) with those based on others theories (close line) for two system bases, [0 0 1] and [0 1 1]. In (a) and (d) Sf1 alone is used; in (b) and (e) the CA uses only Sf1; and finally, in (c) and (f), the CA uses both Sf1 and Sf2.

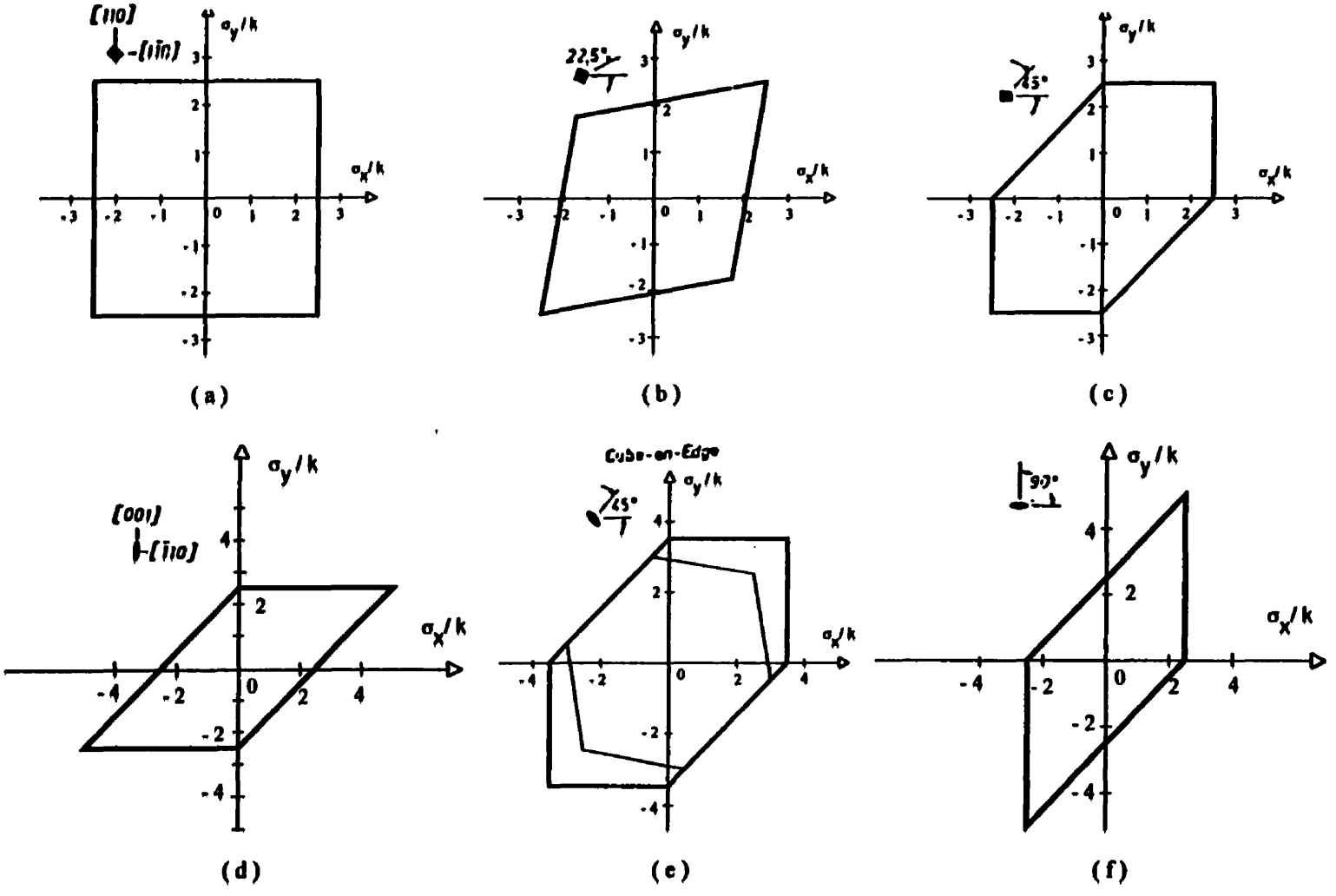

Figure 6.10 Predicted yield loci based on the crystallographic slip analysis and using both upper and lower bound predictions for various textures in f.c.c. metals. From Piehler and Backofen (1969).

6.2 – PREDICTED SIMPLE TESTS RESPONSES

6.2.1 – Monotonic tensile response.

Figure 6.11 compares the predicted stress-strain curves based on the CA theory (solid line) with the experimental data (dotted line) for Rene N4 VF317 at 760° C along the nominal [0 0 1] and [0 1 1] orientations. These curves show the strong anisotropic properties of the material and the orientation dependence of the elastic constants (Young's modulus) as well as the initial yielding. Ultimately, these results show that the predicted model (based on the CA theory) correlates very well with experimental data along both orientations. Significant mismatch was, however, observed between the predicted and experimental responses along the [0 1 3] orientation, about 20° from [0 0 1] in the $[0\,0\,1]$–$[0\,1\,1]$ boundary, (see Figure 6.12). Since an analogous observation has been made with the model of Sheh (1988)[1] along the same orientation, it was seen useful to compare the predicted CA and Sheh theories with experimental data. From the figure of those results, it is seen that in the elastic range, the CA theory predicts very well the actual Young modulus, while in the plastic range, its prediction is closer to the model of Sheh (1988) than it is to experimental data. As concluded in Sheh (1988), this mismatch is thought, to be caused by inaccurate orientation used in the calculation. That conclusion can be justified by the fact that the actual initial yield stress along the [0 1 3] orientation is about 1000 MPa that is higher than the yield stress along the [0 0 1] orientation.

Two other predicted tensile tests for Rene N4 VF317 at 760° C are plotted in Figure 6.13 along the $[\bar{1}\,1\,1]$ and $[\bar{2}\,3\,6]$ orientations. Although there are no experimental data available to compare quantitatively, the observed trends are, however, as expected for such materials.

---

[1] Based on the crystallographic approach

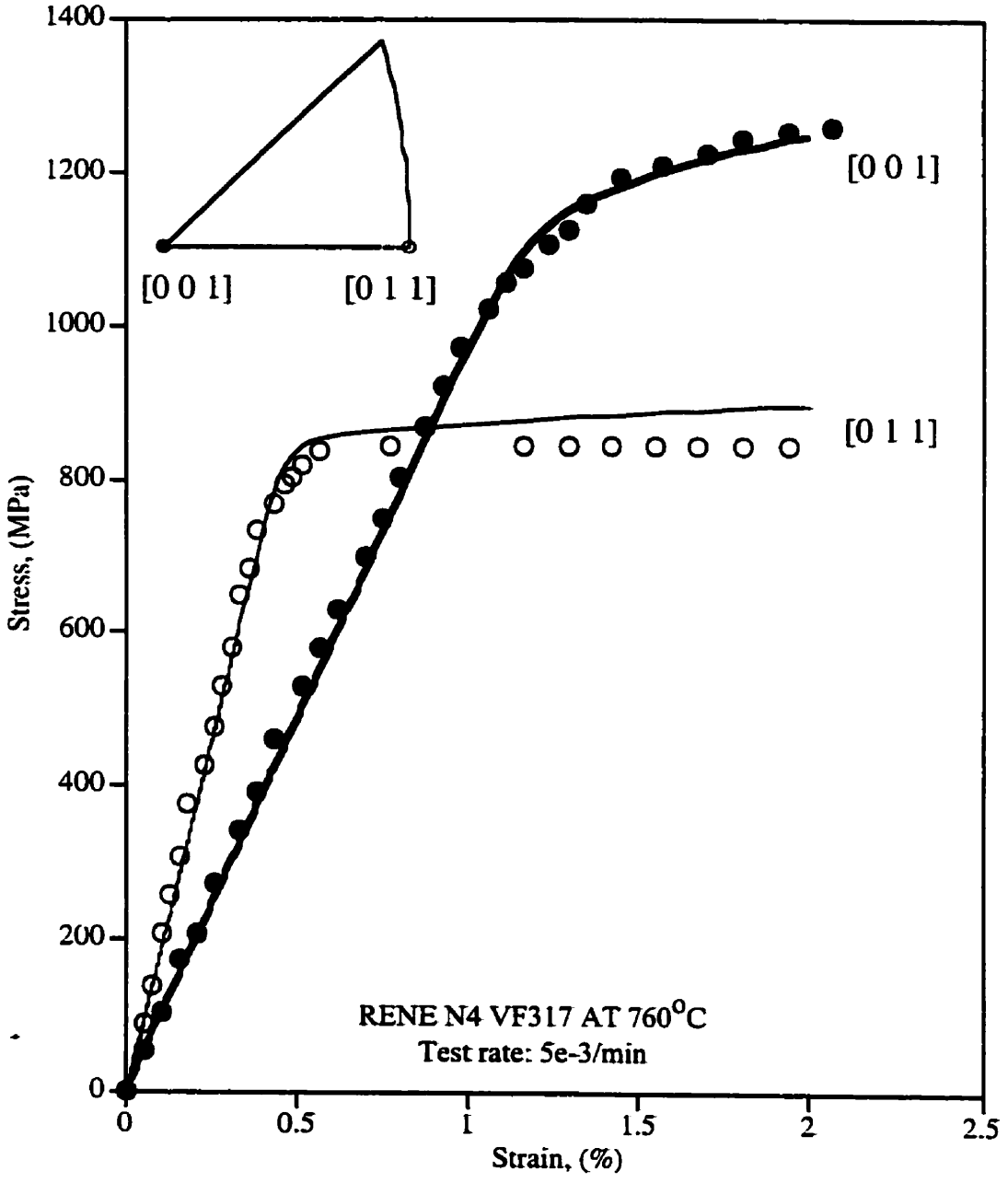

Figure 6.11 Comparison between the CA predictions and experimental data in the nominal [0 0 1] and [0 1 1] orientations for Rene N4 VF317 at 760° C. From Sheh (1988).

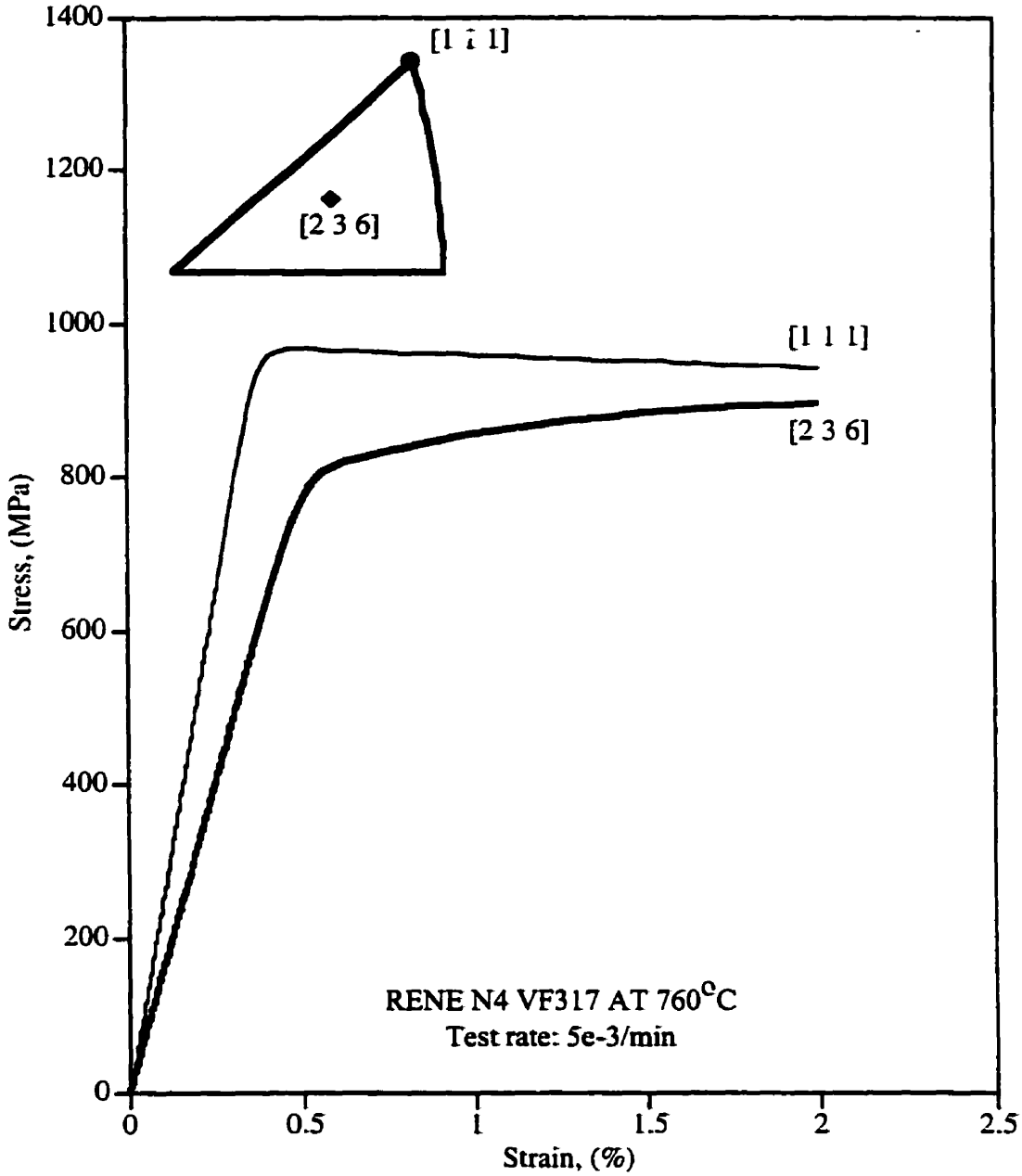

Figure 6.13 Predicted tensile stress-strain responses with the CA theory along the nominal [1 1 1] and [2 3 6] orientations.

6.2.2 – Creep response

The creep response in the [0 0 1] orientation at creep stresses of 621 MPa, 655 MPa, and 758 MPa were calculated and compared with experimental data in Figure 6.14. For the three hold stresses above, the primary and the secondary creep regime of the model correlates relatively well with experimental data. The calculated steady state creep rates also correlate well with the data.

Calculations for creep responses in the [0 0 1], [0 1 1] and [0 342 940] orientations were also calculated and they are compared with experimental data in Figure 6.15 and Figure 6.16. Given the assumptions made in the derivation of material constants of the model, the correlation between the model and the predicted experimental data can be considered to be very good.

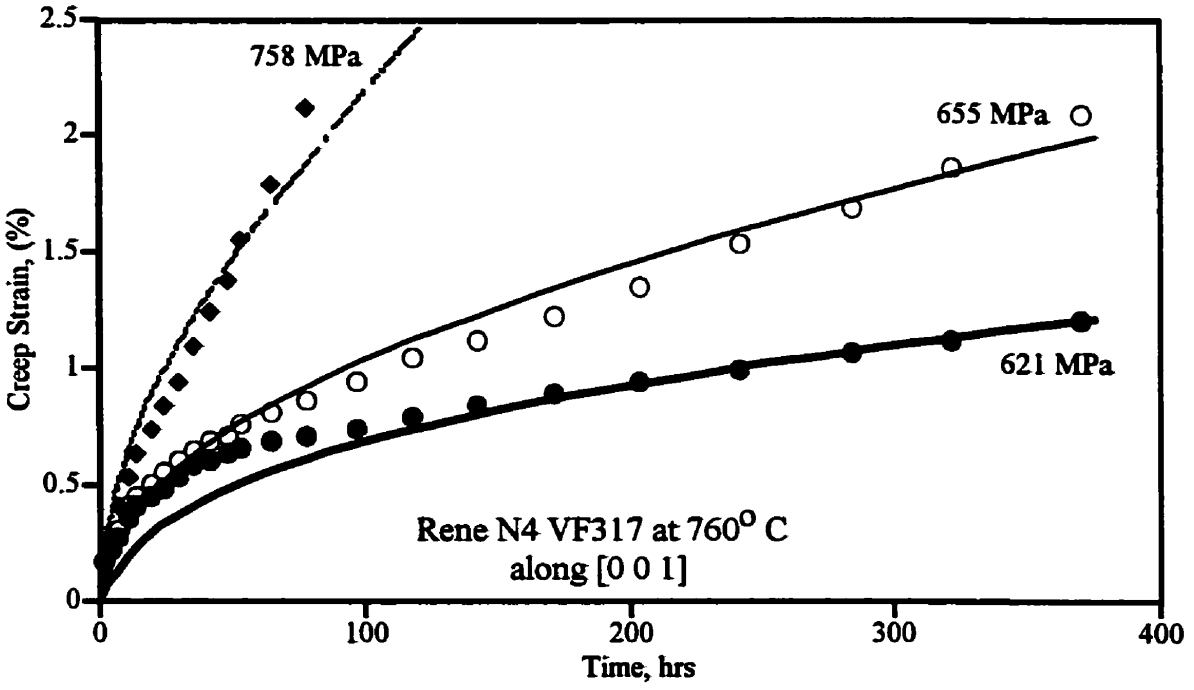

Figure 6.14 Comparison of creep responses for Rene N4 VF317 in the [0 0 1] orientation at creep stresses of 621, 655 and 758 MPa. From Dame (1985).

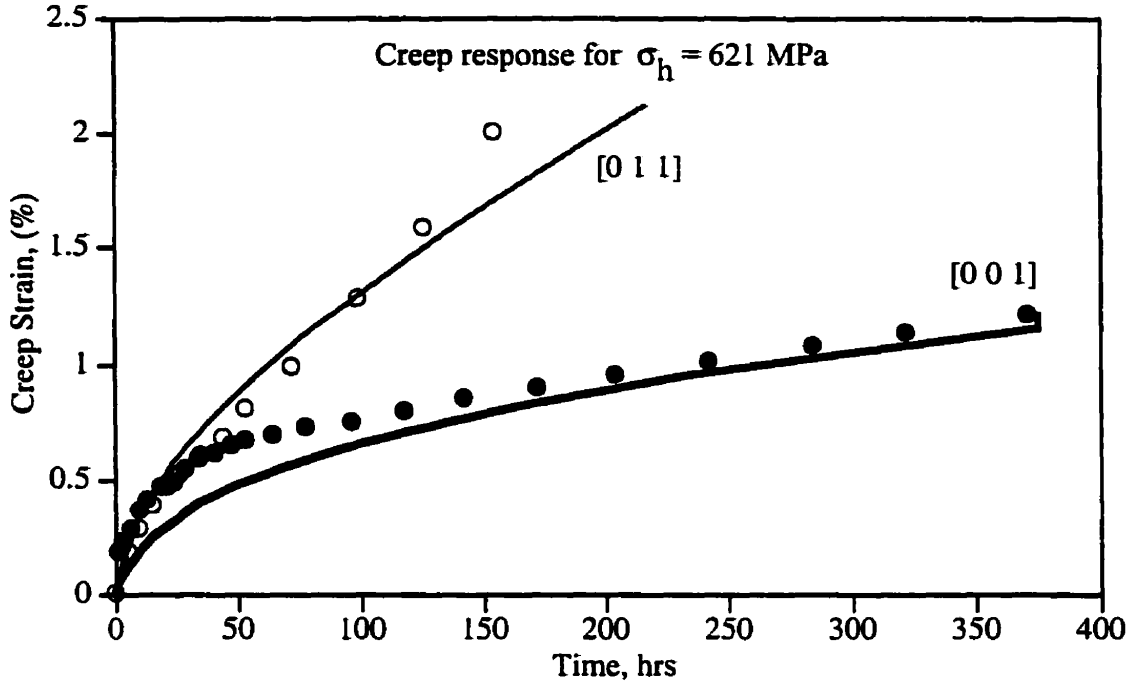

Figure 6.15 Comparison of creep response for Rene N4 VF317 in the [0 0 1] and [0 1 1] orientations at creep stress of 621 MPa. From Dame (1985).

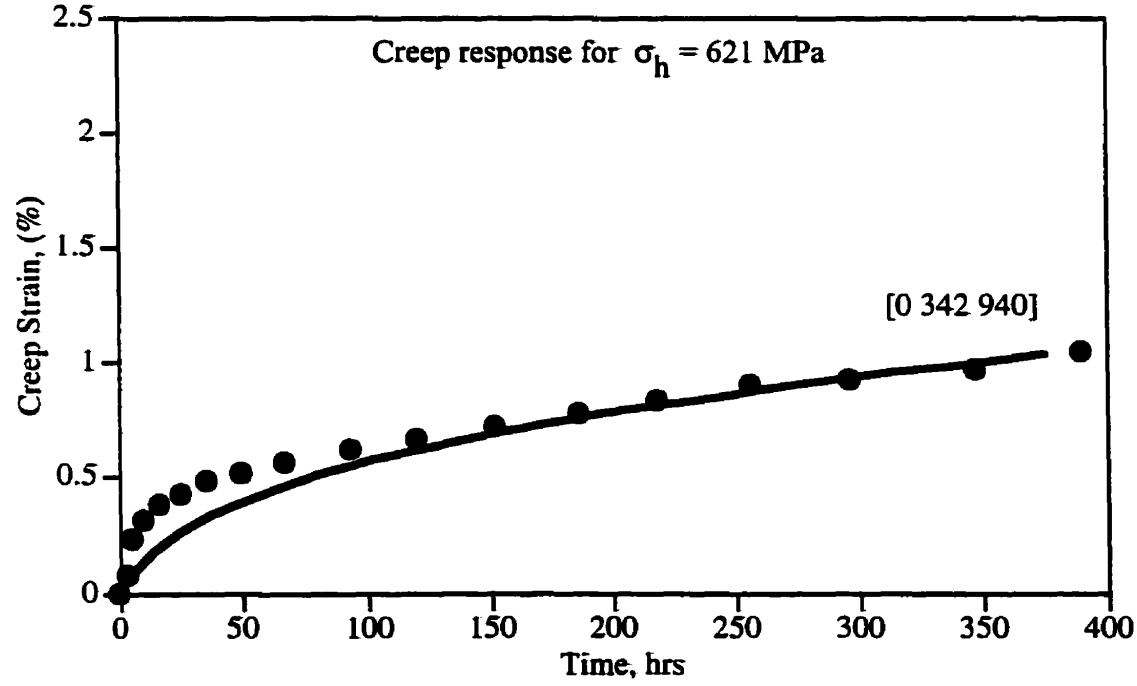

Figure 6.16 Comparison of creep response for Rene N4 VF317 in the [0 342 940] orientation at creep stress of 621 MPa. From Dame (1985).

6.2.3 – Cyclic response

Responses predicted by the CA theory of the first cyclic test for Rene N4 VF317 at 760° C are presented in Figure 6.17 along the orientations [0 0 1], [0 1 1] and $[\bar{1}\,1\,1]$. Because no cyclic data were available for Rene N4 VF317 at that temperature, the comparison between the predicted fully reversed results and experimental data was not possible. However, the predicted results are very similar to the experimental data for Rene N4 at 760° C, presented in Figure 6.18 along the three orientations above. The only difference is in the fact that, for Rene N4 at 760° C, the initial yielding was lower in tension as well as in compression along the three orientations mentioned above. The same observation has been evaluated in Dame (1985) to be about 30% along the [0 0 1] orientation. The source of that observed response was attributed to the slightly different chemistry for VF317.

Finally, as expected, the prediction for the [0 0 1] orientation showed a larger peak stress in tension than it did in compression, while the calculation in the [0 1 1] orientation showed the opposite pattern. That result has been noted in section 6.1, which deals with the orientation dependence of tension/compression asymmetry.

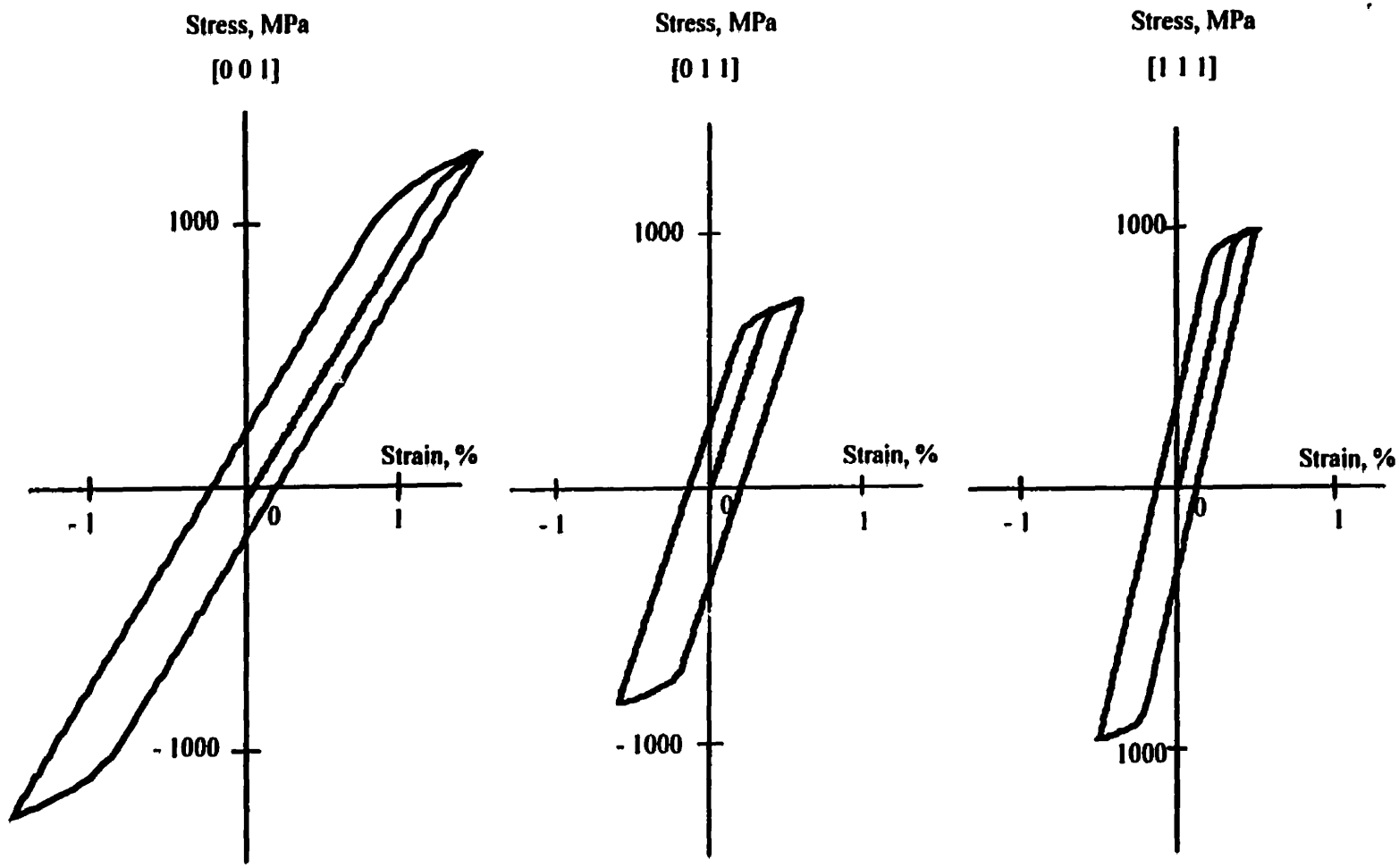

Figure 6.17 Predicted first fully reversed cyclic response for Rene N4 VF317 at 760° C along the [0 0 1], [0 1 1] and [1 1 1] orientations using the CA theory.

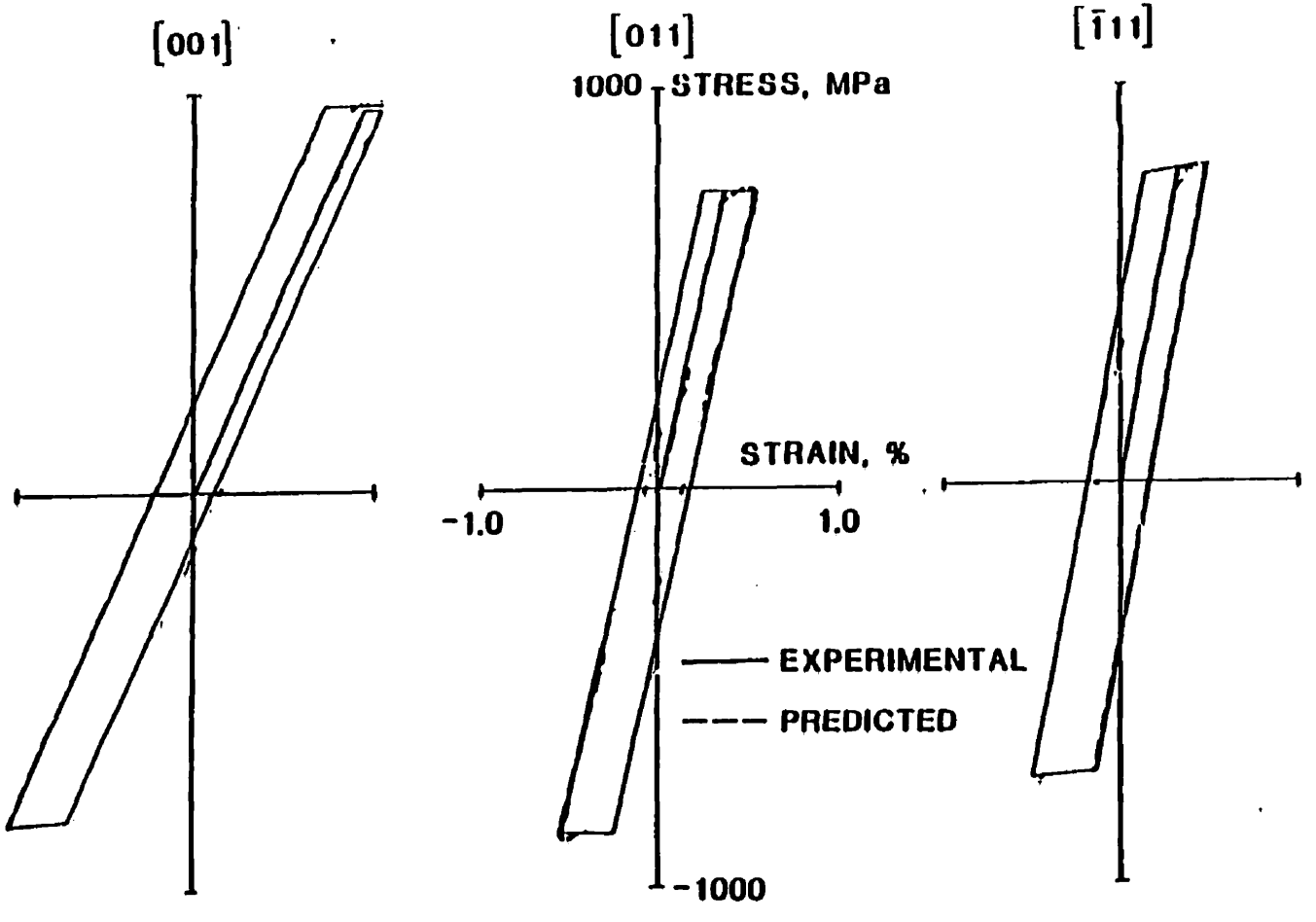

Figure 6.18 Experimental first fully reversed cyclic test response for Rene N4 at 760° C along the [0 0 1], [0 1 1] and [1 1 1] orientations. Data are from Dame (1985).

6.2.4 – Stress relaxation

Although no stress relaxation data are available in the literature for Rene N4 VF317 at 760° C, the stress relaxation responses for specimens oriented in the [0 0 1] and [0 1 1] directions were calculated and then plotted in Figure 6.19. Both predictions are for a constant displacement boundary condition. The qualitative behavior is as expected, with the stress in the [0 1 1] orientated specimen relaxing slightly faster than in the [0 0 1] oriented specimen. The strain rates in the [0 0 1] oriented specimen are in the same range as in the creep tests. However, the strain rates in the [0 1 1] oriented specimen span the range between the tensile and the creep data. Although the predicted relaxation responses appear correct from a qualitative point of view, it would be prudent to validate these results using comparison with experiments.

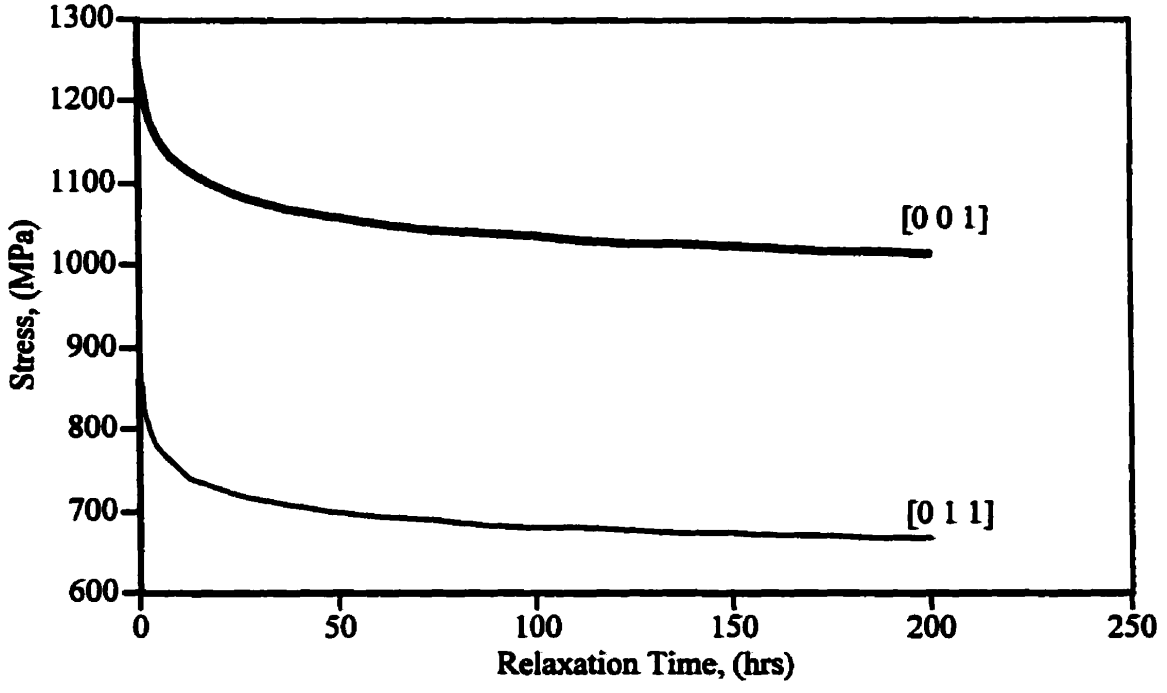

Figure 6.19 Predicted stress relaxation curves for Rene N4 VF 317 at 760° C along the [0 0 1] and [0 1 1] orientations.

CHAPTER VII

DISCUSSION AND SUMMARY OF THE CURRENT MODEL

Early in this research, a significant effort was devoted to highlighting the advantages and disadvantages of the two main approaches (macroscopic and microscopic) used for SC materials analysis. Unlike models based on the microscopic approach, those based on the macroscopic approach are numerically simple. In addition, while implementing these models in a finite element code, they are somewhat less complicated and generally require less calculation. However, their most significant disadvantage is that the actual deformation mechanisms do not correlate well with the theory. This lack of correlation limits their predictive capability for modeling SC materials. From the foregoing observations, the goal of the present research is to propose a new tool, (a phenomenological combined approach) which will enhance predictive capability for modeling single crystal (SC) material.

The success of this theory comes down to the use of accurate deformation mechanisms. Its particularity can be attributed to two major elements: first, the incorporation of the slip factor into the drag stress state variable and second, its capability to express the material parameters as a function of the orientation. These two elements lend a strong

The second element, however, introduces the microscopic properties of the material under given strain rates. This element establishes the physical basis for the model. The results indicate that the active slip system depends on temperature, strain rate and loading orientation relative to the principal axes of the material.

At high strain rates, the deformation mechanism is characterized by dislocations of the γ' particles, while at low strain rates, it is characterized by the interstitial emission and diffusion mechanisms. In order to characterize the effect of a dislocation network for both mechanisms, two terms representing each mechanism have been coupled in the current databases. This was done in such away that, at the high strain rate, one of the terms becomes predominant and the other term negligible, while at the low strain rate, the opposite occurs. This approach appeared to be satisfactory at high and low strain rates. Prediction of behavior at the intermediate strain rate range, however, requires more refinement.

For the SC nickel base superalloys used in this work, three main slip systems were identified: two octahedral slip systems similar to the a/2(1 1 1)$[\bar{1}\,0\,1]$ and a/2(1 1 1) $[\bar{1}\,2\,1]$, and one cube slip system similar to the a/2(1 0 0)$[\bar{1}\,0\,1]$. In accordance with the applied stress orientation and the temperature considered, one of these slip systems had to be predominant. That system was used for the yield condition. For example, during a tension test, two slip systems should be primarily predominant: it concerns the octahedral slip systems similar to a/2 (1 1 1)$[\bar{1}\,0\,1]$, and the cube slip systems similar to a/2(1 0 0)$[\bar{1}\,0\,1]$. Conversely during the compression test, two slip systems should be primarily predominant, the octahedral slip systems similar to a/2(1 1 1)$[\bar{1}\,2\,1]$ and the cube slip systems similar to a/2(1 0 0)[1 0 1].

7.2 – DATA BASE REQUIREMENT

In the short term, it should be possible to implement the current constitutive model into a finite element code and utilize it as a viable mechanical analysis tool with little further development. However, to use the present constitutive model, it would be convenient to develop the database for evaluating the material parameters. Since for turbine blades and vanes operation mostly occurs at temperatures between 600° C to about 1000° C, the test data for the inelastic response of the material should therefore be acquired in this temperature range. These tests are based on the ideal tests required to determine the material parameters, as discussed in Chapter V. For the present model, a test matrix at a single temperature is presented in Table 7.1. The data base must be chosen to activate the octahedral and cube slip systems separately. Thus, most tests should be conducted in the [0 0 1] and [1 1 1] orientations. Tests in the [0 1 1] orientation as well as another orientation where cube slip is not involved are also necessary because the tension/compression asymmetry is significant. Tests should also be conducted in other orientations to verify the validity of the model. It is not expected that the full matrix should be run at all temperatures, however, it should at least be run for temperatures above and below the critical temperature, which is about 760° C, since the deformation mechanisms appear to be different in those cases.

7.3 – LIMITATIONS AND RECOMMENDATIONS

For this first attempt of the CA theory, several features were not evaluated because of the lack of experimental data available for the determination of material parameters at the same temperature. The model has therefore only been used for Rene N4 VF317 at 760° C, temperature in which enough data were available. This problem would be simplified if the material parameters of the model could be derived over a range of temperatures. In that case, a simple non-isothermal implementation could be modeled in the same manner as the isothermal formulation. The material constants could therefore be interpolated for temperature. Although this model has not been calibrated for any other temperatures, that eventuality could be very convenient to improve on the present approach.

Nearly all of the recently developed unified constitutive models include a hardening term and a recovery term in the evolutionary equation of the work hardening. This format has been successful in modeling the inelastic response of many isotropic metals, such as Inconel 718 at 1200° F in Abdel-Kader (1988). In the present formulation, an adequate database for evaluating a recovery term did not exist and the term was therefore excluded. Still, at the temperature-studied (760° C), recovery is probably not as important as at higher temperatures. Future work should, however, include the investigation of a thermal recovery term in the state variable evolutionary equation.

A number of SC nickel base superalloys materials studies show that their crystal lattice structures rotate during deformation. Although the present research deals with small deformations, it is still conceivable that the lattice rotation should be taken into account, at least during creep tests. The reasoning behind this belief comes from the fact that according to Sheh (1988) all rotations are completed in the primary creep stage; it is important to note that these results are consistent with the trends previously stated.

The goal of coupling two terms in the slip factor was to facilitate the description of the two main deformation mechanisms that occur during the creep and high strain rate responses. Although the results seem interesting at high and low strain rates, the response at intermediate strain rates is not well known. Future work should include the investigation of the strain rate sensitivity.

Table 7.1 The constitutive CA model test matrix

Number of tests	Tests	$\dot{\varepsilon}$ (sec^{-1})	σ_{hold} (MPa)	Tests orientations
3	Tension	$\dot{\varepsilon}_1$	-	[0 0 1], [0 1 1] and [h_o k_o l_o]
1	Tension	$\dot{\varepsilon}_2$	-	[0 0 1]
3	Compression	$\dot{\varepsilon}_1$	-	[0 0 1], [0 1 1] and [h_o k_o l_o]
1	Tension	$\dot{\varepsilon}_1$	-	$[\bar{1}\,1\,1]$
1	Compression	$\dot{\varepsilon}_1$	-	$[\bar{1}\,1\,1]$
3	Creep	-	σ_{hold1}	[0 0 1], [0 1 1] and [h_o k_o l_o]
1	Creep	-	σ_{hold2}	[0 0 1]
1	Creep	-	σ_{hold1}	$[\bar{1}\,1\,1]$
1	Stabilized fully reversed cyclic test	$\dot{\varepsilon}_1$	-	[0 0 1]

- [h_o k_o l_o] indicates orientation where cube slip is not involved.
- Tests in the $[\bar{1}\,1\,1]$ orientation are for evaluation of cube slip constants, while tests in the other orientations are for evaluation of octahedral slip constants.
- The strain rates $\dot{\varepsilon}_1$ and $\dot{\varepsilon}_2$ are constant and must be chosen in the high and low strain rate range respectively.
- The hold stresses σ_{hold1} and σ_{hold2} must be different.

REFERENCES

Abder-Kader, M. S., (1986) "*A comparative study of the Chaboche and Bodner theories of viscoplasticity for high temperature applications*". D. Sc. Diss., The George Washington University

Abdel-Kader, M. S., Eftis, J., and Jones, D. L., (1986) "*An extension of the Chaboche theory of viscoplasticity to account for rate dependent initial yield*". Proc. SECTAM XIII, Univ. South Carolina, p. 263

Abdel-Kader, M. S., El-Hefnawy, N. N. and Eleiche, A. M., (1991) "*A theoretical comparison of three unified viscoplasticity theories, and application to uniaxial behavior of inconel 718 at 1100° F*". Nuclear Engineering and Design, North-Holland 128, p. 369

Abdel-Kader, M. S., Eftis, J., and Jones, D. L., (1988) "*An extension of the Chaboche theory of viscoplasticity to account for rate-dependent initial yield*". Proc. SECTAM XIII. (S.Carolina. U.S.A.), p. 263.

Anderson, C. E., Cox, P. A., Johnson, G. R., Mandlin, P. J. (1994) "*A constitutive formulation for anisotropic materials suitable for wave propagation computer programs II*". Computational Mechanics 15, p. 201

Armstrong, P. G., and Frederick, C. O. (1966) "*A mathematical representation of the multiaxial Bauschinger effect*". Rep. RD/B/N731, Central Electricity Generating Board Research and Development Department

Asaro, R. J. and Rice, J. R. (1977) "*Strain localization in ductile single crystals*". Mech. Phys. Solid 25, p. 309

Asaro, R. J., (1983). "*Crystal plasticity*". Journal of Applied Mechanics. ASME 50, p.921.

Asaro, R. J., and Needleman, A. (1984) "*Flow localization in strain hardening crystalline solids*". Scripta Metall., 18, p. 429

Baltov, A. and Sawczuk, A., (1961). "*A rule of anisotropic hardening*". Acta Mech., 1, p. 81.

Beaman, R. L. (1984) "*The determination of the Bodner material coefficients for INCONEL 718 and their effects on cyclic loading*". M. S. thesis, Air Force Institute of Technology

Bingham, E. C. and Green, H., (1919) "*Paint, a plastic material and not a viscous liquid; the measurement of its mobility and yield value*". Proc. ASTM, 19, p. 640

Bingham, E. C., (1922) "*Fluidity and plasticity*". McGraw Hill, New York

Bodner, S. R. and Partom, Y., (1972) "*A large deformation elastic viscoplastic analysis of a thick-walled spherical shell*". J. Applied Mechanics, Trans. ASME, p. 751

Bodner, S. R. and Partom, Y., (1975) "*Constitutive equations for elastic-viscoplastic strain hardening materials*". J. Applied Mechanics, Trans. ASME, p. 385

Bodner, S. R. Partom, I., and Partom, Y., (1979) "*Uniaxial cyclic loading of elastic-viscoplastic materials*". J. Applied Mechanics, Trans. ASME, p. 805

Booker, M.K, (1980) "*Progress toward analytical description of the creep strain-time behavior of engineering alloys*". Conf. 800907-2

Cernocky, E. P., (1982.a) "*An examination of four viscoplastic constitutives theories in uniaxial monotonic loading*". Int. J. Solids Struct. 18, p. 989

Cernocky, E. P., (1982.b) "*Comparison of the unloading and reversed loading behavior of three viscoplastic constitutive theories*". Int. J. Non-linear Mech. 17, p. 255

Chaboche, J. L., (1977) "*Viscoplastic constitutive equations for the description of cyclic and anisotropic behavior of Metals*". Bull. de l'Acad. Polonaise des Sci. 25, p. 33

Chiu, S. S. (1988) "*Application of the Chaboche viscoplastic constitutive theory to low-cycle fatigue life prediction of smooth TI-6AL-4V specimens*". Ph.D. Thesis, The George Washington University

Choi, S. H. and Krempl, E. (1989) "*Viscoplasticity theory based on overstress applied to the modeling of cubic single crystals*". European Journal of Mechanics, A/Solids, 8, N^0 3, p. 219

Dalal, R. P., Thomas, C. R. and Dardi, L. E. (1984) "*The effect of crystallographic orientation on the physical and mechanical properties of investment cast single crystal nickel-base superalloy*". 5th Int. Superalloys, ASM., Metals Park, Ohio, p. 185

Dame, L. T. (1985) "*Anisotropic constitutive model for nickel base single crystal alloys: development and finite element implementation*". Ph.D. Dissertation, University of Cincinnati

Dame, L. T., and Stouffer, D. C. (1986) "*Anisotropic constitutive model for nickel base single crystal alloys; development and finite element implementation*". NASA CR- 175015, Lewis Research Center

Eftis, J., Abdel-Kader, M. S. and Jones, D. L., (1989) "*Comparison between the modified Chaboche and Bodner-Partom viscoplastic constitutive theories at high temperature*". International Journal of Plasticity, 5, p. 1

Eisenberg, M. A. and Yen, C. F. (1981) "*A theory of multiaxial anisotropic viscoplasticity*". J. Applied Mechanics Trans. ASME, 48, p. 276

Eisenberg, M. A. and Yen, C. F. (1983) "*Application of a theory of viscoplasticity to uniaxial cyclic loading*". J. Applied Mechanics Trans. ASME, 105, p. 106

El-Hefnawy, N. N., Abdel-Kader, M. S. and Eleiche, A. M., (1989) "*Inclusion of DSA modeling capability in unified viscoplasticity theories, with application to INCONEL 718 at 1100^0 F*". Proc. 19th Canadian Fracture Conference: Constitutive Laws of Plastic Deformation and Fracture (University of Ottawa, Canada) 8-1 - 8 - 10

Eleiche, A. M. (1991) "*Inelastic shear deformation of stainless steels under quasi-static and impact sequential reverse torsion*". Contract Number 2892-85-12 ED ISP ET, Amendments No. 1& 2

Ewing, J. A. and Rosenhain, W. (1899) "*Experiments in micro-metallography: effects of strain, preliminary notice*". Proc. R. Soc., London 65, p. 85

Ewing, J. A. and Rosenhain, W. (1900) "*The crystalline structure of metals*". Philos. Trans. R. Soc., London 193, p. 353

Fred, A. D., Raj, S. V. and Walker, K. P. (1992) "*Stress versus temperature dependence of activation energies for creep*". Journal of Engineering Materials and Technology, 114, p. 46

Freed, A. D., Walker, K. P. and Verrilli, M. J. (1994) "*Extending the Theory of Creep to Visco-Plasticity*". Journal of Pressure Vessel Technology, 116, p. 67

Frenkel, J. (1926) "*Zur theorie der tlastizitätsgrenze und dert gestigheit kristallinischer*". Körper. Z. Phys. 37, p. 572

Gabb, T. P., Gayda, J. and Miner, R. V. (1986) "*Orientation and temperature dependence of some mechanical properties of the S.C nickel base superalloy Rene N4: Part II. Low cycle fatigue behavior*". Metall. Trans., 17A, p. 497

Gell, M., Duhl, D. N. and Giamei, A. F. (1980) "*The development of single crystal superalloy turbine blades*". Proceedings of Fourth Int. Sym. On Superalloys, ASM Internation, Metals Park, OH, p. 205

Gell, M. and Leverant, G. (1968) "*The fatigue of a nickel-base superalloy, Mar-2000, in single crystal and columnar-grained forms at room temperature*". Trans AIME, 242, p. 1869

Halford, G. R., Meyer, T. G., Nelson, R. S., Nissley, D. M. and Swanson, G. A. (1989) "*Fatigue life prediction modeling for turbine hot section materials*". Journal of Engineering for Gas Turbines and Power, 111, p. 279

Hart, E. W. (1976) "*Constitutive relations for the nonelastic deformation of metals*". J. Engineering Materials and Technology, Trans ASME, p. 193

Helling, D. E. and Miller, A. K. (1987) "*The incorporation of the yield surface distortion into a unified constitutive model, Part 1: equation development*". Acta Mechanica 69, p. 9

Helling, D. E. and Miller, A. K. (1988) "*The incorporation of the yield surface distortion into a unified constitutive model, Part 2: Predictive capabilities*". Acta Mechanica 72, p. 39

Hill, R. (1950) "*The mathematical theory of plasticity*". Oxford University Press

Hill, R. (1966) "*Generalized constitutive relations for incremental deformation of metals by multi slip*". J. Mech. Phys. Solid 14, p. 99

Hill, R. and Rice, J. R. (1972) "*Constitutive analysis of elasto-plastic crystals at arbitrary strain*". J. Mech. Phys. Solid 20, p. 401

Hill, R. and Havner, K. S. (1982) "*Perspectives in the mechanics of elastoplastic crystals*". J. Mech. Phys. Solid 30, p. 5

Hohenemser, K. and Prager, W., (1932) "*Uber die ansatze der mechanick isotroper kontinus*". Zeitschrift f. Angew. Math. U. Mech., 12, p. 216

Hopgood, A. A. and Martin, J. W. (1986) "*The creep behavior of a nickel based single crystal superalloy*". Mat. Sci. Eng., 82, p. 27

James, G. H., Imbrie, P. K., Hill, P. S., Allen, D. H. and Haisler, W. E. (1987) "*An experimental comparison of several current viscoplastic constitutive models at elevated temperature*". Journal of Engineering Materials and Technology 109,

p.130

Jordan, E. H. and Walker, K. P. (1992) "*A viscoplastic model for single crystals*". Journal of Engineering Materials and Technology. 114, p. 19

Kear, B. and Piearcey, B. (1967) "*Tensile and creep properties of single crystals of the nickel base superalloy MAR-M200*". Trans. AIME, 239, p. 1209

Khan, A. S. (1995) "*Continuum theory of plasticity*". New York; Wiley

Korth, G. E., and Smolik, G. R. (1978) "*Status reports of physical and mechanical test data of alloys 718* ". TREE 1254

Krempl, E. and Kallianpur, V. V. (1984) "*Some critical uniaxial experiments for viscoplasticity at room temperature*". J. Mech. Phys. Solids, 32, p. 301

Krempl, E., McMahon, J. J., and Yao, D. (1986) "*Viscoplasticity based on overstress with a differential growth law for the equilibrium stress*". Mechanics of Materials, 5, p. 35

Krieg, R. D., (1975) "*A practical two surface plasticity theory*". J. Applied Mechanics, Trans. ASME, p. 641

Kundel, R., and Kollmann, F. G. (1997) "*Identification of constants of viscoplastic constitutive model for single crystal alloy*". Acta Mechanica 124, p. 27.

Kurtyka, T., and Zyczkowski, M. (1996) "*Evolution equations for distortional plastic hardening*". International Journal of Plasticity, 12, N0. 2, p. 191

Lall, C., Chin, S. and Pope, D. P., (1979) "*The orientation and temperature dependence of the yield stress of Ni3 (Al, Nb) single crystals*". Metallurgical Transactions A. 10A, p. 1323

Lee, D. and Zaverl, F., Jr. (1978) "*A generalized strain-rate dependent constitutive equation for anisotropic metals*". Acta Met., 26, No. 216, p. 1771

Lee, D. and Zaverl, F. (1979) "*A description of history dependent plastic flow behavior of anisotropic metals*". Journal of Engineering Materials and Technology, 101, p. 59

Lekhnitskii, S. G. (1963) "*Theory of elasticity of an anisotropic body*". San Francisco Holden-Day

Lemaître, J. and Chaboche, J. L. (1990) "*Mécanique des matériaux solides*". Cambridge University Press

Leverant, G. and Kear, A. H. (1970) "*The mechanism of creep in gamma prime precipitation-hardened nickel-base alloys at intermediate temperatures*". Metall. Trans., 1, p. 491

Li, S. X., Ellison, E. G. and Smith, D. J. (1994) "*The influence of orientation on the elastic and low cycle fatigue properties of several single crystal nickel base superalloys*". The Journal of strain Analysis, 29. N0 2, p. 147

Li, S. X. and Smith, D. J. (1995a) "*Modeling of anisotropic creep deformation and damage in single crystal superalloys*". Scripta Metallurgica et Materialia, 33, N^0 5, p. 711

Li, S. X. and Smith, D. J. (1995b) "*High temperature fatigue-creep behavior of single crystal SRR90 nickel base superalloys, Part I - cyclic mechanical response*". Engineering Materials and Structures, 18. N^0 5, p. 617

Li, S. X. and Smith, D. J. (1995c) "*High temperature fatigue-creep behavior of single crystal SRR90 nickel base superalloys, Part II - fatigue creep life behavior*". Engineering Materials and Structures. 18. N^0 5, p. 631

Li, S. X. and Smith, D. J. (1995d) "*Temperature and orientation dependence of elastic and yield properties of single crystal nickel base superalloy: PWA 1480*". Materials Science and Technology, 11, p. 12

Lin, T. L. and Maowen (1990) "*The deformation mechanism of a precipitation-hardened nickel-base superalloy*". Materials Science and Engineering A, 128, p. 23

Liu, M. C., and Krempl, E. (1979) "*A uniaxial viscoplastic model based on total strain and overstress*". J. Mech. Phys. Solids, 27, p. 377

Mackay, R. A. and Maier, R. D. (1982) "*The influence on the stress rupture properties of nickel-base single crystals*". Metall. Trans., 13A, p. 1747

Masson, D. P. and Van Aken, D. C. (1993) "*Creep deformation studies in directionally solidified $MoSi_2$-Mo_5Si_3 eutectic*". Mat. Res. Soc. Symp. Proc. 288. Materials Research Society

Marchionni, M., Goldschmidt, D. and Maldini, M. (1993) "*Evaluation of high-temperature behavior of CMSX4 + Yttrium single-crystal nickel-base superalloy*". Journal of Materials Engineering and Performance, 2 (4), p. 497

Méric, L., Poubanne, P. and Cailletaud, G. (1991) "*Single crystal modeling for structural calculations: Part I- Model presentation*". Journal of Engineering Materials and Technology, 113, p. 162

Miller, A. K. (1976) "*An inelastic constitutive model for monotonic, cyclic and creep deformation: Part I – Equations development and analytical procedures, Part II Application to type 304 stainless steel*". J. Engineering Materials and Technology, Trans. ASME, 96, p. 97

Miller, A. K. (1980) "*Modeling of cyclic plasticity with unified constitutive equations: improvements in simulating normal and anomalous Bauschinger effects*". J. Engineering Materials and Technology, Trans. ASME, 102, p. 215

Milligan, W. W. and Antolovich, S. D. (1987) "*Yielding and deformation behavior of the single crystal superalloy PWA 1480*". Metallurgical Transactions A.18A, p. 85

Milly, T. M. and Allen, D. H. (1982) "*A comparative study of nonlinear rate-dependent mechanical constitutive theories for crystalline solids at elevated temperatures*". Virginia Poly. Tech. Inst. Rep. VP1-E-92-5

Miner, R. V., Voigt, R. C., Gayda, J. and Gabb, T. P. (1986.a) "*Orientation and temperature dependence of some mechanical properties of the single crystal nickel base superalloy Rene N4: Part I. Tensile behavior*". Metall. Trans., 17A, p. 491

Miner, R. V., Gabb, T. P., Gayda, J. and Hemker, K. J. (1986.b) "*Orientation and temperature dependence of some mechanical properties of the single crystal nickel base superalloy Rene N4: Part III. Tensile compressive anisotropy*". .Metall. Trans., 17A, p. 507

Nathal, M. V. and Ebert, L. J. (1985) "*Elevated temperature creep-rupture behavior of the single crystal nickel-base superalloy NASAIR 100*". Metal. Trans. 16A, p. 427

Nissley, D. M. and Swanson, G. A. (1989) "*Fatigue life Prediction Modeling for Turbine Hot Section Materials*". Journal of Engineering for Gas Turbines and Power, 111, p. 279

Nissley, D. M. and Meyer, T. G. (1992.a) "*Life prediction and constitutive models for engine hot section anisotropic materials program*". United Technologies Corporation, NASA Contractor Report 189222

Nissley, D. M. and Meyer, T. G. (1992.b) "*Life prediction and constitutive models for engine hot section anisotropic materials program*". United Technologies Corporation, NASA Contractor Report 189223.

Nouailhas, D. (1988) "*Modélisation de l'écrouissage et de la restauration en viscoplasticité cyclique*". Revue Phys. Appl. 23, p. 339

Nouailhas, D. (1990) "*Lois de comportement en viscoplasticité cyclique anisotrope: Application aux cas des matériaux à symétrie cubique*". La recherche aerospaciale, 3, p. 11

Nouailhas, D. and Cailletaud, G. (1995) "*Tension-Torsion behavior of single crystal superalloys: experiment and finite element Analysis*". International Journal of Plasticity, 4, p. 451

Nouailhas, D. and Freed, A. D. (1992) "*Viscoplastic theory for anisotropic materials*". Submitted to ASME Journal of Engineering Materials and Technology, 114, p. 97

Ohno N. and Takeuchi T. (1994) "*Anisotropy in multiaxial creep of nickel-based single-crystal superalloys CMSX-2 (experiments and Identification of active slip systems)*". JSME International Journal, series A, 37, N0. 2, p. 129

Olszak, W. and Ostrowska-Maciejewska, J. (1985) "*The plastic potential in the theory of anisotropic elastic-plastic solids*". Engineering Fracture Mechanics, 21, N0. 4. p. 625

Orowan, W. (1934) "*Zur Kristallplastizitat III. Uber den Mechanismus des gleituorganges*". Z. Phys. 89, p. 634

Piehler, H. R. and Backofen, W. A. (1969) "*In textures in research and Practice*". Wasserman, G. and Grewen, G. eds., Springer-Verlar, Berlin 1969), p. 436

Peirce, D., Azaro, R. J. and Needleman, A. (1982) "*An analysis on non uniform and localized deformation in ductile single crystals*". Acta Metall., 30, p. 1087

Peirce, D., Azaro, R. J. and Needleman, A. (1983) "*Material rate dependence and localized deformation in crystalline solids*". Acta Metall., 31, p. 1951

Perzyna, P. (1963.a) "*The constitutive equations for work hardening and rate sensitive plastic materials*". Proc. Vibr. Probl., 4, p. 281

Perzyna, P. (1963.b) "*The constitutive equations for rate sensitive plastic materials*". Quart. Appl. Math. 20, p. 321

Perzyna, P. (1963.c) "*The study of the dynamical behavior of rate sensitive plastic materials*". Arch. Mech. Stos., 15, p. 199

Perzyna, P. (1966) "*Fundamental problems in viscoplasticity*". Advances in Applied Mechanics, 19, p. 243

Philips, A. and Wu, H. C. (1973) "*A theory of viscoplasticity*". Int. J. Solids Structures, 9, p. 15

Polanyi, V. M. (1934) "*Über eine art gitter-Storung die eine kristall plastischamachen konnte* ". Z. Phys. 89, p. 660

Prager, W. (1961) "*The theory of plasticity: a survey of recent achievements* ". Proc. of the Instn. of Mech. Engineering., 169, p. 21

Prager, W. (1961) "*Introduction to mechanics of continua*". Ginn and Company, Boston

Robinson, D. N. (1978) "*A unified creep plasticity model for structural metals at high temperatures*". ORNL/TM 5969.

Robinson, D. N., (1983) "*Constitutive relationships for anisotropic high-temperature alloys*". NASA Technical Memorandum 83437

Salvatore, C. (1994) "*Computational aspects of the integration of the Von Mises linear hardening constitutive laws*". International Journal of Plasticity. 10, p. 935

Shah, D. and Duhl, D. (1984) "*The effect of orientation, temperature and gamma prime size on the yield strength of a single crystal nickel base superalloy*". Proceedings of the fifth international symposium on superalloys, ASM, Metals Park, Ohio

Schmid, E. (1924) Proc. Int. Congr. Appl. Mech. (Delft). p. 342

Schmidt, C. G. and Miller, A. K. (1981) Res., Mech., 3, p. 175

Sheh, Y. M. (1988) "*Anisotropic constitutive modeling for nickel-base single crystal Superalloys*". Ph.D. Dissertation, University of Cincinnati

Stouffer, D. C. and Bodner, S. R., (1979) "*A constitutive model for the deformation induced anisotropic plastic flow of metals*". Int. J. of Engineering Science, 17, p. 757

Suh, Y. S., Saunders, F. I., and Wagoner, R. H. (1996) "*Anisotropic yield functions with plastic-strain-Induced anisotropy*". International Journal of Plasticity 12, N0.3, p. 417

Swanson, G. (1984.a) "*Life prediction and constitutive models for engine hot section anisotropic materials program*". Contract NAS3-23939, Monthly Report PWA-5968-8

Swanson, G. (1984.b) "*Life prediction and constitutive models for engine hot section anisotropic materials program*". Contract NAS3-23939, Monthly Report PWA-5968-9

Swanson, G. A., Linask, I. and Nisley, D. M. (1986) "*Life prediction and constitutive models for engine hot section anisotropic materials program*". Annual Status Report; Contract NAS3-2393

Takeuchi, S. and Kuramoto, E., (1973) "*Temperature and orientation dependence of the yield stress in Ni3Ca single crystals*". Acta Metallurgica 21, p. 415

Taylor, G. I. (1934) "*The mechanism of plastic deformation of crystals. Part I – theoretical*". *Proc. R. Soc., London Sec.* A. 145, p. 362

Taylor, G. I. (1938) "*Plastic strain in metals*". J. Inst. Metals 62, p. 307

Valanis, K. C., (1974) "*Effect of prior deformation on cyclic response of metals*". J. Applied Mechanics, Trans. ASME, 41, p. 411

Valanis, K. C. (1971) "*A theory of viscoplasticity without a yield surface, Part I: general theory, Part II: Application to mechanical behavior of metals*". Archives of mechanics, 23, p. 517

Wagoner, R. H. and Chenot, J. L. (1996) "*Fundamentals of metal forming*". Copyright, by John Wiley & Sons, Inc.

Walker, K. P. (1980) "*Representation of hastelloy-X behavior at elevated temperatures with a functional theory of viscoplasticity*". ASME Pressure Vessels Conference. San Francisco

Wegener, K., and Schlegel, M. (1996) "*Suitability of yield functions for the approximation of subsequent yield surfaces*". International Journal of Plasticity, 12, N0. 9, p. 1151

Wukusick, C. (1980) "*Directional solidification alloy development*". NADC-78136-60, Naval Air Systems Command

Yun, Z. and Dongliang, L. (1993) "*Creep behavior of directionally solidified Ni_3Al alloy*". Mat. Res. Soc. Symp. Proc. Materials Research Society, 288

Zaverl, F. and Lee, D. (1978) "Constitutive relations for nuclear reactor core materials". Journal of Nuclear Materials, 75, p. 14

Zhou, Y. Neale, K. W. and Toth, L. S. (1993) "*A modified model for simulating latent hardening during the plastic deformation of rate-dependent fcc polycrystals* ". International Journal of Plasticity. 9, p. 961

APPENDIX A

This appendix establishes the sign convention for positive slip directions on the (1 1 1) octahedral planes (Figure A.1) and (0 1 0) cube planes (Figure A.2). In addition, it establishes the three corresponding structural matrices [B_m], [C_m] and [H_m] defined in the single crystal and used for the purpose of the present work.

A.1 – Octahedral plane

In the faced centred cubic (f.c.c) single crystal material, the sign conventions for positive slip directions on the (1 1 1) octahedral planes are shown in Figure A.1. The positives units normal to the four octahedral planes are given by:

$$\begin{aligned} \mathbf{n}^1 &= 1/\sqrt{3}(\mathbf{i}+\mathbf{j}+\mathbf{k}), \\ \mathbf{n}^2 &= 1/\sqrt{3}(-\mathbf{i}+\mathbf{j}-\mathbf{k}), \\ \mathbf{n}^3 &= 1/\sqrt{3}(\mathbf{i}-\mathbf{j}-\mathbf{k}), \text{ and} \\ \mathbf{n}^4 &= 1/\sqrt{3}(-\mathbf{i}-\mathbf{j}+\mathbf{k}), \end{aligned} \tag{A.1}$$

where **i**, **j** and **k** are the unit vectors in the principal material directions.

The positive sign conventions for the $[1\,0\,\bar{1}]$ directions on the octahedral planes are:

$$\begin{aligned} &\mathbf{s}^{11} = 1/\sqrt{2}(\mathbf{i}-\mathbf{k}), \quad \mathbf{s}^{12} = 1/\sqrt{2}(-\mathbf{j}+\mathbf{k}), \quad \mathbf{s}^{13} = 1/\sqrt{2}(\mathbf{i}-\mathbf{j}), \\ &\mathbf{s}^{21} = 1/\sqrt{2}(\mathbf{i}-\mathbf{k}), \quad \mathbf{s}^{22} = 1/\sqrt{2}(\mathbf{i}+\mathbf{j}), \quad \mathbf{s}^{23} = 1/\sqrt{2}(\mathbf{j}+\mathbf{k}), \\ &\mathbf{s}^{31} = 1/\sqrt{2}(\mathbf{i}+\mathbf{j}), \quad \mathbf{s}^{32} = 1/\sqrt{2}(-\mathbf{j}+\mathbf{k}), \quad \mathbf{s}^{33} = 1/\sqrt{2}(\mathbf{i}+\mathbf{j}), \\ &\mathbf{s}^{41} = 1/\sqrt{2}(\mathbf{j}+\mathbf{k}), \quad \mathbf{s}^{42} = 1/\sqrt{2}(\mathbf{i}+\mathbf{k}), \quad \mathbf{s}^{43} = 1/\sqrt{2}(\mathbf{i}+\mathbf{j}); \end{aligned} \tag{A.2}$$

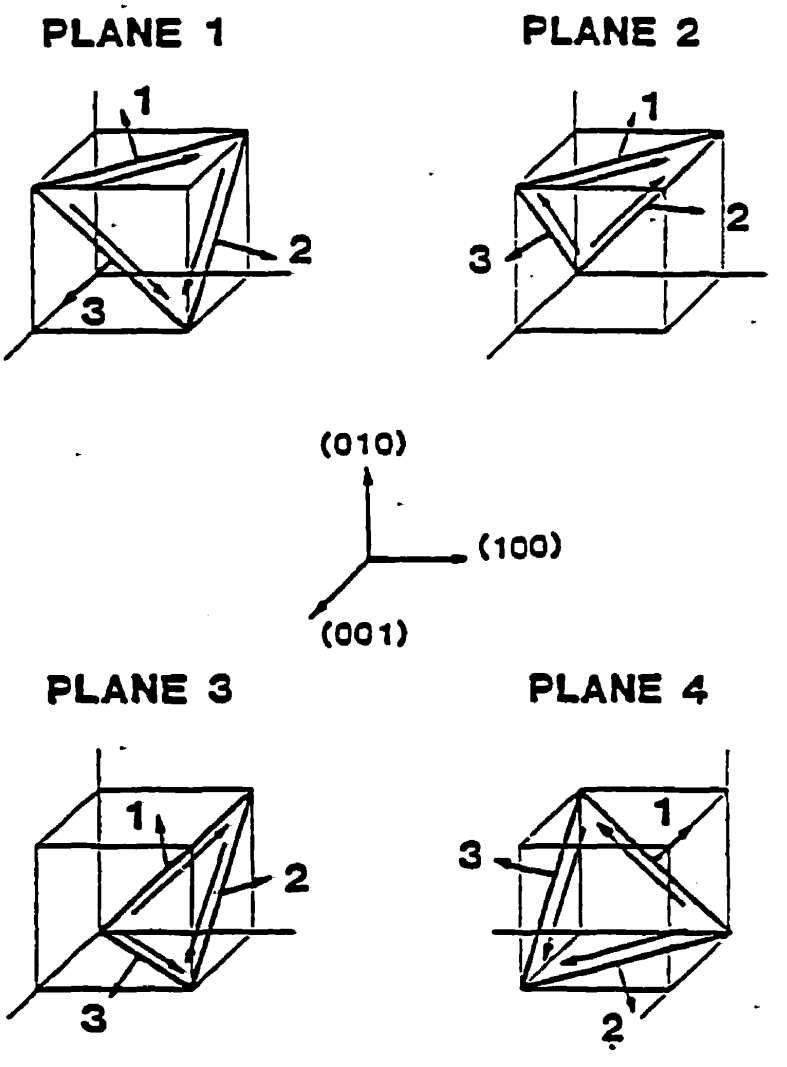

Figure A.1 Octahedral a/2(1 1 0) and a/2(1 1 2) slip systems

Those for the $[\bar{1}\,2\,\bar{1}]$ directions on the octahedral planes are

$$\begin{aligned}
&z^{11} = 1/\sqrt{6}(-i+2j-k),\ z^{12} = 1/\sqrt{6}(2i-j-k),\ z^{13} = 1/\sqrt{6}(-i-j+2k),\\
&z^{21} = 1/\sqrt{6}(i+2j+k),\ z^{22} = 1/\sqrt{6}(i-j-2k),\ z^{33} = 1/\sqrt{6}(-2i-j+k),\\
&z^{31} = 1/\sqrt{6}(-i+j-2k),\ z^{32} = 1/\sqrt{6}(2i+j+k),\ z^{33} = 1/\sqrt{6}(-i-2j+k),\\
&z^{41} = 1/\sqrt{6}(-2i+j-k),\ z^{42} = 1/\sqrt{6}(i-2j-k),\ z^{43} = 1/\sqrt{6}(i+j+2k),
\end{aligned} \tag{A.3}$$

It is now possible to calculate the resolved shear stress vector $\{\tau\}$, corresponding to each slip system of the crystal material that is loaded with an arbitrary stress, $\{\sigma^*\}$. For example, let us apply an external load in a SC nickel base super-alloys sample, and let us assume that the corresponding stress at any given point of that sample is $\{\sigma^*\}$. Then the yield condition in the α^{th} octahedral slip system is expressed in the crystallographic co-ordinate system as follows.

$$\tau^{(\alpha)} \equiv \pm s_i^{(\alpha)}\ \sigma_{ij}^{*} n_j^{(\alpha)} \geq \tau_c^{(\alpha)}, \alpha = 1,2,..,12. \tag{A.4}$$

Where

- α represents one of the slip directions of the crystal mentioned above,
- $\{s\}^{(\alpha)}$ is a slip vector along the α^{th} slip direction,
- $\{n\}^{(\alpha)}$ is a normal to the α^{th} slip direction,
- $s_i^{(\alpha)}$ and $n_j^{(\alpha)}$ are the components of vectors $\{s\}^{(\alpha)}$ and $\{n\}$ respectively,
- $\tau^{(\alpha)}$ and $\tau_c^{(\alpha)}$ are respectively the magnitude of the resolved shear stress (RSS) and the critical resolved shear stress (CRSS) in the α^{th} slip direction,
- σ^*_{ij} are components of the second order tensor σ^* in the crystallographic system

Eq.(A.4) may restated as

$$\pm m_i^{(\alpha)} \sigma_i \equiv \tau^{(\alpha)} \geq \tau_c^{(\alpha)} \tag{A.5}$$

where, $m_i^{(\alpha)}$, defined in Eq.(A.6), may be expressed in function of $s_i^{(\alpha)}$ and $n_j^{(\alpha)}$, the components of vectors $\{ s \}^{(\alpha)}$ and $\{ n \}^{(\alpha)}$, respectively.

$$\begin{bmatrix} m_1 \\ m_2 \\ m_3 \\ m_4 \\ m_5 \\ m_6 \end{bmatrix}^{(\alpha)} = \begin{bmatrix} s_1 n_1 \\ s_2 n_2 \\ s_3 n_3 \\ (s_2 n_3 + s_3 n_2) \\ (s_1 n_2 + s_2 n_1) \\ (s_1 n_3 + s_3 n_1) \end{bmatrix}^{(\alpha)} \tag{A.6}$$

Using Eqs.(A.4) and (A.6), all of the shear stress in the crystal on the octahedral planes along an orientation similar to the $[1\,0\,\bar{1}]$ directions can be expressed in the vector form as:

$$\begin{Bmatrix} \tau^{11} \\ \tau^{12} \\ \tau^{13} \\ \tau^{21} \\ \tau^{22} \\ \tau^{23} \\ \tau^{31} \\ \tau^{32} \\ \tau^{33} \\ \tau^{41} \\ \tau^{42} \\ \tau^{43} \end{Bmatrix} = \frac{1}{\sqrt{6}} \begin{bmatrix} 1 & 0 & -1 & 1 & 0 & -1 \\ 0 & -1 & 1 & -1 & 1 & 0 \\ 1 & -1 & 0 & 0 & 1 & -1 \\ -1 & 0 & 1 & 1 & 0 & -1 \\ -1 & 1 & 0 & 0 & -1 & -1 \\ 0 & 1 & -1 & -1 & -1 & 0 \\ 1 & -1 & 0 & 0 & -1 & -1 \\ 0 & 1 & -1 & -1 & 1 & 0 \\ 1 & 0 & -1 & -1 & 0 & -1 \\ 0 & -1 & 1 & -1 & -1 & 0 \\ -1 & 0 & 1 & -1 & 0 & -1 \\ -1 & 1 & 0 & 0 & 1 & -1 \end{bmatrix} \begin{Bmatrix} \sigma_1^* \\ \sigma_2^* \\ \sigma_3^* \\ \sigma_4^* \\ \sigma_5^* \\ \sigma_6^* \end{Bmatrix} \tag{A.7}$$

Eq.(A.7) may be rewritten in the shorthand form as

$$\{\tau\} = [B_m]\{\sigma^*\} \tag{A.8}$$

Where

$$[B_m]=\frac{1}{\sqrt{6}}\begin{bmatrix} 1 & 0 & -1 & 1 & 0 & -1 \\ 0 & -1 & 1 & -1 & 1 & 0 \\ 1 & -1 & 0 & 0 & 1 & -1 \\ -1 & 0 & 1 & 1 & 0 & -1 \\ -1 & 1 & 0 & 0 & -1 & -1 \\ 0 & 1 & -1 & -1 & -1 & 0 \\ 1 & -1 & 0 & 0 & -1 & -1 \\ 0 & 1 & -1 & -1 & 1 & 0 \\ 1 & 0 & -1 & -1 & 0 & -1 \\ 0 & -1 & 1 & -1 & -1 & 0 \\ -1 & 0 & 1 & -1 & 0 & -1 \\ -1 & 1 & 0 & 0 & 1 & -1 \end{bmatrix} \qquad \text{(A.9)}$$

In the same way, all of the shear stress of the crystal on the octahedral planes along an orientation similar to the $[\bar{1}\,2\,\bar{1}]$ directions can be expressed in the shorthand form as:

$$\{\tau\}=[C_m]\{\sigma^*\} \qquad \text{(A.10)}$$

Where

$$[C_m]=\frac{1}{\sqrt{18}}\begin{bmatrix} -1 & 2 & -1 & 1 & -2 & 1 \\ 2 & -1 & -1 & 1 & 1 & -2 \\ -1 & -1 & 2 & -2 & 1 & 1 \\ -1 & 2 & -1 & -1 & -2 & -1 \\ -1 & -1 & 2 & 2 & 1 & -1 \\ 2 & -1 & -1 & -1 & 1 & 2 \\ -1 & -1 & 2 & 2 & -1 & 1 \\ 2 & -1 & -1 & -1 & -1 & -2 \\ -1 & 2 & -1 & -1 & 2 & 1 \\ 2 & -1 & -1 & 1 & -1 & 2 \\ -1 & 2 & -1 & 1 & 2 & -1 \\ -1 & -1 & 2 & -2 & -1 & -1 \end{bmatrix} \qquad \text{(A.11)}$$

A.2 – Cube plane

Similarly, the sign conventions for positive slip directions on the (0 1 0) cube planes are shown in Figure (A.2). The positive units normal to the three cube planes are given by:

$$\mathbf{n}^1 = \mathbf{i}\ ,$$
$$\mathbf{n}^2 = \mathbf{j}\ , \quad \text{and} \tag{A.12}$$
$$\mathbf{n}^3 = \mathbf{k}\ ,$$

The sign conventions for positive slip directions on the cube planes are:

$$\mathbf{s}^{11} = 1/\sqrt{2}(\mathbf{j}+\mathbf{k})\ ,\ \mathbf{s}^{12} = 1/\sqrt{2}(\mathbf{j}-\mathbf{k})\ ,$$
$$\mathbf{s}^{21} = 1/\sqrt{2}(\mathbf{i}+\mathbf{k})\ ,\ \mathbf{s}^{22} = 1/\sqrt{2}(\mathbf{i}-\mathbf{k})\ , \quad \text{and} \tag{A.13}$$
$$\mathbf{s}^{31} = 1/\sqrt{2}(\mathbf{i}+\mathbf{j})\ ,\ \mathbf{s}^{32} = 1/\sqrt{2}(-\mathbf{j}+\mathbf{j})\ ,$$

Using the same reasoning as in the previous case, all of the shear stress of the crystal on the cube planes along an orientation similar to the $[\bar{1}\,0\,\bar{1}]$ directions can be expressed in the shorthand form as:

$$\{\tau\} = [H_m]\{\sigma^*\} \tag{A.14}$$

Where

$$[H_m] = \frac{1}{\sqrt{2}}\begin{bmatrix} 0 & 0 & 0 & 1 & 1 & 0 \\ 0 & 0 & 0 & 1 & -1 & 0 \\ 0 & 0 & 0 & 1 & 0 & 1 \\ 0 & 0 & 0 & 1 & 0 & -1 \\ 0 & 0 & 0 & 0 & 1 & 1 \\ 0 & 0 & 0 & 0 & -1 & 1 \end{bmatrix} \tag{A.15}$$

Finally, $[B_m]$, $[C_m]$, and $[H_m]$ are defined to be structural matrices relative to the octahedral slip system along $[\bar{1}\,0\,1]$ and $[\bar{1}\,2\,\bar{1}]$ orientations, and relative to the cube slip system along $[\bar{1}\,0\,1]$ orientation. These matrices are by definition constants, and thus they depend on the structure of the crystal.

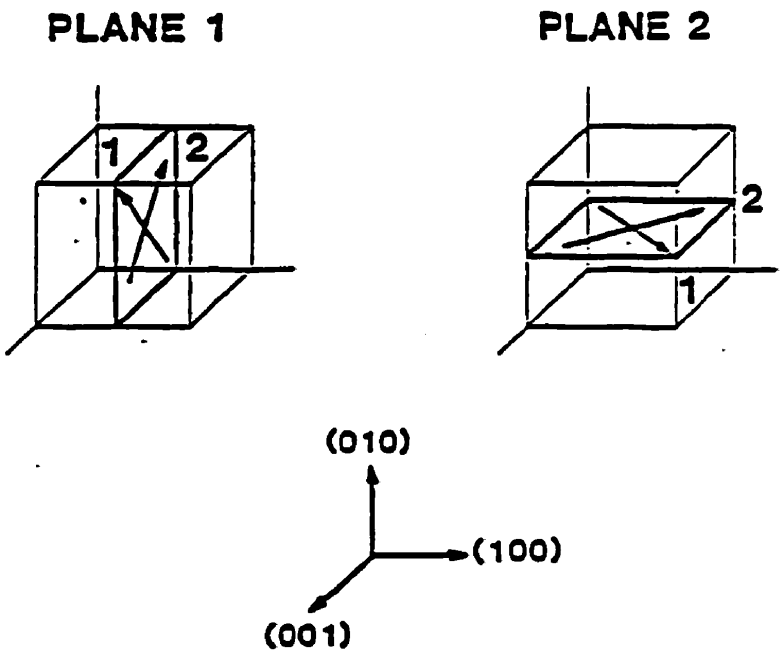

Figure A.2 Cube a/2(1 1 0) slip systems

APPENDIX B

This appendix presents a summary of the crystalline structure of metals necessary for an understanding of the microscopic mechanisms of plastic deformation used in the development of the *combined approach*'s theory proposed in the present work.

It is well known today that metals are crystalline solids that consist of atoms arranged in a pattern that is repeated periodically. The patterns in which the atoms are arranged are called a crystal lattice. Therefore a crystal or space lattice is an infinite, three-dimensional array of points with periodic structure. This structure is dependent on the material.

B.1 – Elementary Cells

The full description of crystalline metals is based on the smallest crystal unit known as the *elementary cell*. The cell can take one of a number of different shapes: cubic, tetragonal, hexagonal, orthorhombic, monoclinic and triclinic. The most common lattice types are the followings three:

1. *Faced-centered-cubic (f.c.c) lattice*. The unit cell of this lattice is shown in Figure B.1. The length of every edge of the cell is equal and is denoted by a. There is one atom at each of the 8 corners of the cubic cell and one atom in the middle position on each of the 6 faces of a cell. Many pure metals crystallize in this lattice structure, such as aluminum, copper, gold, silver and nickel.

2. *Body-centered-cubic (b.c.c) lattice*. The unit cell of this lattice is shown in Figure B.2. Like f.c.c crystals, the lengths of the edges of a cell are equal, and there is one atom at each of the eight corners of the cell. There is one extra atom at the centroid of the cell and no atom on the faces. Metals crystallizing in this structure include iron, niobium, tantalum, molybdenum, and tungsten.

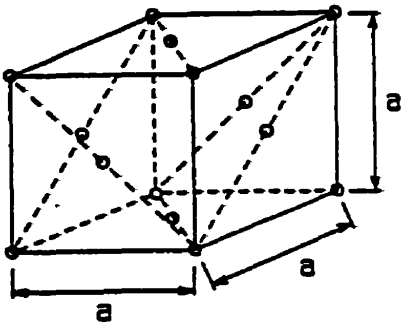

Figure B.1 – Face-centered-cubic cell

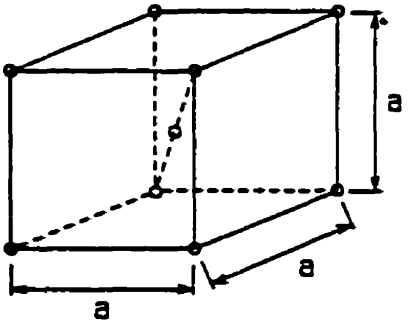

Figure B.2 – Body-centered-cubic cell

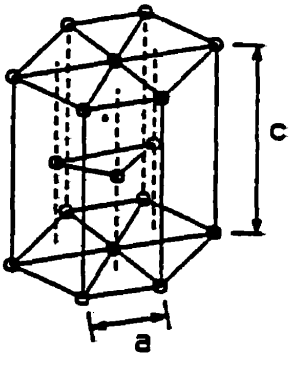

Figure B.3 – Closed-packed hexagonal cell

3. *Hexagonal or closed-packed hexagonal (h.c.p) lattice.* The elementary unit of this lattice structure is shown in Figure B.3. As can be seen from the figure, the upper and the lower basal planes are regular hexagons with side length *a*. The distance between the basal planes is given by *c*. The ratio *c/a* is a very important parameter in determining the slip plane discussed in section B4. Examples of h.c.p metals are zinc, cadmium, and magnesium.

For the purpose of the present work, only the cubic lattice structure will be considered, since single crystal nickel base superalloys (principal material used in this work) crystallizes in the f.c.c lattice.

B.2 – Miller Indices

Miller indices are used to describe the directions and planes in a crystal.

B.2.1 - Indices of a lattice plane

A plane in space can be described by the equation

$$\frac{x}{c_1}+\frac{y}{c_2}+\frac{z}{c_3}=1 \qquad \text{(B.1)}$$

where c_1, c_2 and c_3 are the intercepts of this plane on the x, y, and z axes, respectively. To describe the crystallographic planes, the axes are taken along three non-coplanar edges of the unit cell and the intercepts are measured in terms of unit length, which is usually the length of one edge of the atomic cell. The axes and unit lengths of a cubic cell are shown in Figure B.4. Note that the edge length is assigned to be one unit although its actual length is *a*, as shown in Figure B.1. To find the Miller indices for the crystallographic plane, one may proceed in three steps:

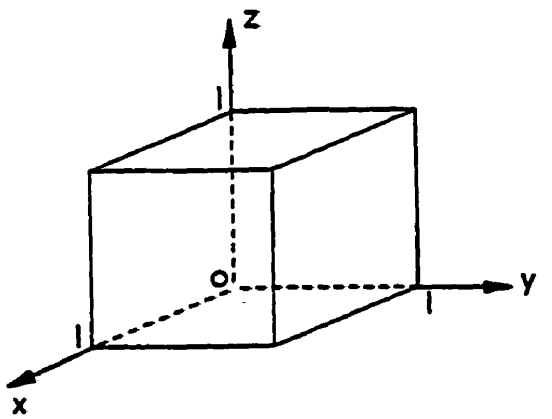

Figure B.4 – Face-centered-cubic cell

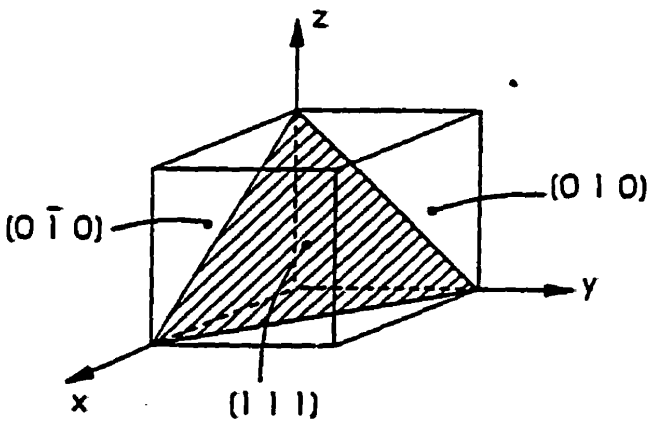

Figure B.5 – Miller indices of planes

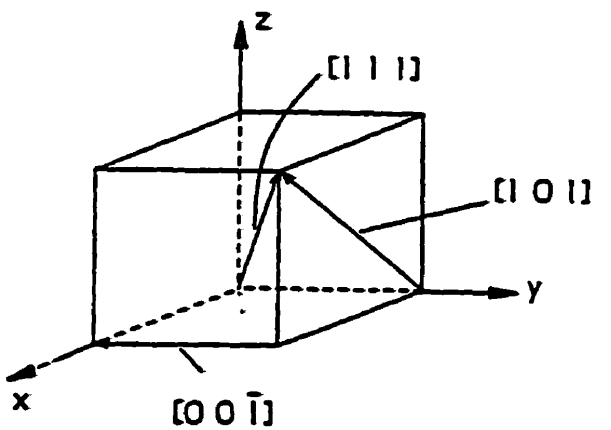

Figure B.6 – Miller indices of directions

1. Find the three intercepts c_1, c_2 and c_3.
2. Calculate the reciprocal of each of them ($1/c_1, 1/c_2$ and $1/c_3$).
3. Reduce the reciprocals into their smallest integers by dividing by the largest common factor.

When obtained in this way for a crystallographic plane, these indices are called Miller indices and are enclosed in parentheses as (U V W). A bar on an integer represents a negative number. Because of the symmetry of the crystal structure, several planes can have the same atomic distributions. They are called crystallographically equivalent planes and are represented by the indices of one of the planes. So in f.c.c crystals, there are a total of six equivalent cube planes, represented in this work by (0 1 0), and eight equivalent octahedral planes represented by (1 1 1) as shown in Figure B.5.

B.2.2 - Indices of a lattice direction

The indices of the direction are simply the vector components of the direction resolved along each of the coordinate axes and reduced to smallest integers. These indices are enclosed in a bracket as [h k l]. Again, a bar an integer represents a negative number. Indices for three distinct directions are represented in Figure B.6.

B.3 – STEREOGRAPHIC PROJECTION

In a single crystal rod for example, the principal axes of the crystal (axes along cell edges) do not usually coincide with the axis of the rod. The standard way to describe the orientation of a crystal is to use the stereographic projection characteristic of the crystal structure. Consider a unit cell of crystal sitting at the origin of a sphere as shown in Figure B.7. The normal of various planes to the crystal cell is drawn to intercept the sphere at various points. Each point represents a particular plane or a particular direction along the normal to the plane. All of the points are then projected onto a plane surface, producing a circular plot called a stereographic projection. Every point representing a particular plane falls within this circular plot. The angles between various plane normals can then be measured with a circular stereographic net.

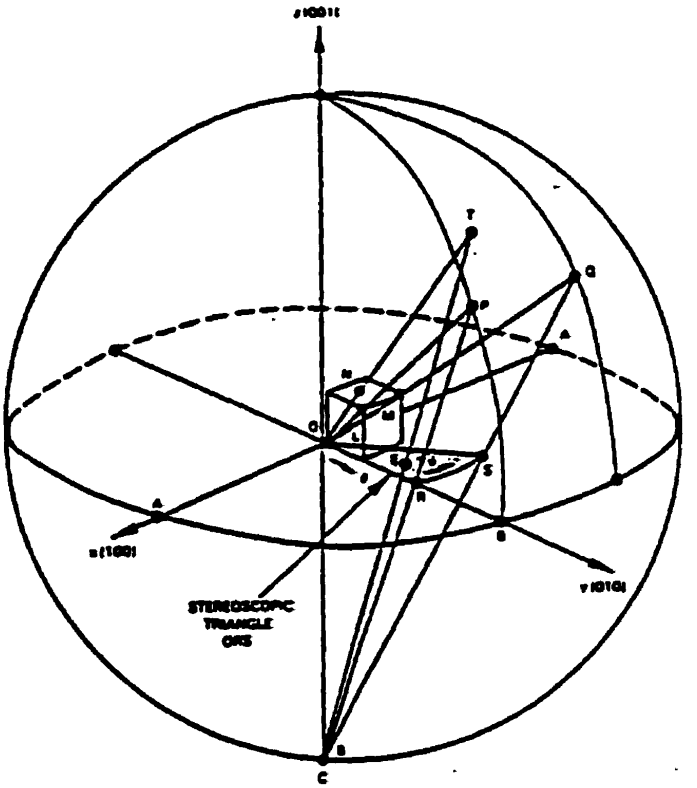

Figure B.7 Single crystal bar oriented along the direction ON respect to the cubic crystal axes AA, BB, and CC can be located in the stereographic triangle ORS at point E.

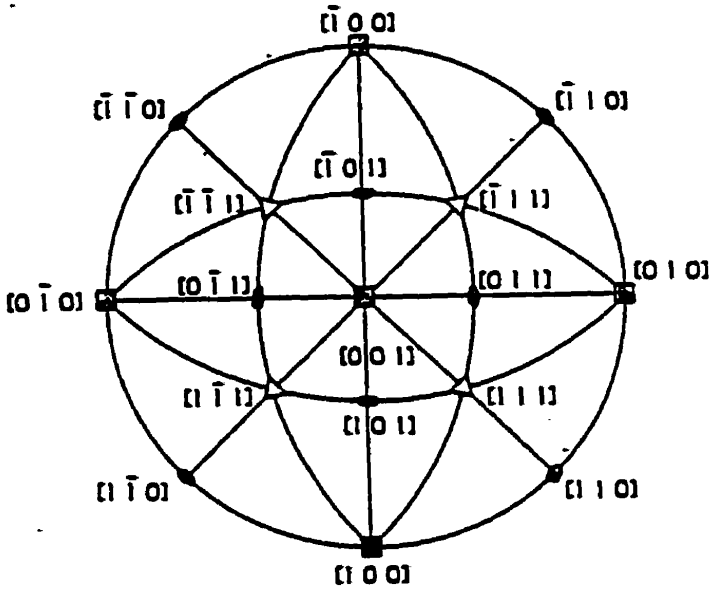

Figure B.8 – Standard [0 0 1] stereographic projection of FCC crystal

For cubic crystals, the usual practice is to use the standard projection, which is produced in such a way that the center of the projection is the normal of the plane [0 0 1]. A standard [0 0 1] stereographic projection of f.c.c crystal is shown in Figure B.8, where some other important planes or directions are labeled. Note that each point in the plot represents a plane or a direction along that plane normal.

It is seen from Figure B.8 that the projection is divided by great circles into 24 unit stereographic triangles, which, due to the symmetry of the crystal structure, are crystallographically identical. Therefore, in the specification of a crystal orientation only one triangle is normally used and it is the triangle bounded by $[0\,0\,1]$, $[0\,1\,1]$ and $[\bar{1}\,1\,1]$ in the center of the projection. All possible orientations of crystals of f.c.c structure can then be specified by plotting the position of the rod axis within this triangle or along its boundaries. In practice, to represent the relative orientations of a crystal rod, the angles between the rod axis and at least two of the $[0\,0\,1]$, $[0\,1\,1]$ and $[\bar{1}\,1\,1]$ directions are measured. The rod axis can then be plotted in the standard triangle by using these measurements and a stereographic net, as shown in Figure B.9.

B.4 – Slip System

It is well known that plastic deformation occurs by slip on certain crystallographic planes in certain crystallographic directions. Such crystallographic planes are called *slip* or *glide planes,* while the directions along which slip occurs are referred to as *slip* or *glide directions*. The combination of any one of the slip planes with any one of the slip directions on that plane is called a *slip* or *glide system.*

Experimental observation shows that in most metals, the slip planes are usually those planes with the closest atomic packing, while the slip directions are always the closest packed ones along the slip planes. In f.c.c metals, the slip occurs on (1 1 1) planes in $\langle 0\,1\,1 \rangle$ directions, while in b.c.c metals, the slip directions are $\langle 1\,1\,1 \rangle$ but the slip plane may be one of (0 1 1), (1 1 2) or (1 2 3).

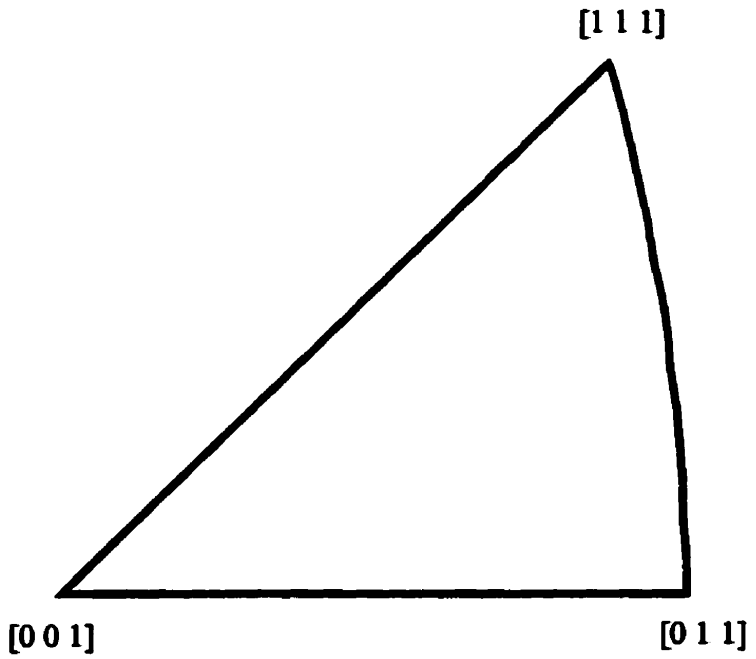

Figure B.9 Standard triangle